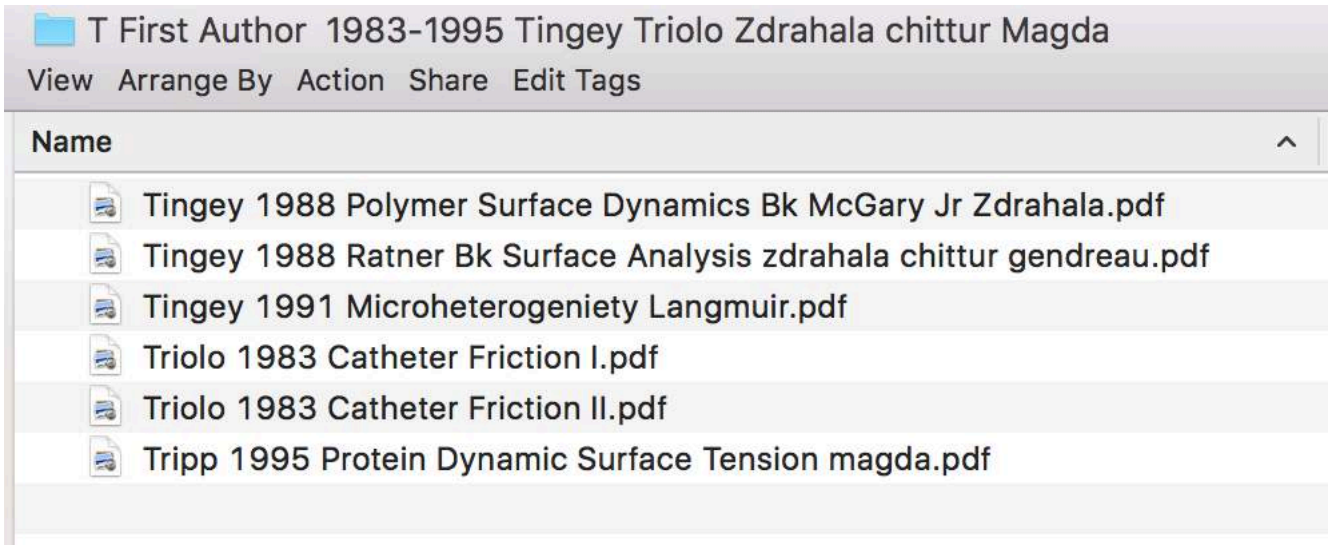
T First Author 1983-1995 Tingey Triolo Zdrahala chittur Magda
View Arrange By Action Share Edit Tags
Name
Tingey 1988 Polymer Surface Dynamics Bk McGary Jr Zdrahala.pdf
Tingey 1988 Ratner Bk Surface Analysis zdrahala chittur gendreau.pdf
Tingey 1991 Microheterogeniety Langmuir.pdf
Triolo 1983 Catheter Friction I.pdf
Triolo 1983 Catheter Friction II.pdf
Tripp 1995 Protein Dynamic Surface Tension magda.pdf

SURFACE ANALYSIS OF COMMERCIAL BIOMEDICAL POLYURETHANES

K. G. Tingey, J. D. Andrade, C. W. McGary Jr.*
and R. J. Zdrahala*

Dept. of Bioengineering, University of Utah,
Salt Lake City, Utah, 84112
* Deseret Polymer Research, Dayton, Ohio, 45401

ABSTRACT

Surface analysis of commercial biomedical polyurethanes including Vialon® 510X formulations, Pellethane®, Mitrathane®, Biomer®, and Lycra Spandex® have been conducted to evaluate surface reorientation, contamination, phase partitioning, and heterogeniety. Analysis of polyurethane films has included the Wilhelmy Plate technique for measuring dynamic contact angles. These results may be used to indicate reorientation of separated microphase domains in segmented polyurethanes upon exposure to differing environments. Evidence is presented showing the heterogeniety of phases at the surface. X-ray photoelectron spectroscopy (XPS) measurements were also conducted to verify surface compositional differences from that of the bulk, a reflection of preferential surface orientation. Data indicating surface variations due to hydration time, composition and morphology indicate that polyurethane surface properties are dependent on time, composition and processing history.

INTRODUCTION

Polyetherurethanes (PEUs), due in part to microphase separation of hard and soft segment components, exhibit unique bulk and surface properties. The phase separation observed in polyurethanes is known to contribute to properties that yield durable elastomers valuable as components in many biomedical products, and may also effect the thromboresistance in blood contacting applications. It has been shown that slight variations in synthesis technique, chemical composition, and processing all lead to variations in the chemical and morphological properties of polyurethanes[1-5]. The degree of phase separation, for example, is observable in dynamic mechanical analysis and reveals that phase separation increases with increasing polyol molecular weight, even vs. odd number of chain extender carbons, and diamine vs diol chain extender types[6-8]. It has been shown that the properties of the surface relative to the bulk also vary due to slight variations in composition and processing for common commercial polyurethanes[7,9,10].

The blood compatibility of a polymer is primarily a function of its surface properties. Correlations between polyurethane surface composition and

platelet adhesion have been published[11,12]. They do appear, however, to lead to ambiguous conclusions regarding optimal surface composition. Furthermore, hypotheses regarding blood compatibility as a function of dispersive and polar components of the solid surface tension[13], heterogeneous microphase separated surface structure[14] and possible complete dominance of soft-segment overlayers at the surface[15,16] indicate the importance and relevance of characterization of the surface of biomedical polyurethanes.

Part of the confusion regarding the mechanism of polyurethane biocompatibility may be attributed to the dynamic nature of polyetherurethane surfaces. This study focuses on the characterization of the surface composition and properties of polyurethanes. We attempt to better understand the dynamics of polyurethane surfaces which may eventually provide further insights into meaningful correlations between polyurethane chemical and/or processing parameters with applicable measures of blood compatibility. Our characterization has thus far relied heavily on X-ray photoelectron spectroscopy (ESCA) and the Wilhelmy Plate technique for measuring dynamic contact angles. This chapter discusses our progress thus far in determining the surface chemistry and morphological structures of selected commercial polyurethanes.

Polyurethanes are a family of polymers characterized by their phase-segregated morphology. They are generally composed of hard and soft segment regions[15]. The soft segment of most PEUs is generally a hydrophobic polyether. Structural order or crystallinity of the polyether soft segment depends on its chemical structure and molecular weight. Due to smaller intermolecular forces in the polyether segments, significantly less order or crystallinity is observed relative to the hard segment regions in most polyurethanes. The hard segment, composed of diisocyanate, and diol or diamine chain extender, does include permanent dipoles and hydrogen bonding sites. This results in a more hydrophilic region and a higher degree of intermolecular ordering. Frequently the hard and soft segment regions form two

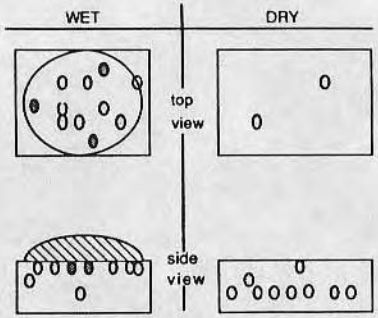

Figure 1 The presence of water, a polar solvent, on PEUs induces the polar hard segment to migrate to the surface to minimize the interfacial free energy. Surface free energy under hydrophobic air conditions is minimized by allowing the more hydrophobic soft segment matrix to dominate at the surface.

incompatible phases. The nature and morphology of continuous and dispersed phases depends on chemical composition, molecular weight and hard to soft segment ratio. The microphase separation of common elastomeric polyurethanes is frequently modeled as island domains of hard segment in a sea or matrix of soft segment. Due to the high degree of ordering in the hard segment and its inherent glass transition, usually well above room temperature, hard segment domains are rather fixed. The soft segment is considered quite mobile and is the origin of high degrees of elasticity in urethanes.

The matrix mobility allows the two phases to move relative to one another and could account for the dynamic behavior observed in polyurethane surfaces. Figure 1 illustrates the theoretical shifting of phases at the surface due to hydrophobic/hydrophilic surface interactions. The more hydrophobic soft segment matrix would tend to dominate in vacuum or air, and recede slightly to expose hydrophilic hard segment domains at a PEU-water interface. The driving force is minimization of interfacial free energy. This dynamic character complicates the surface characterization of a material and leads to very interesting in situ surface and bulk properties.

A major advantage of polyurethanes is their inherent tailorability. By varying composition or morphology the desired properties may often be developed. This particular study involves characterization of commercial polyurethanes with largely proprietary compositions. Although starting composition information is unavailable we can catagorize the polyetherurethanes into 3 general groups. Biomer® (Ethicon Inc.), Lycra® (DuPont deNemours and Co.) and Mitrathane® (Mitral Medical International Inc.) are considered to be of similiar formulation composed of methylene bis(p-phenyl isocyanate) (MDI) with a diamine chain extended hard segment and a polyether soft segment of undefined molecular weight. These are frequently referred to as polyurethaneureas. Pellethane® (Upjohn Co.) and Vialon® 510X (Deseret Polymer Research) are similar using MDI with a butanediol chain extended hard segment and a soft segment composed of polytetramethylene oxide (PTMO). The Vialon® H/H (Deseret Polymer Research) series differs from the Vialon® 510X series only by substituting blocks of PTMO with polyethylene oxide (PEO) varying from 0 to 100 %.

EXPERIMENTAL

Sample Preparation

Four different types of Vialon® 510X were received in extended ribbon form, differentiated as 510X-45, -55, -65, and -75, in which the suffix distinguishes the Shore D hardness of the composition[17]. Each type was received from single lots with as many as 4 individually packaged ribbons of each type. The samples were stored in the dark at room temperature to minimize degradation or change with time. In addition to the Vialon® 510X series, Deseret Polymer Research supplied a second prototypical H/H series which were also prepared, packaged and stored similarly to the Vialon® 510X samples. The H/H polymers are based on a hard segment concentration of 55%, composed of MDI chain extended with butanediol. The soft segment is composed of PTMO of molecular weight 1000 and PEO of molecular weight 1450. H/H-1 corresponds to a soft segment of 100% PTMO, H/H-5 is based on 100% PEO, and H/H-9 and H/H-10 are based on 2:1 and 1:2 PTMO:PEO ratios respectively.

Additional samples of commercial polyurethanes were provided from local sources, including Biomer® (20wt% in DMAC), Pellethane® 2363-90AE, Mitrathane® M2007 (25 wt% in DMAC), and Lycra Spandex® 126C. Biomer® and

Mitrathane® solutions were diluted with reagent grade N,N-dimethylacetamide (DMAC) to 3% polymer solutions. The other polymers were all dissolved in reagent N,N-dimethylformamide (DMF) to form 3% solutions. The polymer solutions were filtered under 30 psi pressure using polytetrafluoroethylene (PTFE) Millipore® filters. Biomer® and Lycra® were filtered with 0.5 micron filters and Mitrathane® and Pellethane® in 0.1 micron filters.

Films were dip cast from the filtered solutions onto cleaned Corning® glass cover slips (cleaned for 30 minutes in 80°C chromic acid solution) for contact angle measurements. Films were also dip cast on chromic acid cleaned soda lime glass plates under the same conditions for ESCA analysis. The cast films were allowed to hang vertically and dried under forced nitrogen flow for 4 hours at 75°C. Samples were then placed in a vacuum dessicator (15 in. Hg) for 24 hours to insure removal of residual solvent.

Instrument Analysis

A Hewlett Packard 5950B monochromatic X-ray photoelectron spectrometer was utilized for the ESCA studies. Ribbon samples were removed from sealed pouches and cast samples from isolated but ambient pressure conditions and immediately loaded into the vacuum prep chamber to minimize surface contamination. X-rays from the Al ($K\alpha_{1,2}$) line were used for excitation and an 8-10 eV electron flood gun was used to compensate sample charging. All bands were referenced to the 284.6 eV band of the alkyl carbon 1s spectrum for each sample. Samples were scanned 20 times with a scan width of 20 eV centered around the peak of interest; carbon 1s (270-290 eV), nitrogen 1s (385-405eV), oxygen 1s (515- 535eV), and silicon 2p (85-105 eV). Oxygen, due to its large Scoffield cross section, was scanned only 10 times. Spectra from 0 to 1000 eV were also collected from 4 scans. Peak areas for oxygen, carbon, nitrogen, and silicon were determined digitally. The carbon peaks were curve resolved into alkyl, ether, and carbamate carbons through the use of software (Surface Science Laboratories, Mountain View, Ca), based on the chi square fit optimization of gaussian distributions of collected electrons.

Dynamic contact angle data was collected by using the Wilhelmy Plate technique as previously described[18]. Cast films on glass cover slips were used as prepared and the dimensions of the clean cover slips were used in determining the contact angle. Polyurethane ribbon samples were cut using a die of 50 mm. X 22 mm., corresponding to the glass cover slip dimensions. Following sample cutting all ribbon samples were wiped clean with Tex-Wipe® (Thousand Saddle, N. J.) ultra-clean wipes. Samples were permitted to equilibrate under room temperature, pressure and relative humidity conditions for 24 hours before analysis. Contact angle experiments were performed in purified water filtered through a Milli-Q® ultrafiltration system (Millipore, El Paso, TX). Both advancing and receding contact angle measurements were made. Contact angle hysteresis loops were obtained until the measured hysteresis values equilibrated. Equilibrated ratios are reported. Following contact angle measurements of each sample, the test water was replaced with clean water to minimize cross contamination by extractables.

ANALYTICAL BACKGROUND

ESCA

The use of ESCA in probing polymer surfaces has been well documented[19,20,21] and a number of studies have been conducted on polyetherurethanes.[2,7,10,11,12,16,19,22] ESCA is considered to be quantitative to ± 10%[8]. Error may arise as a function of variations in the X-ray flux, photoionization cross-section, instrument transmission function and electron mean free path at various kinetic energies[20]. From proper manipulation of these parameters, semiquantitative photo-electron intensities can be determined. Unfortunately, impurities which may exist as low molecular weight oligomers appear similiar to the high molecular weight bulk polymer. The low molecular weight components may cause major property changes in the surface of the polyetherurethanes due to their variation in mobility, and interaction with other surface species.

Characterization of commercial proprietary PEUs limits our study and for this reason we will assume that all nitrogen and carbamate carbon is indicative of hard segment regions. The use of ESCA in identifying and characterizing separated phase domains is however difficult[8,16]. Knutsen et. al. have indicated that some nitrogen and carbamate carbons used to identify hard segment domains may actually be present in soft segment matrix areas or phase boundary regions[4]. Ratner has cleverly attempted to measure hard and soft segment nitrogen and carbamates by chemically derivatizing hard segment chain extenders which yield stronger more sensitive electron emission information and eliminate signal originating from hard segment components interspersed in the soft segment matrix[7].

The phase mobility of the polyurethane should also be considered. In a vacuum the surface environment is much different than in aqueous environments or even ambient air conditions. If PEUs are truly dynamic then the surface we identify in a vacuum with ESCA may be very different than the surface in water, where the polymer may reorient to minimize surface free energy. Under this limitiation, that the surface is the top 0-100 angstroms in a dry hydrophobic environment, we consider our ESCA analysis a good quantitative measure of surface molecular composition. It has been further assumed that the soft segment is largely characterized by ether carbons while the hard segment can be identified with nitrogen or carbamate carbon. Small amounts of ether signal are anticipated and discernable from the hard segment regions but are not accounted for in determining soft segment concentration. It should be further noted that the "as-received" polymer surface is the surface of interest and in most cases should not be assumed to be free of impurity or correctly represent the surface of ultra-pure polyurethane polymer. Essentially, due to phase mobility, impurities, and poorly defined phases or phase boundaries, all of which may be present, we have limited ourselves to "as-received" surfaces and our estimates of composition or morphology are at best semi-quantitative.

Contact Angle

Contact angle studies of surfaces hold significant value in characterization of polymer surface properties. Polyurethanes have been studied using static and dynamic contact angle, and using the underwater captive bubble and droplet techniques[9,18,23]. These studies, by nature, are indicative of surface energetics and do not yield intrinsic compositional information. Dynamic contact angle data in particular may yield insights into other important surface parameters. Johnson and Dettre[24] have indicated the complexity of contact angle hysteresis loops. They report that hysteresis may occur due to surface heterogeneity, roughness or physical surface deformation. Andrade adds that dynamic transitions, swelling, or entropy effects must also be included as hysteresis factors[18]. Contact angle studies may also be used to evaluate the leachablity of low molecular weight polymer components or impurities. Separation or isolation of any of these variables is very difficult and hence characterization of polymer surfaces by analysis of contact angle hysteresis is a bit tenuous. Contact angle data from polyurethanes tested in our studies, although somewhat ambiguous, manifests very interesting trends which suggest

surface related phenomena. In cooperation with other analytical methods, contact angle data does offer some valuable insights. Polyurethane variations observed using contact angle analyses may be presumed to indicate differences in surface composition, and polymer chain mobility. These may be considered functions of chain length of the soft segment, chain length of the hard segment, degree of crystallinity or ordering of the hard segment, and degree of phase mixing.

RESULTS AND DISCUSSION

ESCA Results

The relative concentrations derived from quantitative X-ray photoelectron spectroscopy of carbon, nitrogen and oxygen in their molecular environments are reported in Table 1. Spectra from different samples of a single lot were analyzed and revealed concentration variations of less than 2 %. Aliphatic, ether, and carbamate carbon, as well as oxygen, and nitrogen were quantitated for all polyurethanes studied and are presented in the above mentioned table. The ether carbon to nitrogen ratios were also determined to establish a surface soft to hard segment relationship. Also in Table 1, where possible, theoretical bulk ether carbon to nitrogen ratios are reported. This data originates from manufacturer supplied monomeric ratios. The experimentally derived surface ether carbon to nitrogen ratio also is calculated and the comparison of theoretical and experimental ratios results in a surface enhancement index which acts as a measure of the partitioning of soft segment ether carbon at the surface relative to the bulk.

A few general observations may be noted from the accumulated ESCA data. The Lycra sample with very low carbamate carbon and total nitrogen apparently has a very low concentration of hard segment in the surface region. Because Lycra® is not a biomedical PEU and substantially less care is taken in inhibiting contamination, surface composition may be explained as a hydro-

TABLE 1
RELATIVE SURFACE CONCENTRATION FROM ESCA

Polymer	%PEO	C-H	C-O	O=C-N	N	O	Theory C-O / N	ESCA C-O / N	Enhancement Soft to Hard Segment
Biomer		47	26	0.75	1.4	19	---	34	---
Mitra.		43	31	0.65	1.5	20	---	21	---
Pelleth.		51	23	1.43	2.8	18	---	16	---
Lycra		50	12	0.16	0.5	22	---	25	---
510X-45		50	27	2.00	1.6	18	5.2	16	2.8
-55		48	26	1.80	2.1	19	4.2	14	3.2
-65		49	29	2.40	2.7	17	3.1	11	3.6
-75		48	28	2.40	3.3	18	2.0	9	5.1
H/H- 1	0	46	32	1.50	3.0	18	3.1	11	5.0
- 9	33	40	32	1.70	2.8	22	4.0	11	3.7
-10	66	39	33	1.70	2.7	22	4.9	12	3.2
-5	100	28	38	2.40	3.0	26	5.8	13	2.4

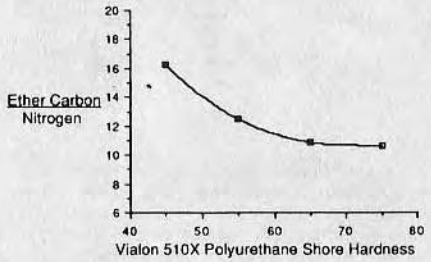

Figure 2 Ratio of soft segment polyethers to hard segment index at the vacuum interfacing surface as a function of PEU composition.

carbon contamination overlayer which acts to mask the true PEU surface. However, Biomer® and Mitrathane®, both diamine chain extended PEUs similiar to Lycra® also show significantly lower nitrogen and carbamate carbon concentrations than the diol extended PEU samples. Although these polyurethane ureas are thought to contain polyethers of higher molecular weight than the polyetherurethanes, this decrease in nitrogen is nonetheless surprising because the chain extender of these polymers also contain nitrogen, thereby further increasing the bulk nitrogen content. This indicates that the nitrogen containing hard segment may be partitioned away from the surface and suggests that the diamine extended PEUs are more phase separated relative to diol extended PEUs, allowing the hard segment to move somewhat independently of the soft segment.

The similiarity between Pellethane® and the Vialon® 510X series PEUs should also be noted. Chemical composition, although proprietary, is thought to be quite similiar for Vialon® 510X and Pellethane polyetherurethanes. The Vialon® 510X polyurethanes increasing in Shore hardness from 45-75 do show a trend of increasing nitrogen and carbamate carbon with increasing hardness. This is anticipated in that hardness increases as the ratio of highly ordered high Tg material increases relative to the disordered low Tg soft segment. This phenomenon, observed as a hard segment index of nitrogen and a soft segment index of ether carbon, is shown in Figure 2. ESCA data show that surface composition in the Vialon® 510X series are quite similiar. The relative invariability of the Vialon® polymers may indicate that very little if any appreciable differential surface composition within the series occurs, even though the bulk mechanical properties differ significantly based on Shore hardness values. The relative consistency of surface molecular concentration may be indicative of a minimization of surface free energy at an optimal composition corresponding to that seen experimentally. The enhancement of soft segment at the surface relative to the bulk is evident and this trend will be discussed further in this paper.

Contact Angle

Contact angle data is valuable because it allows one to monitor the energetics of the true surface layer and to explore the potential of dynamic

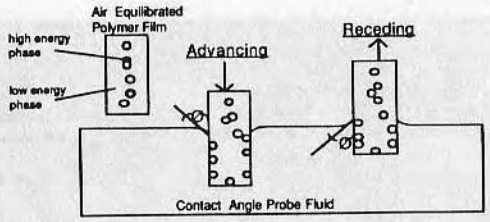

Figure 3 Wilhelmy Plate Contact Angle method to observe dynamic character of PEUs and the hypothetical movement of phases with changing environment.

phenomena. Figure 3 illustrates the dynamic nature of the surfaces being measured using the Wilhelmy Plate technique, based on the hypothesis that mobile phases reorient to minimize interfacial free energy. As the air equilibrated film approaches the water an increased concentration of soft segment, relative to bulk concentration, dominates at the surface. The higher valued advancing contact angle is measured (as shown in the figure above) as the water is repelled by the more hydrophobic soft segment. As the film becomes hydrated, however, the more hydrophilic hard segment migrates to the surface to minimize interfacial free energy. When the hydrated sample is withdrawn the air/water interface probes the altered more hydrophilic surface resulting in the lower receding contact angle. The hysteresis observed is considered to be indicative, in part, of short time scale surface transistions. Both advancing and receding contact angles were determined from hysteresis loops. Variation in a single lot was observed to be less than 6%

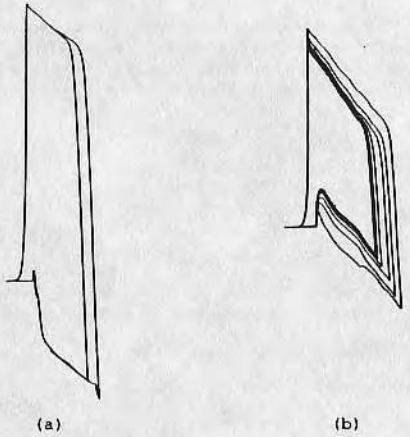

(a) (b)

Figure 4 Contact angle hysteresis loops formed using the Wilhelmy technique of (a) Biomer® and (b) Vialon® 510X-45.

Table 2
As Received Polyurethane Contact Angle Data

Polyurethane			Øadv	Ørec	Hysteresis
Vialon®	PTMO	H/H -1	82	51	31
	33% PEO	H/H -9	79	33	46
	66% PEO	H/H-10	71	31	40
	PEO	H/H -5	55	30	25
Vialon®	510X-45		87	51	36
	510X-55		86	50	30
	510X-65		82	51	31
	510X-75		87	51	36
Pellethane			88	50	38
Mitrathane			93	45	48
Biomer			90	0	90
Lycra			105	29	76

for most samples. The polyurethanes studied vary dramatically in both advancing and receding contact angles as well as hysteresis. Figure 4 illustrates representative contact angle hysteresis loops for Biomer® and Vialon® 510X-45 polyetherurethanes. Differences in surface energetics suggesting differences in constant or dynamic composition, morphology or molecular motion are apparent. Table 2 tabulates the contact angles of the as received commercial polyetherurethanes.

It should be noted that Biomer®, Lycra®, and Mitrathane®, the three diamine chain extended polyurethanes observed in this study, exhibit very high advancing and low receding contact angles. The large hysteresis suggests that either short time scale molecular orientations are occurring as the surface environment changes or that heterogenieties exist at the surface. This may signify some combination of greater degrees of phase separation and concommitant phase mobility or surface phase enhancement, surface heterogeniety, or surface roughness--all parameters determining contact angle character. Since Pellethane® and Vialon® 510X PEU's bulk compositions are similiar it is not suprising that their contact angle data correspond quite closely. ESCA surface composition data is also very similiar indicating comparable compositional surface properties. The advancing and receding contact angles are seen to be quite intermediate with a relatively low degree of hysteresis. This may indicate that phase mobility properties, a function in part of morphology, are also quite similiar for Pellethane® and Vialon.® The difference observed between these polymers and Biomer®, Lycra®, and Mitrathane® suggest that these two butane diol extended polymers have a less phase separated or less mobile surface composition.

The Vialon® H/H series, increasing in PEO/PTMO concentration ratio, shows decreasing contact angle or increasing wettability as the concentration ratio of the more hydrophilic PEO component of the polyether increases. The advancing and receding angles in this series do reveal trends which suggest that surface heterogeniety does exist. This phenomena will be discussed in a further section.

Preliminary hydration studies of these PEU films indicate that both the advancing and receding contact angle decrease with increasing hydration. Figure 5 presents part of this data and demonstrates that long time-scale reorientation may take place to present a more hydrophilic surface. It might

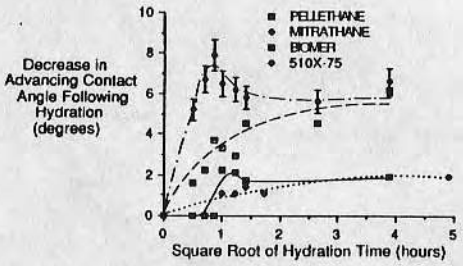

Figure 5 Decrease in advancing contact angle of various PEUs with hydration time. Error bars shown for Mitrathane® are representative for all samples shown.

be argued that water absorption and polymer swelling would account for variations in surface energetics with time and may in part explain this data. Water absorption appears to be on a much longer time scale leveling out after about 150 hours. Contact angle indicated transitions appear to be completed after less than 16 hours.

A rough approximation of the effect of water absorption on contact angle may be made by calculating the weighted average of the contact angle for a multicomponent surface as proposed by Cassie[25],

$$\cos \theta = Q_1 \cos \theta_1 + Q_2 \cos \theta_2 , \qquad Q_1 + Q_2 = 1.0$$

where Q_i is the fraction of component i at the surface, θ_i is the contact angle of the pure component i and θ is the theoretical contact angle of the mixture. The effect of hydration would assume that the weight % bulk absorption would be equivalent to Q_1. The contact angle of water in water would be 0 thus cos θ_1 would be 1.0. The contact angle of component 2, θ_2, would be the contact angle of the dry polyurethane film. Solving for Q_1, based on the equilibrium contact angle of the hydrated film, indicates a water surface coverage of 3.7%. This calculation does assume that no surface excess or deficiency is present. Equilibrium bulk water absorption data indicates that 2.1% absorption occurs after about 21 days. This suggests that sorbed water may account for a large fraction, but probably not all of the decrease in advancing contact angle upon hydration.

Okawa has also observed this phenomenon and indicates that it may in part be due to structural reorientation of surface side chains to minimize the interfacial free energy[26].

Contamination

Recent studies of polyurethane surfaces have demonstrated that polyether-urethanes frequently contain a significant fraction of low molecular weight

TABLE 3

SURFACE SILICON OBSERVED USING ESCA

POLYURETHANE			mole% Si
Lycra			15.9
Biomer			5.7
Mitrathane			4.0
Pellethane			3.7
Vialon®	510X-45		2.6
	510X-55		4.1
	510X-65		0.0
	510X-75		0.0
Vialon®	H/H -5	PEO	3.0
	H/H-10	66% PEO	2.8
	H/H -9	33% PEO	2.4
	H/H -1	PTMO	0.0

material which tends to migrate from the bulk[22,27]. This low molecular weight material has been shown to be compositionally quite different from the bulk and may have its origin in processing aids, release agents, or oligomers of the polyether component or urethane fraction. It has been proposed that in some cases the bulk impurities which aggregate at the surface may improve blood compatibility[16,28,29]. Ward et. al. have proposed that intentionally adding inert low molecular weight additives may act to render the surface less thrombogenic by migrating to, and masking, the surface region[30]. Other studies however indicate improved biocompatibility upon impurity extraction[27,31]. Angular dependent ESCA data can be used to depth profile impurity concen- trations[22]. Table 3 shows that these samples contain surface silicon. The existence of silicon may be indicative of poly(dimethyl siloxane)(PDMSO), a common mold release agent, which may dramatically alter the surface properties of the polyurethane. Lycra® and Biomer® show the largest concentration of silicon at the surface (>5%) while most other polyurethanes analyzed revealed intermediate concentrations (2.4--4.1%

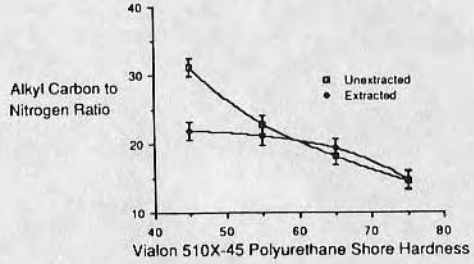

Figure 6 Ratio of Alkyl carbon to hard segment nitrogen at the vacuum interfacing surface of extracted and unextracted PEU compositions.

silicon) at the surface. It is interesting to note that Vialon® 510X-65 and -75 showed no appreciable silicon at the surface. ESCA data was also collected from Vialon® 510X PEUs following 24 hour extraction in purified water. Following extraction a dramatic decrease in alkyl carbon relative to nitrogen is observed for Vialon® 510X-45 as seen in Figure 6. Water extraction (24 hours, 70°C) results in approximately 0.025 wt% extractable low molecular weight components. Although of low bulk concentration, extractable components will most likely be heavily concentrated at the surface and may be primarily responsible for this observation.

Contact angle studies also indicated the presence of surface extractables for all polyetherurethanes in this study with the exception of Vialon® 510X-65 and 510X-75. Extraction was monitored by measuring the surface tension of water against perfectly wetting glass both prior to and following exposure to cast or sheet polyurethane films. The surface tension of water decreases if surface active extractables are present. Contact angle extraction results correspond with those samples which showed surface silicon analyzed by ESCA.

Surface Partitioning

Surface partitioning can best be investigated by variable angle ESCA although reasonable quantitation of soft to hard segment concentration in the upper 100 angstroms of material may be represented as the ether carbon to nitrogen ratio from fixed angle ESCA. Figure 7 illustrates a correlation between the surface soft segment enhancement ratio and Shore D hardness. The correlation shown argues that hydrophobic soft segment surface enhancement increases with increasing hardness. Since the hardness increases with increasing hard segment concentration, the probability of soft segment surface enhancement should decrease with increasing hardness. This apparent conflict may, however, be rationalized in terms of the extent of the phase separation. The increase in the hard segment content leads to formation of higher molecular weight hard segment chains. This, in turn, minimizes the chance for phase mixing and produces purer, larger and better defined hard and soft segment domains. Assuming that the soft domains are composed of loosely packed chains, and thus are larger in size, more surface could be covered with the soft segment. Our ESCA surface analysis data shows that the surface concentration of hard segment components increases with hardness. This implies that greater phase segregated regions appear to be more mobile and either migrate more strongly to the surface or dynamically rotate to the surface more easily in a hydrophobic environment relative to the less concentrated more disperse low hardness samples. This may be due to a stronger driving force to aggregate and to minimize surface free energy due primarily to increased concentration of hard segment material.

The Vialon® PEO/PTMO soft segment PEUs also serve as an example of phase dynamics. Hwang et.al studied polyurethanes of MDI, BDO and polyether soft segments and observed that PEO interacts more with the hard segment than either poly(propylene oxide)(PPO) or PTMO, suggesting maximal phase mixing for PEO polyetherurethanes[32]. Similiar arguments show that phase compatibility increases from olefinic to polyether soft segment prepolymer and from high to low aliphatic character polyethers[33]. Other investigators have shown that large Tg changes with variations in composition or processing parameters may be indicative of high phase mixing[34]. Glass transition temperature variations observed for PEO, PPO, and PTMO show that the most rapid Tg changes occur for the PEO polyurethanes[10]. The use of PEO as the soft segment would increase the relative compatibilities of the hard segment diisocyanate domains and the

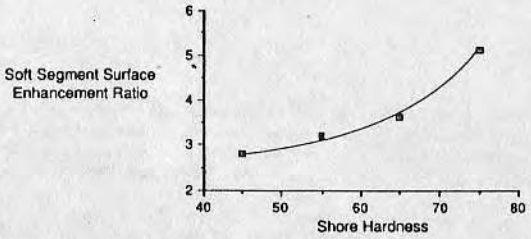

Figure 7 Enhancement of soft segment at the surface observed with ESCA for Vialon® 510X polyurethanes implying Hardness related to greater phase segregation leads to greater phase mobility.

soft polyether matrix material resulting in a higher degree of phase mixing throughout the bulk of the polymer. The more disperse the hard segment regions in the polyether matrix, the lower, one might anticipate, would be the enhancement of the soft segment at the surface. Figure 8 shows the correlation between experimentally derived soft segment enhancement at the surface relative to the bulk as a function of PEO content. As hypothesized, the soft segment surface enhancement decreases with increasing ratio of more compatible PEO polyether.

These correlations seem to indicate that phase compatibility and hardness, a function of hard segment concentration and phase separation, have a strong effect on surface enhancement of soft segment material in a vacuum environment. The data suggests that as phase separation decreases, surface/bulk enhancement of polyether soft segment also decreases. These two

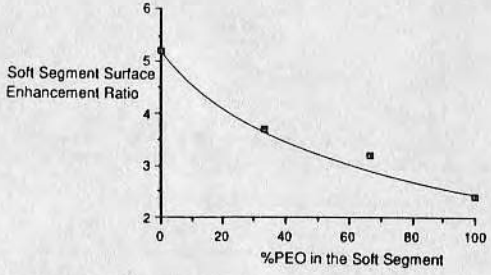

Figure 8 Enhancement of soft segment at the surface observed with ESCA for PEO-PTMO polyurethanes implying greater phase mixing correlates with a decreasing driving force for minimization of surface free energy.

examples of surface enhancement of the soft segment phase argue that apparent surface structure and phase dynamics may be governed by controlling the compatibility of the phases through selection of hard and soft segment relative concentrations, surface energetics, and solubility parameters.

Heterogeneous Surfaces

Surface heterogeniety is thought to exist in highly phase separated systems. Some spectroscopic analyses of PEUs seem to indicate that polyurethane surfaces are completely dominated by a polyether soft segment overlayer[16]. Muhmud et. al. have shown that as the average molecular weight of the soft segment increases the relative ratio of soft segment to hard segment at the surface increases and approaches infinity at soft segment molecular weights of about 4,500[35]. Using FTIR-ATR Knutson and Lyman have varied internal reflection angle and shown that morphology of the domain-matrix polyurethanes is a function of IR sampling depth, indicating greater phase separation at the surface than in the polymer bulk[4]. These findings indicate that surface heterogeniety does exist for intermediate molecular weight soft segments and the surface is more completely phase separated than the bulk. Schwartz and Garoff present a theoretical development that indicates the importance of patch size, shape, and relative position, in addition to surface coverage, in predicting wetting behavior. Their analysis suggests that hysteresis diminishes and perhaps vanishes for micron size particles at low surface concentration[36]. Ruckenstein and Gourisankar show that the contact angle of a solid surface varies as a function of its environmental fluid and that dynamic restructuring and reorientation may take place over time[37]. This phenomenon is observed for single phase materials but may be more pronounced for multiphase surfaces.

Johnson and Dettre[24] have modeled a heterogeneous surface and observed that contact angles and contact angle hysteresis vary with the percentage of low contact angle material surface coverage as presented in Figure 9. This model system has been substantiated with a hydrophobic partial monolayer on glass[38] and on primarily low energy polymer and starch systems[39]. Their findings argue that the contact angles are a balance between liquid vibrations and the free energy barriers of the surface. This figure further indicates

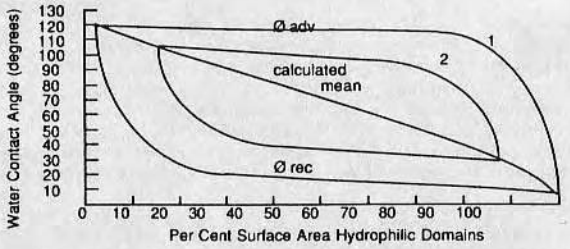

Figure 9 Dynamic contact angle of heterogeneous surfaces based on the model of Johnson and Dettre[24]. Heterogeneous domain size decreases in the order from 1-2.

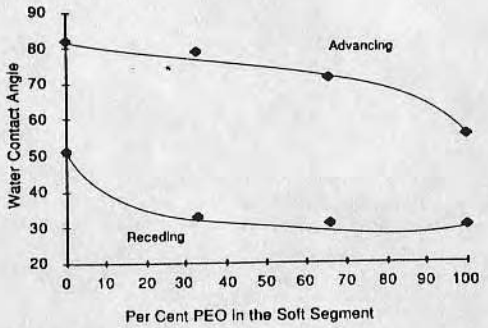

Figure 10 Water contact angle of PEO-PTMO polyetherurethanes of similiar composition or relative size of heterogeneous domains.

how the contact angles approach Cassie's curve[25], or the median of the advancing and receding angle, as the size of the heterogeneous regions grow smaller.

Figure 10 shows the correlation between per cent PEO and both advancing and receding contact angle for H/H PEUs. The trend indicates that as the PEO/PTMO ratio increases only a slight change in contact angle is observed until quite large concentrations of PEO are present in the bulk. The receding contact angles conversely remain fairly constant until almost no PEO is present in the bulk. The previous ESCA correlation to surface enhancement, shown in Figure 6, suggests lower phase separation at high PEO bulk concentrations and highly-phase separated, increasingly surface enhanced soft segment at low PEO bulk concentrations. Because ESCA data shows that the concentration of soft segment does not decrease but remains constant, while the enhancement of soft segment decreases with decreasing PTMO, it may be interpreted that phase domains are becoming less well defined and smaller. In light of Johnson and Dettre's findings, one would expect that, as the MDI hard segments grow smaller and more diffuse, the advancing contact angle would remain fairly constant until the domain size decreased to very small values, at which point the energy barrier of the heterogenous domain is readily overcome. At this point the advancing angle would fall rapidly to the value predicted by Cassie's curve for homogeneous mixtures. Conversely, the receding angle would be very low until the hard segment domains size or concentration are at their maximum, at which point the receding angle would rapidly approach Cassie's curve. Our contact angle data appears to correlate well with Johnson's model for heterogeneous surfaces.

Because so many variables are involved in contact angle experiments the analysis and definition of mechanism is difficult. In general, however, the major cause of hysteresis on optically smooth, non-deformable surfaces is surface heterogeniety, which appears to be the primary component of hysteresis

in this case[24]. The H/H prototypical PEO-PTMO polyurethane model system is further complicated in light of Takahara's conclusion[40] that the surface free energy for this system increases in the order PTMO< hard segment < PEO so not only will domain size change but, as the concentration ratio of PEO/PTMO approaches infinity, the hard segment becomes the hydrophobic component and the soft segment becomes the hydrophilic component. This polyurethane may exist with 3 discernable phases rich in either PEO, PTMO, or MDI. This contact angle data indicates that the prototypical H/H PEUs are dynamic and yield data consistent with a heterogeneous surface as modeled by Johnson et. al.

CONCLUSIONS

Although additional analyses of these commercial polyurethanes is planned, a number of conclusions can be derived from the results to date. Many of the PEUs studied are surface contaminated, and the impurities or extractables observed at the surface may dramatically alter the surface properties.

ESCA data has shown an increased surface enhancement of soft segment for a more hydrophobic polyether, implying that minimization of surface free energy may be a driving force in surface phase segregation dynamics. From ESCA we have observed that hardness increases with increasing concentration of hard segment and that the enrichment of soft segment at the surface is enhanced by greater bulk hardness. This may be related to increases in phase separation proportional to hardness which would permit greater phase mobility. Phase mobility is also suggested in contact angle studies which show that surface energetics change dramatically upon long and short time scale hydration.

Contact angle hysteresis, observed to be much greater for the diamine chain extended PEUs, suggests greater phase mobility for diamine extended systems than for diol extended systems. Additionally, advancing and receding contact angle data plotted against polyether composition corresponds to accepted models of surface heterogeniety, indicating that these polyether-urethane surfaces behave dynamically and suggesting that both polyether and diisocyanate rich phases do indeed exist at the surface and respond to hydrophobic or hydrophilic environments.

ACKNOWLEDGEMENTS

The authors acknowledge the assistance of P. D. Dryden of the University of Utah Surface Analysis Lab for his assistance in the ESCA analysis. The work was supported by a grant from Becton Dickinson Polymer Research.

REFERENCES

1. Alu, B. B., Ward, R. S. Jr. A New Criterion of Phase Separation: The Effect of Diamine Chain Extenders on the Properties of Polyurethane-ureas., *JAPS*, **27**, 2167-2177, 1982
2. Takahara, A., Tashita, J., Kajiyama, T., Takayanagai, M., McKnight, W. J., Microphase Separated Structure and Blood Compatibility of Segmented Poly(urethaneureas) with Different Diamines in the Hard Segment. *Polymer* **26**, 978, 1985

3. Lin, S. B., Hwang, K. S., Tsay, S. Y., Cooper, S. L. Segmental Orientation Studies of Polyurethane Block Copolymers with Different Hard Segment Lengths and Distribution., *Coll. Polym. Sci.* **263**, 128-140, 1985
4. Knutson, K. S., Lyman, D. J., The Effect of Polyether Segment Molecular Weight On the Bulk and Surface Morphologies of Copolyetherurethaneureas in *Biomaterials-Interfacial Phenomona and Applications* (Cooper, S. L., Peppas M. A., Eds.) *Adv. Chem. Ser.* **199** 109-132, 1982
5. Zdrahala, R. J., Hager, S. L., Gerkin, R. M., Critchfield, F. E., Polyether Based Thermoplastic Polyurethanes. Effect of the Soft Segment Molecular Weight. *Elastomers and Plastics* 12, 225-244 (1980)
6. Zdrahala, R. J., Gerkin, R. M., Hager, S. L., Critchfield, F. E., Polyether Based Thermoplastic Polyurethanes. I. Effect of Hard Segment Content, *JAPS* 24, 2041-2050 (1979)
7. Yoon, S. C., Ratner, B. D., Surface Structure of Segmented Polyetherurethanes and Polyetherurethaneureas with Various Perfluoro Chain Extenders. An X-Ray Photoelectron Spectroscopic Investigation., *Macromolecules* **19**, 1068-1079, 1986
8. Grasel, T. G., Cooper, S. L., Surface Properties and Blood Compatibility of Polyurethaneureas, *Biomaterials* **7**, 315, 1986
9. Lelah, M. D., Grasel, T. G., Pierce, J. A., Cooper, S. L., Ex Vivo' Interactions and Surface Property Relationships of Polyetherurethanes., *J. Biomed. Mater. Res.* **20**, 433-468, 1986
10. Takahara, A., Tashita, J., Kajiyama, T., Takayemaji, M, McKnight, W. J., Microphase Separated Structure, Surface Composition and Blood Compatibility of Segmented Poly(urethaneureas) With Various Soft Segment Components. *Polymer* **26**, 987-996, 1985
11. Merrill, E. W., Muhmud, N., Wan, S., Polymer Surface Studies, XPS Characterization, *Proc. IUPAC Macromol. Symp.* Amherst Mass 1982, p. 685
12. Hanson, S. R., Harker, L. A., Ratner, B. D., Hoffmann, A. S., In vivo Evaluation of Artificial Surfaces With a Nonhuman Primate Model of Arterial Thrombosis, *J Lab Clin Med* **95**, 289-304, 1980
13. Baier, R. E., Applied Chemistry at Protein Interfaces., *Adv. Chem. Ser.* **145**, 1, 1975
14. Aoguayi, T., Uruno, M., Akami, H., Shinohara, I., Okano, T., Kataoka, K., Sakurai, Y., Compatibility in Blood of Block Copolymers Having Microphase Separated Structure. *Kobunshi Ronbunshu*, **42**, 647-54, 1985
15. Yoon, S. C., Ratner, B. D., Thermal and Solvent Effects on the Surface Structure of Fluorinated Polyurethanes. Program and Abstracts of the 8th Rocky Mountain Regional ACS Meeting, Denver CO, June 1986.
16. Ratner, B. D.,Paynter, R. W., Polyurethane Surfaces: The Importance of Molecular Weight Distributions, Bulk Chemistry and Casting Conditions, in *Polyurethanes in Biomedical Engineering* (Planck, H., Egbers, G., Syre, R. eds.) Elsevier Science Publishers, Amsterdam, 1984
17. Zdrahala, R.J., Solomon, D. D., Lentz, D. J., McGary, C. W. Jr., Thermoplastic Polyurethanes, Materials for Vascular Catheters. in *Progress in Biomedical Engineering Volume III, Polyurethanes in Biomedical Engineering*, Elsevier Science Publishers, Amsterdam, 1987
18. Andrade, J. D., Smith, L. M., Gregonis, D. E., The Contact Angle and Interface Energetics in *Surface and Interfacial Aspects of Biomedical Polymers* 249-292 (Andrade, J. D. Ed.) Plenum Press, NY, 1985
19. Ratner, B. D., Surface Charaterization of Biomaterials by Electron Spectroscopy for Chemical Analysis., *Ann. of Biomed. Eng.* **11** 313-336, 1983
20. Andrade, J. D. X-Ray Photoelectron Spectroscopy in *Surface and Interfacial Aspects of Biomedical Polymers* 105-195 (Andrade, J. D. Ed.) Plenum Press NY, 1985
21. Paynter, R. W., Ratner, B. D., Thomas, H. R., Polyurethane Surfaces-An XPS Study, *Polym. Prepr.* **24** 13, 1983

22. Hu, C. B., Sung, C. S. P., Surface Chemical Composition Depth Profile o Polyetherpolyurethaneureas as Studied by FTIR and ESCA., *Polym. Prepr.* **21**, 1956, 1980
23. Lelah, M. D., Stafford, R. J., Lambrecht, L. K., Young, B. R., Cooper, S. L., Cast Vrs Extruded Biomer For Biomedical Applications. *TASAIO* **27**, 506, 1981
24. Johnson, R. E., Dettre, R. H., Wettability and Contact Angles in *Surfac and Colloid Science* **2** 85-154 (Matijevic, E. Ed) Wiley, NY, 1969
25. Baxter, S., Cassie, A.B.D., The Water Repellency and a New Water Repellency Test, *J. Textile Inst.* **36** T67, 1945
26. Okawa, A. *The Hydration of Polymer Thin Films and its Effect on Blood Compatibility* Senior Thesis, Dept. of Materials Science and Engineering, University of Utah, 1983
27. Ratner, B. D., Polyetherurethane Surfaces: Chemical and Morphological Changes Upon Extraction, *Proc. IUPAC Macromol. Symp.* Amherst, Mass, 1982 p. 677
28. Lelah, M. D., Cooper, S. L. *Polyurethanes in Medicine*, CRC Press, Bato Rogue, LA, 1986
29. Ratner, B. D., ESCA Studies of Extracted Polyurethanes and Polyurethane Extracts; Biomedical Implications in *Physiochemical Aspects of Polyme Surfaces* (Mittel, K. L., ed.) Vol. 2 p. 969-983, Plenum, NY 1983
30. Ward, R. S., White, K. A., Yilgor, I. Contact Angle Hysteresis of Polymers Modified with Surface Active Amphipathic Polymeric Additives Program and Abstracts of the 8th Rocky Mountain Regional ACS Meeting, Denver CO, June 1986.
31. Marchant, R. E., Anderson, J. M., Hiltner, A., Castillo, E. J., Gleit, J., Ratner B. D., The Biocompatibility of Solution Cast and Acetone Extracted Biomer. , *J. Biomed. Maters. Res.* **20** 799-815, 1986
32. Hwang, K. K. S., Hemker, D. J., Cooper, S. L., Phase Diagrams and Morphology of a Urethane Model Hard Segment and Polyether Macroglycols *Macromolecules* **17** 307, 1985
33. Chamberlin, Y., Pascault, J. P., Phase Segregation Kinetics in Segmente Linear Polyurethanes: Relations Between Equilibrium Time and Chain Mobility *Polym.Sci* **22** 1835, 1984
34. Xu, M., McKnight, W. J., Chen, C. H. Y., Thomas, E. L., Structure and Morphology of Segmented Polyurethanes. I. Influence of Incompatabilit on Hard Segment Sequence Length, *Polymer* **24** 1327, 1983
35. Muhamud, N. A., Merrill, E. W., XPS Studies of Segmented Polyurethaneur Surfaces *Polym. Sci. Eng.* **55** 751, 1986
36. Schwartz, L. W., Garoff, S., Contact Angle Hysteresis on Heterogeneous Surfaces *Langmuir* **1**, 219-230, 1985
37. Ruckenstein, E., Gourisankar, S. V., Enviromentally Induced Restructuri of Polymer Surfaces and Its Influence on their Wetting Characteristics in An Aqueous Environment. *J. Coll. Interf. Sci.* **107** 485-502, 1985
38. Dettre, R. H., Johnson, R. E. Jr., Contact Angle Hysteresis IV. Contac Angle Measurements on Heterogeneous Surfaces *J. Phys. Chem.* **69** 1507, 1965
39. Ray, B. R., Andersen, J. R., Scholz, J. J., Wetting of Polymer Surfaces I. Contact Angle of Liquids on Starch, Amylase, Amylopectin, Cellulose and Poly(Vinyl Alcohol) *J. Phys. Chem.* **62** 1220, 1958
40. Takahara, A., Atsushi, M., Kajiyama, T., Tashito, J., Effect of Polyether Components on Surface Composition and Blood Compatibility of Polyurethanes, *Nippon Kagaku Kaishi* **6**, 1293-1301, 1985

POLYMER SURFACE DYNAMICS

Edited by
J. D. Andrade
The University of Utah
Salt Lake City, Utah

1988

PLENUM PRESS • NEW YORK AND LONDON

ERRATUM

Surface Characterization of Biomaterials, edited by B.D. Ratner

Pages 255–269: Surface Analysis of polyether and polysiloxane soft segment polyurethanes, by K.G. Tingey, J.D. Andrade, R.J. Zdrahala, K.K. Chittur and R.M. Gendreau.

1. p. 256, line 25, correct to "composed of 15% and 5% 1000"
2. p. 258, Table 1, in column labeled

	ESCA C-O/N
Biomer	19
Pellethane	8

3. p. 259, equation 1 second line should read

$$+\lambda^2\sin^2\theta\frac{N_2-N_1}{x_2-x_1}\ [\exp(-x_1/\lambda\sin\theta)-\exp(-x_2/\sin\theta)] \quad (1)$$

4. p. 265, Figure 5
   Theta identified on the left (advancing) portion of the figure should be corrected to be the complement of the indicated angle.
5. p. 266, line 12 omit "PEO matrix or"
   line 18 correct to "concentration of hard segment"
6. p. 267, Figure 6, model of U/S-2
   Remove PEO soft segment domains

Surface Characterization of Biomaterials, edited by B.D. Ratner
Elsevier Science Publishers B.V., Amsterdam, 1988 — Printed in The Netherlands

SURFACE ANALYSIS OF POLYETHER AND POLYSILOXANE SOFT SEGMENT POLYURETHANES

K.G. Tingey[1], J.D. Andrade[1], R.J. Zdrahala[2], K.K. Chittur[3], R.M. Gendreau[3]
[1]Dept. of Bioengineering, University of Utah, Salt Lake, Utah, 84112
[2]Becton Dickinson Polymer Research, 11125 Yankee, Dayton, OH, 45401
[3]National Center for Biomedical Infrared Spectroscopy, Battelle, 505 King Ave, Columbus, OH 43201-2693

SUMMARY

Surface analysis of commercial biomedical polyurethanes, including Pellethane®, Mitrathane®, Biomer®, Cardiothane®, Cardiomat® and Vialon® formulations with polyethylene oxide, poly (tetramethylene oxide), and silicone containing soft segments, have been conducted to evaluate surface reorientation, phase partitioning, and heterogeneity. Analysis of polyurethane films has included the Wilhelmy Plate technique for measuring dynamic contact angles, fixed angle and variable angle X-ray photoelectron spectroscopy, and Fourier transform infrared spectroscopy with attenuated total reflectance optics. These results may be used to indicate reorientation of separated microphase domains in segmented polyurethanes upon exposure to differing environments. Evidence is presented showing the heterogeneity of phases at the surface. Compositional differences between the surface and the bulk, a reflection of preferential surface phase partitioning are presented. Models of the polyurethanes studied are presented, which indicate significant variation in surface composition, morphology, and dynamic character.

INTRODUCTION

Segmented polyurethanes (SPUs), due in part to microphase separation of hard and soft segment components, exhibit unique bulk and surface properties. Slight variations in synthesis technique, chemical composition, or processing lead to variations in the chemical and morphological properties of polyurethanes (refs. 1-5). The properties of the surface relative to the bulk may also vary (refs. 6-8). The phase separation observed in polyurethanes may affect the thromboresistance in blood contacting applications (ref. 9). Hypotheses regarding blood compatibility as a function of dispersive and polar components of the solid surface tension (ref. 10), heterogeneous microphase separated surface structure (ref. 11) and possible complete dominance of soft-segment overlayers at the surface (ref. 12,13) indicate the importance and relevance of characterization of the surface of biomedical polyurethanes.

The soft segment of SPUs is considered quite mobile and this matrix mobility allows the two phases to move relative to one another. This may account for the dynamic behavior observed in polyurethane surfaces, leading to the confusion regarding the mechanism of polyurethane biocompatibility. The more hydrophobic soft segment matrix would tend to dominate in vacuum or air, and recede slightly to expose hydrophilic hard segment domains at a SPU-water interface. The driving force is minimization of interfacial free energy. This dynamic character complicates the surface characterization of SPUs.

EXPERIMENTAL

Sample Preparation

This study involves characterization of commercial SPUs with largely proprietary compositions. Although starting composition information is unavailable we can categorize the SPUs into 3 general groups. Biomer®(Ethicon Inc.) and Mitrathane®(Mitral Medical International Inc.) are considered to be of similar formulation composed of methylene bis(p-phenyl isocyanate) (MDI) with a diamine chain extended hard segment and a polyether soft segment of undefined molecular weight. These are frequently referred to as polyurethaneureas(SPUUs). Cardiomat® (Kontron), Pellethane® (Upjohn Co.) and Vialon® 510X (Becton Dickinson Polymer Research) are similar using MDI with a butanediol chain extender as hard segment and a soft segment composed of polytetramethylene oxide (PTMO). The Vialon® H/H (Becton Dickinson Polymer Research) series differs from the Vialon® 510X series only by substituting portions of PTMO with polyethylene oxide (PEO) varying from 0 to 100%. The Vialon® U/S series has polydimethylsiloxane (PDMSO) components coupled with the ether portion of the soft segment in various molecular weights or concentrations. Cardiothane® 51 (Kontron), also a diol extended PDMSO soft segment urethane, is also included in this study.

The Vialon® films were received from Becton Dickinson as sealed extruded ribbons and analyzed with no additional preparation. Four different types of Vialon® 510X were studied, differentiated as 510X-45, -55, -65, and -75, in which the suffix distinguishes the Shore D hardness of the composition (ref. 14). The H/H polymers are based on a hard segment concentration of 55%, composed of MDI chain extended with butanediol. The soft segment is composed of varying ratios of PTMO of molecular weight 1000 and PEO of molecular weight 1450. H/H-1 corresponds to a soft segment of 100% PTMO, H/H-5 is based on 100% PEO, and H/H-9 and H/H-10 are based on 2:1 and 1:2 PTMO:PEO ratios, respectively. The U/S polymers are based on a hard segment concentration of 50%. The U/S-1 and U/S-7 soft segment is composed of 5% and 15% 1000 molecular weight PDMSO, respectively, in a block copolymer with polyethylene oxide (PEO). The U/S-2 and U/S-3 samples are also 5% and 15% of ABA block copolymer of 3000 molecular weight. The A block is 25% as large as the B block and is composed of polypropylene oxide (PPO) with a B block of PDMSO. The U/S-4 sample PDMSO soft segment is 1000 molecular weight and is terminated with single molecules of ethylene oxide.

Additional samples of commercial polyurethanes include Biomer® (20wt% in DMAC), Pellethane® 2363-90AE, Mitrathane® M2007 (25 wt% in DMAC), Cardiothane 51 (15 wt% in 2:1 tetrahydrofuran (THF): dioxane) and Cardiomat 610 (15 wt% in 2:1 THF: dioxane). Biomer® and Mitrathane® solutions were diluted with reagent grade N,N-dimethylacetamide(DMAC) to 3% polymer solutions. Pellethane® was dissolved in reagent N,N-dimethylformamide (DMF) to form 3% solutions. Cardiomat and Cardiothane were diluted with 2;1 ratios of THF: dioxane to 1% solutions. All solution cast films were dip cast using techniques previously described (ref. 15).

Instrumental Analysis

Contact angle analysis was performed using the Wilhelmy plate technique and fixed angle XPS measurements were made as described previously by the authors (ref. 15) Variable angle ESCA was performed on the Hewlett Packard 5950B monochromatic X-ray photoelectron spectrometer with variable angle probe as described previously (ref. 16). Take off angles are expressed as the angle subtended by the sample film plane and the detector central axis--that is the smallest effective penetration depths will correspond to low angles. XPS spectra were collected at angles from 8 to 75°.

FT-IR analysis was performed on a Digilab FTS-15 spectrometer in the ATR mode. A 1% polymer solution was used to spin cast films onto 45° germanium flow cell crystals as described by Gendreau (ref. 18). The films were cast and cured for 12 hours at 20 inches of mercury vacuum at 65°C. Prior to IR analysis the films were allowed to equilibrate to room conditions for at least 2 hours. Spectra were collected as 2000 coadded scans at 2 wave number resolution. After suitable dry blanks were collected, water was permitted to flow at 25 ml/sec over the cast film. Water subtraction factors were calculated by comparing hydrated film water band intensities to dry blanks.

RESULTS

ESCA Results

The relative concentrations derived from quantitative X-ray photoelectron spectroscopy of carbon, nitrogen and oxygen in their molecular environments are reported in Table 1. Spectra from different samples of a single lot revealed concentration variations of less than 2%. Aliphatic, ether, and carbamate carbon, as well as oxygen, and nitrogen, were quantitated for all polyurethanes studied. The ether carbon to nitrogen ratios were determined to establish a surface soft to hard segment relationship. Also in Table 1, theoretical bulk ether carbon to nitrogen ratios are reported, where possible. These data originate from manufacturer supplied monomer ratios. The experimentally derived surface ether carbon to nitrogen ratio also is calculated and the comparison of theoretical and experimental ratios results in a surface enhancement index which acts as a measure of the partitioning of soft segment ether carbon at the surface relative to the bulk.

Biomer® and Mitrathane®, both diamine chain extended SPUs, show significantly lower nitrogen and carbamate carbon concentrations than the diol extended SPU samples. This indicates that the nitrogen containing hard segment may be partitioned away from the surface and suggests that the diamine extended SPUUs are more phase separated relative to diol

TABLE 1

Relative surface concentration from ESCA

Polymer	C-H	C-O	O=C-N	N	O	Si	Theory C-O / N	ESCA C-O / N	Enhance. Soft seg. to Hard	%PEO
Biomer	47	26	0.75	1.4	19	5.7	---	34	---	
Mitra.	43	31	0.65	1.5	20	4.0	---	21	---	
Cardiomat	48	26	1.40	2.3	19	4.0	---	11	---	
Pelleth.	51	23	1.43	2.8	18	3.7	---	16	---	
510X-45	50	27	2.00	1.6	18	2.6	5.2	16	3.1	
-55	48	26	1.80	2.1	19	4.1	4.2	14	3.3	
-65	49	29	2.40	2.7	17	0.0	3.1	11	3.5	
-75	48	28	2.40	3.3	18	0.0	2.0	9	4.5	
H/H -1	46	32	1.50	3.0	18	0.0	3.1	11	3.5	0
-9	40	32	1.70	2.8	22	2.4	4.0	11	2.8	33
-10	39	33	1.70	2.7	22	2.8	4.9	12	2.	66
-5	28	38	2.40	3.0	26	3.0	5.8	13	2.2	100
U/S -1	43	17	1.10	2.1	24	12.2	4.9	8	1.6	
-7	42	24	1.40	2.1	23	8.1	4.7	11	2.3	
-2	48	17	0.40	0.9	25	9.6	4.8	18	3.8	
-3	37	27	0.00	0.0	25	10.7	4.4	0	0	
Cardiothane	49	6	0.00	0.0	23	22.7	---	0	---	

extended SPUs, allowing the hard segment to move somewhat independently of the soft segment. The ability of the PDMSO to migrate to the surface of polyurethanes has been reported (ref. 18) and is apparent in our data. Cardiothane XPS data is essentially stoichiometric PDMSO, indicating that at least the top 50 angstroms is dominated by PDMSO. The U/S-2 and U/S-3 samples also indicate little if any hard segment at the surface.

The similarity in composition between Pellethane®, Cardiomat®, and the Vialon® 510X series SPUs is manifest in ESCA data. The Vialon 510X polymers, which increase in bulk hard segment from -45 to -75, show a relative consistency of surface molecular concentration. This may be indicative of a minimization of surface free energy at an optimal surface composition.

Variable Angle XPS

Variable angle data was collected for Vialon® 510x-45 and Vialon® H/H-9 PEO/PTMO SPU. Figure 1 presents the adjusted ratio of hard segment nitrogen to soft segment ether carbon as a function of take-off angle. It is clear that a strong partitioning of soft segment occurs toward the surface, in agreement with the work of Ratner (ref. 6). The calculated bulk hard segment nitrogen to soft segment ether carbon are presented to indicate phase partitioning.

Using the algorithm of Paynter (ref. 19), a simple model of the phases, their dimensions and their relative concentrations, is postulated. The theoretical molecular electron intensities were computed based on an overlayer model (refs. 19-20). The model is characterized as having 2 gradient concentration regions separated by a constant region and surrounded by a constant overlayer region at the surface, and one into the polymer, representative of the bulk.

The intensity ratios are back calculated from assumed profiles based upon physical and chemical realities of the system as shown in equation (1):

$$I(\theta) \propto N_1\lambda\sin\theta + \lambda^2\sin^2\theta \frac{N_4 - N_3}{x_4 - x_3}\left[\exp(-x_3/\lambda\sin\theta) - \exp(-x_4/\lambda\sin\theta)\right] + \frac{N_2 - N_1}{x_2 - x_1}\left[\exp(-x_1/\lambda\sin\theta) - \exp(-x_2/\lambda\sin\theta)\right] \quad (1)$$

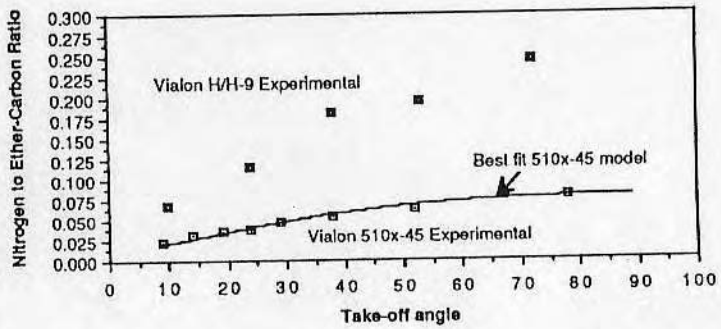

Figure 1 Variable angle XPS data for Vialon 510X-45 and H/H-9 polyurethanes. The best fit of the data based on the Paynter algorithm is displayed for Vialon 510X-45.

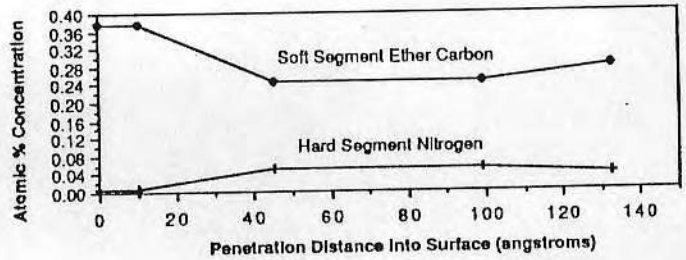

Figure 2 Best fit parameters against the experimental data for Vialon 510X-45. The atom% concentrations of ether carbon (above) and nitrogen (below) and their variation with depth are shown.

The mean free paths (λ) were calculated by the method of Ashley (ref. 21). N_i, x_i, and θ_i are the component concentration, polymer depth, and take-off angle, respectively, based on the assumed profile model. Figure 2 displays the best fit from several assumed polymer profiles for

these SPUs. Applying trial and error methods alone the best fit suggests that only small amounts of hard segment are present at the surface in this vacuum environment.

Contact Angle

Contact angle data allows one to monitor the energetics of the true surface layer and explore the potential of dynamic phenomena. The hysteresis observed is considered to be indicative, in part, of short time scale surface transitions, roughness, and surface heterogeneity. Both advancing and receding contact angles were determined from hysteresis loops. Variation in a single lot was observed to be less than 6% for most samples. Differences in surface energetics suggest differences in constant or dynamic composition. Table 2 tabulates the contact angles of the as received commercial polyetherurethanes.

It should be noted that Biomer® and Mitrathane® exhibit very high advancing and low receding contact angles. The hysteresis suggests that either short time scale molecular orientations are occurring as the surface environment changes or that heterogeneities exist at the surface. This may signify some combination of greater degrees of phase separation and concomitant phase mobility or surface phase enhancement, surface heterogeneity, surface or leachable impurity or surface roughness--all parameters determining the contact angle.

Table 2
As received polyurethane contact angle data

Polyurethane	Øadv	Ørec	Hysteresis
Biomer	102	26	76
Mitrathane	93	45	48
Cardiomat	88	42	46
Pellethane	88	50	38
Vialon® 510X-45	87	51	36
510X-55	86	50	30
510X-65	82	51	31
510X-75	87	51	36
Vialon® PTMO H/H-1	82	51	31
33% PEO H/H-9	79	33	46
66% PEO H/H-10	71	31	40
PEO H/H-5	55	30	25
Vialon® PDMSO U/S-1	99	53	44
U/S-7	101	54	47
U/S-2	79	55	24
U/S-3	62	62	0
U/S-4	105	63	42
Cardiothane	115	57	58

Since the bulk compositions of Pellethane® and Vialon® 510X PEUs are similar, it is not surprising that their contact angle data correspond quite closely. ESCA surface composition data is also very similar, indicating comparable compositional surface properties. The

advancing and receding contact angles are seen to be quite intermediate with a relatively low degree of hysteresis. This may indicate that phase mobility properties, a function in part of morphology, are also quite similar for Pellethane® and Vialon.® The difference observed between these polymers and Biomer® and Mitrathane® (diamine extended polymers) suggest that the two butane diol extended polymers are less phase separated or have a less mobile surface composition.

Contact angle data of the PDMSO-containing SPUs reveals a stronger correlation with the type of soft segment than to the amount of PDMSO in the soft segment. This emphasizes the importance of considering the entire chemistry of the soft segment and not assuming that PDMSO will predominate regardless of soft segment linkage type. The Cardiothane 51 advancing contact angle value is consistent with the fixed angle XPS data, indicating that PDMSO dominates at the surface, presenting a very hydrophobic surface. U/S-2 and U/S-3 samples containing long PDMSO segments reveal surprisingly low advancing contact angles relative to the US-1 and US-7 samples with smaller molecular weight PDMSO soft segment blocks. Apparently the PPO linkages play an important role in determining the surface energetics. The fact that no hysteresis is observed in the U/S-3 sample indicates that the surface must be neither rough, heterogeneous, nor subject to reorientation. The XPS data gives strong reason to believe that large amounts of PPO and PDMSO are present at the surface. This suggests that a homogeneous mixture of PPO and PDMSO dominate at the surface and that microdomains are smaller than 50-100 angstroms in diameter, a proposed dimensional microdomain limit to distinguish multiphase character with contact angle techniques (ref. 22).

Preliminary hydration studies of these SPU films indicate that both the advancing and receding contact angle decrease with increasing hydration. Figure 3 presents part of this data and demonstrates that long time-scale reorientation may take place to present a more hydrophilic surface. Ruckenstein and Gourisankar (ref. 23) and Okawa (ref. 24) show that the contact angle of a solid surface varies as a function of its environmental fluid and that dynamic restructuring and reorientation may take place over time. Calculations relating water absorption to contact angle of a multicomponent surface, assuming no surface deficiency or excess, indicate that absorption may contribute to advancing contact angle changes but can not account totally for the effect (ref. 15).

FTIR ANALYSIS

Infrared spectra of Biomer and Vialon H/H-5 were collected in dry and hydrated environments. Preliminary spectra of dry and hydrated samples are shown below in Figure 4 and reveal spectral changes. The spectral variations may be interpreted as chemical changes in the polymer upon water exposure. Spectral signals can be separated into hard and soft segment bands. The hard segment bands monitored include the 1700/1730 wavenumber bonded/non-bonded carbonyl stretch, the 1527 C-N stretch/N-H bend, and the 1080 ester linked

ether stretch. The soft segment bands observed include 2850-2920 and 1430-1480 C-H stretch and the 1110 aliphatic linked ether stretch. Figure 4 shows the dry H/H-5 FTIR ATR spectrum and the resultant difference spectrum when compared with the polymer after 2 hours of water hydration.

Spectral analysis of the changes in the polymer suggest that some reorientation does take place and that most reorientation occurs in the first hour. The PEO containing H/H-5

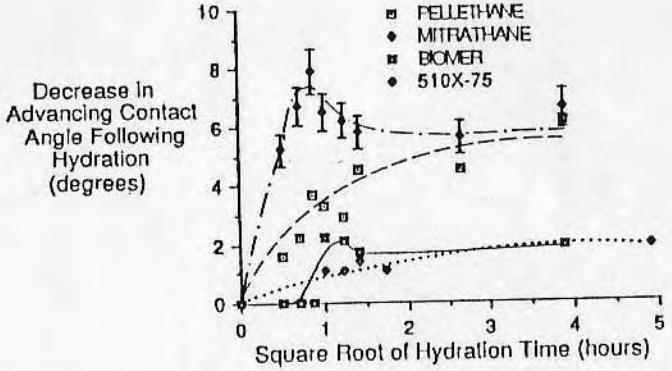

Figure 3 Decrease in advancing contact angle of various PEUs with hydration time. Error bars shown for Mitrathane® are representative for all samples shown. From ref 15 with permission of author and Plenum Press.

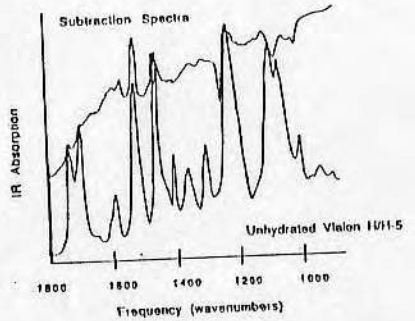

Figure 4 Dry H/H-5 polyurethane and its difference spectrum upon comparison with the hydrated polymer.

polymer shows much more dramatic soft segment spectral changes than does Biomer, which contains the PTMEG soft segment. The hard segment also appears more stable in Biomer, consistant with the higher stability observed with SPUUs.

Although this data is still preliminary and more complete FTIR analysis of hydrated polyurethane films is continuing, it is evident that chemical or physical changes do occur upon hydration of dry polyurethane films. ATR-FTIR is at best subsurface sensitive, however, it is reasonable to believe that the solution interfacing surface may change significantly in response to its environment.

Water subtraction from the hydrated polymer spectra is somewhat subjective although an error analysis of the major bands of interest in this study revealed that a large deviation in the water subtraction factor, led to variations in band intensity, width and position of less than 2%.

DISCUSSION

Surface Partitioning

Surface partitioning can best be investigated by variable angle ESCA, although reasonable quantitation of soft to hard segment concentration in the upper 100 angstroms of material may be represented as the ether carbon to nitrogen ratio from fixed angle ESCA. The ESCA results for Vialon 510X-45 through -75 indicate a correlation between increasing hydrophobic soft segment surface enhancement with hardness or phase separation. Similarly the H/H results lead to a correlation with increasing PTMO composition in the soft segment suggesting that phase separation yields greater phase mobility . The relationships between hardness, phase separation, and phase mobility have been previously discussed (ref.15).

These correlations indicate that phase compatibility and hardness, a function of hard segment concentration and phase separation, have a strong effect on surface enhancement of soft segment material in a vacuum environment. The data suggests that as phase separation decreases, surface/bulk enhancement of polyether soft segment also decreases. These two examples of surface enhancement of the soft segment phase argue that apparent surface structure and phase dynamics may be governed by controlling the compatibility of the phases through selection of relative hard and soft segment concentrations, surface energetics, and solubility parameters.

To an even greater extent the variable angle XPS data maps the partitioning of soft segment toward the surface. It should be noted how dramatically the profiles differ between the two samples analyzed. The H/H-9 sample approaches the bulk concentration much more rapidly than does the 510X-45 indicating a greater propensity for partitioning in the two phase Vialon 510X series under a vacuum environment. This may be explained by considering interfacial energetics and the incompatibility of the phases present in the polymers. The Vialon 510X-45 will tend to present the hydrophobic soft segment to the surface to minimize interfacial free energy. The H/H-9 soft segment is composed partially of hydrophilic PEO linked with the more hydrophobic PTMO. The surface energy of the hard segment lies between that of the blocks of the soft segment. The competing surface free energy driving forces--one toward the

surface, one away from the surface -- will minimize the ability of the phases to partition more completely and the depth profile ratio of hard/soft segment phases will change more rapidly to accommodate the more disperse shallower hard segment. This is consistent with surface enhancement changing with increasing Shore hardness as argued above.

Surface Heterogeneity

Surface heterogeneity is thought to exist in highly phase separated systems. Some spectroscopic analyses of SPUs seem to indicate that polyurethane surfaces are completely dominated by a polyether soft segment overlayer (ref. 13). Muhmud et al. (ref. 25) have shown that as the average molecular weight of the soft segment increases the relative ratio of soft segment to hard segment at the surface increases and approaches infinity at soft segment molecular weights of about 4,500. This suggests that for intermediate molecular weight soft segments, surface heterogeneity does exist. Schwartz and Garoff (ref. 22) present a theoretical development that indicates the importance of patch size, shape, and relative position, in addition to surface coverage, in predicting wetting behavior. Their analysis suggests that hysteresis diminishes and perhaps vanishes for small patches at low surface concentration.

Johnson proposes that the major cause of hysteresis on optically smooth, non-deformable surfaces is surface heterogeneity. He modeled a heterogeneous surface and observed that contact angles and contact angle hysteresis vary with the surface coverage of low contact angle material (refs. 26, 27).

We have previously presented data for Vialon H/H polyethers which correlate well with Johnson's model for heterogeneous surfaces (ref. 15). The trend indicates that as the PEO/PTMO ratio increases only a slight change in contact angle is observed until quite large concentrations of PEO are present in the bulk. The receding contact angles conversely remain fairly constant until almost no PEO is present in the bulk. The previously discussed ESCA correlation of surface enhancement with per cent of hydrophilic soft segment, suggests lower phase separation at high PEO bulk concentrations and highly-phase separated, increasingly surface enhanced soft segment, at low PEO bulk concentrations. Because ESCA data shows that the concentration of soft segment does not decrease but remains constant, while the enhancement of soft segment decreases with decreasing PTMO, it may be interpreted that phase domains are becoming less well defined and smaller.

There is no direct and unique way to transform the variable angle XPS data to a concentration profile. The profile is consistent with the XPS data, but other assumed profiles might also be as suitable. It is clear that the most promising predicted models include non-trivial amounts of hard segment nitrogen at the surface. The small concentrations of nitrogen may be indicative of soluble hard segment in the soft segment phase rather than hard segment domains, although Knutson has pointed out that similar urethane-ureas are more well separated near the surface than in the bulk (ref. 4). It appears from this preliminary variable angle XPS data that high vacuum may inhibit surface heterogeneity but small amounts of the hard segment may exist despite strong soft segment surface partitioning.

Surface Phase Mobility

In a vacuum the surface environment is much different then in aqueous environments or even in ambient air conditions. If SPUs are truly dynamic then the surface we identify in a vacuum with XPS may be very different from the surface in water, where the polymer may reorient to minimize its interfacial free energy.

The advancing contact angle, which probes primarily the hydrophobic component of the surface, was shown to decrease upon hydration, suggesting that in water the high interfacial free energy between soft segment and water is unstable. This high interfacial free energy draws high energy hard segment to the surface, lowering the interfacial free energy. A schematic consistent with this hypothesis is shown below in Figure 5. As of yet no obvious correlations between contact angle change and composition have been made.

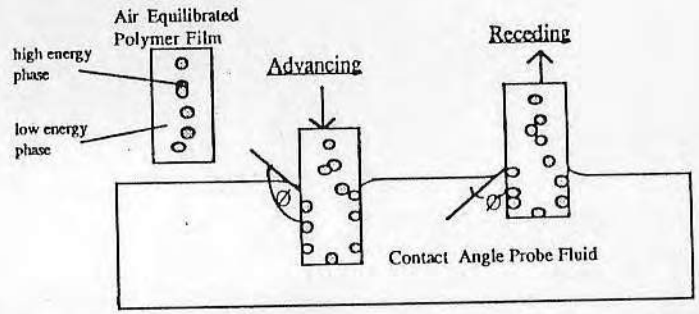

Figure 5 Wilhelmy Plate contact angle techniques to observe dynamic character of PEUs: hypothetical movement of phases with changing environment. From ref 15 with permission of author and Plenum Press.

The FTIR-ATR data previously presented shows spectral variations upon hydration. Although the data is preliminary it appears to indicate variations in the hydrophobic soft segment resulting in less exposed volume of the soft segment or purification of the interfacial region. Increased hard segment material at the surface is likely the effective result of soft segment aggregation upon wetting.

Polymer Surface Models

Although surface analytical data is still incomplete and multiphase polyurethane surfaces are very complex, compilation of the available information into surface models may aid

in future approaches to SPU surface characterization. Figure 6 attempts to illustrate model surface concentration and morphology consistent with our data thus far. An attempt has been made to differentiate wetted and dry polymer films which apparently is important to completely characterize the surface.

Cardiothane was shown to have a PDMSO overlayer but large hysteresis suggesting that side chain transitions may account for advancing and receding contact angle differences. U/S-3 was shown to have a mixture of PDMSO and aliphatic organic ether at the surface but no hysteresis was observed, suggesting that a homogeneous, multicomponent mixture of PPO and PDMSO exists at the surface and excludes most or all of the high energy PEO. The U/S-2 sample, similar to U/S-3 suggests similar surface properties, but the PDMSO-PPO soft segment block concentration is reduced and may not be able to completely exclude the higher energy PEO matrix or hard segment from the surface. The U/S-1 and U/S-7 samples appear to have similar properties which appear to be a function of both PDMSO side chain transitions, and either hard and soft segment surface components or phase transition upon environmental fluctuation.

The lower hysteresis and phase partitioning evident in the diol extended PTMO SPUs (Vialon 510X, Pellethane, H/H-1) suggests poorer phase separation and a small, but significant, concentration of soft segment at the surface under vacuum. Some soft segment unfolding may occur upon wetting to account for hysteresis effects in addition to the variable angle data, which indicates the existence of a two phase surface. The PEO soft segment SPUs appear to be morphologically very similar to the PTMO soft segment polymers. The data accumulated so far suggests that the urethane ureas (Biomer and Mitrathane) are better phase separated, and partition more strongly, but because they are poorly mixed they are mobile enough to cause hard segment phase exposure under aqueous environments. The model for PEO/PTMO soft segment mixtures appears to be a combination of the models for the pure PEO and PTMO soft segment polymers. The presence of all phases at the surface as seen with ESCA, and the large contact angle hysteresis indicate environmental restructuring.

CONCLUSIONS

Although additional analyses of these commercial SPUs is planned, a number of conclusions can be derived from the results to date. XPS data has shown an increased surface enhancement of soft segment for a more hydrophobic polyether, implying that minimization of surface free energy may be a driving force in surface phase segregation dynamics. Material properties that cause an increase in phase separation appear to permit greater phase mobility. Phase mobility is also suggested in contact angle studies which show that surface energetics change dramatically upon long and short time scale hydration and in FTIR analyses that reveal spectral changes on exposure to water.

Contact angle hysteresis, observed to be much greater for the diamine chain extended SPUs, suggests greater phase mobility for diamine extended systems than for diol extended systems. Advancing and receding contact angle data plotted against polyether composition

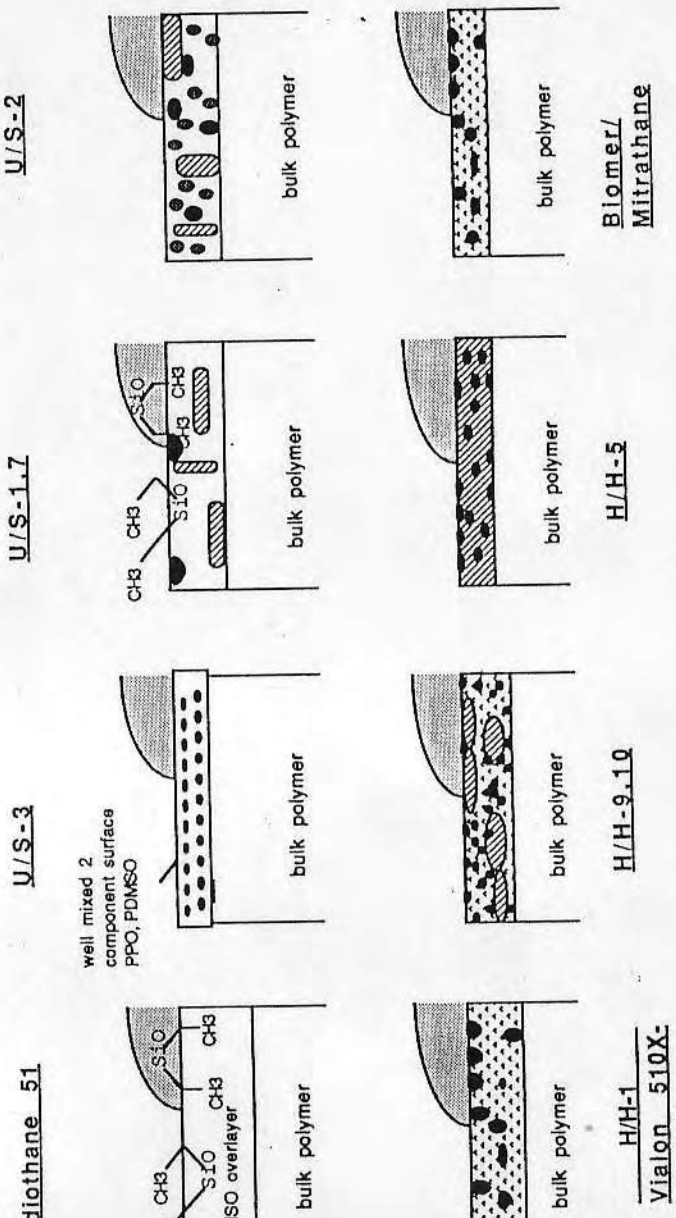

Figure 6. Surface models of sample SPUs based on XPS, contact angle, and FTIR-ATR, and their dynamic response to environmental changes.

corresponds to accepted models of surface heterogeneity, indicating that these SPU surfaces behave dynamically and suggesting that both polyether and diisocyanate-rich phases do indeed exist at the surface and respond to hydrophobic or hydrophilic environments. Variable angle XPS data also suggest that 2 phase surfaces do exist despite strong phase partitioning at the surface under vacuum.

ACKNOWLEDGMENTS

The work was supported by a grant from Becton Dickinson Polymer Research, and funding from the National Center for Biomedical Infrared Spectroscopy, grant RRO11367, originating from the division of Research Resources at NIH.

REFERENCES

1. Hu, C. B., Ward, R. S. Jr. A New Criterion of Phase Separation: The Effect of Diamine Chain Extenders on the Properties of Polyurethaneureas., Jl. Appl Polym. Sci 27, (1982) 2167-2177,
2. Takahara, A., Tashita, J., Kajiyama, T., Takayanagai, M., McKnight, W. J., Micro-phase Separated Structure and Blood Compatibility of Segmented Poly(urethaneureas) with Different Diamines in the Hard Segment. Polymer 26, (1985) 978,
3. Lin, S. B., Hwang, K. S., Tsay, S. Y., Cooper, S. L. Segmental Orientation Studies of Polyurethane Block Copolymers with Different Hard Segment Lengths and Distribution., Coll. Polym. Sci. 263, (1985) 128-140
4. Knutson, K. S., Lyman, D. J., The Effect of Polyether Segment Molecular Weight On the Bulk and Surface Morphologies of Copolyetherurethaneureas in: Cooper, S. L., Peppas M. A., (Eds.)Biomaterials-Interfacial Phenomona and Applications Adv. Chem. Ser. Vol. 199 , 1982 pp109-132
5. Zdrahala, R. J., Hager, S. L., Gerkin, R. M., Critchfield, F. E., Polyether Based Thermoplastic Polyurethanes. Effect of the Soft Segment Molecular Weight. Elastomers and Plastics 12, (1980) pp.225-244
6. Yoon, S. C., Ratner, B. D., Surface Structure of Segmented Polyetherurethanes and Polyetherurethaneureas with Various Perfluoro Chain Extenders. An X-Ray Photoelectron Spectroscopic Investigation., Macromolecules 19, (1986) 1068-1079
7. Lelah, M. D., Grasel, T. G., Pierce, J. A., Cooper, S. L., Ex Vivo Interactions and Surface Properties Relationships of Polyetherurethanes., J. Biomed. Mater. Res. 20, (1986) 433-468,
8. Takahara, A., Tashita, J., Kajiyama, T., Takayemaji, M, McKnight, W. J., Microphase Separated Structure, Surface Composition and Blood Compatibility of Segmented Poly(urethaneureas) With Various Soft Segment Components. Polymer 26, (1985) 987-996
9. Okano, T., Aoyagi, T., Kataoka, K., Abe, K., Sakurai, Y., Shimada, M., Shinohara, I., Hydrophilic-Hydrophobic Microdomain Surfaces Having An Ability to Suppress Platelet Aggregation and Their in vitro Antithrombogenicity, J. Biomed Mater. Res. 20, (1986) 919,
10. Baier, R. E., Applied Chemistry at Protein Interfaces., Adv. Chem. Ser. 145, (1975) 1
11. Aoguayi, T., Uruno, M., Akami, H., Shinohara, I., Okano, T., Kataoka, K., Sakurai, Y., Compatibility in Blood of Block Copolymers Having Microphase Separated Structure. Kobunshi Ronbunshu, 42, (1985) 647-54,
12. Yoon, S. C., Ratner, B. D., Thermal and Solvent Effects on the Surface Structure of Fluorinated Polyurethanes. in: Andrade, J. D., (Ed) Polymer Surface Dynamics Plenum , NY, 1988 in press
13. Ratner, B. D.,Paynter, R. W., Polyurethane Surfaces: The Importance of Molecular Weight Distributions, Bulk Chemistry and Casting Conditions, in: Planck, H., Egbers, G., Syre, R. (Eds.) Polyurethanes in Biomedical Engineering Elsevier Science Publishers, Amsterdam, 1984

14. Zdrahala, R.J., Solomon, D. D., Lentz, D. J., McGary, C. W. Jr., Thermoplastic Polyurethanes, Materials for Vascular Catheters in Progress in Biomedical Engineering Volume III, Polyurethanes in Biomedical Engineering, Elsevier Science Publishers, Amsterdam, 1987
15. Tingey, K.G., Andrade, J. D., McGary, C. W., Zadrahala, R. J., Surface Analysis of Commercial Biomedical Polyurethanes In: Andrade, J. D. (Ed) Polymer Surface Dynamics Plenum, NY, 1988 in press
16. Hansen, J., Ely, K., Horseley, D., Herron, J., Hlady, V., Andrade, J., The Adsorption of Lysozymes: A Model System, Mackromol Chem:Macromol Symp. In press
17. Gendreau, R. M., Biomedical Fourier Transform Infrared Spectroscopy: Equipment and Experimental Considerations in: R.M. Gendreau (Ed)Spectroscopy in the Biomedical Sciences CRC Press, Boca Raton FA 1986
18. Ward, R. S., White, K. A., Yilgor, I. Contact Angle Hysteresis of Polymers Modified with Surface Active Amphipathic Polymeric Additives Program and Abstracts of the 8th Rocky Mountain Regional ACS Meeting, Denver CO, June 1986
19. Paynter, R. W., Modification of the Beer-Lambert Equation for Application to Concentration Gradients, Ph.D. Thesis, University of Surrey, England, October, 1981: Surface Interface Analysis Vol. 3, 186-187
20. Andrade, J. D. X-Ray Photoelectron Spectroscopy in: Andrade, J. D. (Ed.) Surface and Interfacial Aspects of Biomedical Polymers 105-195 Plenum Press NY, 1985
21. Ashley, J. C., Simple Model for Electron Inelastic Mean Free Paths, J. Electron Spect. 28, (1982) 177-94
22. Schwartz, L. W., Garoff, S., Contact Angle Hysteresis on Heterogeneous Surfaces Langmuir 1, (1985) 219-230
23. Ruckenstein, E., Gourisankar, S. V., Enviromentally Induced Restructuring of Polymer Surfaces and Its Influence on their Wetting Characteristics In An Aqueous Environment. J. Coll. Interf. Sci. 107 (1985) 485-502
24. Okawa, A. The Hydration of Polymer Thin Films and Its Effect on Blood Compatibility Senior Thesis, Dept. of Materials Science and Engineering, University of Utah, 1983
25. Muhamud, N. A., Merrill, E. W., XPS Studies of Segmented Polyurethaneurea Surfaces Polym. Sci. Eng. 55 (1986) 751
26. Johnson, R. E., Dettre, R. H., Wettability and Contact Angles In: Matijevic, E. (Ed) Surface and Colloid Science Vol. Wiley Interscience, NY, 1969 pp. 2 85-154
27. Dettre, R. H., Johnson, R. E. Jr., Contact Angle Hysteresis IV. Contact Angle Measurements on Heterogeneous Surfaces J. Phys. Chem. 69 (1965) 1507

Probing Surface Microheterogeneity of Poly(ether urethanes) in an Aqueous Environment

K. G. Tingey* and J. D. Andrade

Department of Bioengineering, University of Utah, Salt Lake, Utah 84112

Received August 1, 1990. In Final Form: December 19, 1990

The morphology and microheterogeneous composition of polymeric surfaces partially determines their adsorption and absorption characteristics. The surface structure, often significantly different from that of the bulk, is influenced by the environment, and especially by the interfacial energetics of the surrounding medium. These effects result in dynamic properties with relaxation times that affect the sorptive properties of the materials. Microheterogeneity on surfaces has been shown to have significant effects on the biological interactions between synthetic materials and proteins and/or cells; however, the in situ surface character, which determines the blood compatibility of biomedical copolymers, has only recently come under investigation. The objective of this paper is to present a perspective view of several methods for the characterization of microheterogeneity of dynamic surfaces in an aqueous- or fluid-phase environment. This work focuses on the investigation of the dynamic properties of microheterogeneous biomedical polyurethanes, and on the characterization of these surfaces with novel spectroscopic, surface energetic, and surface imaging techniques. Contact angle, infrared spectroscopy, and inverse chromatography are used to characterize the surface reorientation and heterogeneous microphase nature of polyurethane surfaces. The polyurethanes studied are shown to have a multicomponent surface with detectable hard-segment domains. The chemical structure of the copolymers suggests that the material is composed of domains 150 Å in diameter. Evidence of these domains at the surface is presented. We have observed that the concentration of hard-segment surface groups, identified by the aromatic groups in the hard segment, varies as a function of polymer composition. The composition of surface hard segment is minimized with increasing phase purity, indicating the significance of morphology in determining surface composition of these polyurethanes and the ability of the surface to reorient in response to their environment. We have observed polyurethane surface structural rearrangements induced by hydration of the polymer film. These infrared and contact angle data indicate reorientation of the surface phase structure to enhance the surface concentration of the more polar phase in an aqueous environment. From these studies, structural models of selected polyurethane surfaces have been presented and additional analytical methods sensitive to in situ surface morphology have been proposed.

Introduction

Surface and interfacial properties significant in polymer materials development dictate the materials interaction with their environment and affect adhesion, diffusion and transport, and adsorption of molecules that interact with their surface. These general properties have applications in a broad spectrum of areas, including biomaterials, membranes, adhesives, chromatographic supports, composite materials, drug delivery systems, and other areas involving polymer-based materials. The morphology of polymers plays a significant role in determining the thermal and mechanical properties of the bulk material.

The surface composition and structure of polymeric materials may be very different from that of the bulk. Surfaces are known to concentrate surface-active molecules from the polymer bulk and from the air environment.[1] This tendency has been used to concentrate specifically targeted chemical species at the surface.[2] The ability of the surface to structure differently than the bulk can be an advantage if the surface dynamics can be predicted and controlled. Although the analytical tools used to study surface structure are different from those used to study bulk properties, the atomic and molecular composition of most surfaces can be routinely studied. Morphology studies of polymers having domains of the order of 50–250 Å, typical of polyurethane block copolymers, require indirect methods of characterization.

One additional complication in investigating low glass transition temperature polymeric materials is the ability of their surfaces to restructure in response to their environment. Under vacuum, a common environment for analysis of surfaces, apolar features tend to dominate at the surface. Many materials restructure to present a more hydrophobic surface under vacuum conditions. When that same surface is exposed to water, reduction of the interfacial free energy drives surface restructuring, and more polar species tend to be presented at the polymer surface. This restructuring has been observed as functional group rotations[3] or as hydrophilic phases partitioning toward the surface to replace or reduce regions of more apolar character.[4,5] Environmentally dependent surface reorientation requires appropriate tools for the study of surfaces in their in situ conformation.

The methods for characterization of surface structure in an aqueous environment are different from those used to study bulk composition. Table I outlines candidate analytical tools for evaluating aqueous surface structure. We have attempted to describe some of the key limitations of some of the most promising methods. The limiting factors include surface sensitivity, resolution in the lateral plane, quantitative nature of the method, and suitability to an aqueous environment.

* Present address: Becton Dickinson Vascular Access, Sandy, UT 84070.

(1) Ratner, B. D. In *Physicochemical Aspects of Polymer Surfaces*; Mittal, K. L., Ed.; Plenum: New York, 1983; Vol. 2, p 969.
(2) Ward, R. S. *Org. Coat.* 1980, *42*, 227.
(3) Good, R. J.; Kotsidas, E. D. *J. Colloid Interface Sci.* 1978, *66*, 360.
(4) Takahara, A.; Jo, J.-I.; Takamori, K.; Kajiyama, T. In *Progress in Biomedical Polymers*; Gebelein, C. G., Dunn, R., Eds.; Plenum: New York, 1989.
(5) Andrade, J. D. In *Polymer Surface Dynamics*; Andrade, J. D., Ed.; Plenum: New York, 1988; Chapter 1.

0743-7463/91/2407-2471$02.50/0

Table I. Analytical Methods and Their Limitations for Studying Microheterogeneity in an in Situ Environment

method	limitation
Quantitative	
computer simulation	atomic
AFM	molecular
electron microscopy	1–5%
ESCA	1–5%
infrared spectroscopy	1–20%
inverse chromatography	5–10%
contact angle	5–15%
fluorescence	semiquantitative
calorimetry	semiquantitative
in Water Analysis	
contact angle	yes
infrared spectroscopy	yes
inverse chromatography	yes
fluorescence	yes
AFM	yes
computer simulation	modeled
calorimetry	limited
electron microscopy	frozen/hydrated
ESCA	frozen/hydrated
Surface Sensitivity	
computer simulation	<1 Å
contact angle	5–10 Å
AFM	15–100 Å
fluorescence	20–50 Å
ESCA	20–50 Å
electron microscopy	20–50 Å
inverse chromatography	20–50 Å
calorimetry	~1000 Å
infrared spectroscopy	~1000 Å
Resolution in the Lateral Plane	
computer simulation	<1 Å
electron microscopy	10–100 Å
AFM	50–100 Å
fluorescence	100 Å
contact angle	1000 Å
infrared spectroscopy	50000 Å
ESCA	300000 Å
calorimetry	none
inverse chromatography	none

Contact angle hysteresis has been shown to be sensitive to surface[6] (1) composition, (2) mechanical modulus, (3) reorientation, (4) concentration of leachable components, (5) topography or roughness, and (6) microphase heterogeneity. Although these are all related to surface structure, it is difficult to sort out the specifics of the surface if only contact angle data are available.

Johnson and Dettre,[7] and Schwartz and Garoff[8] have described the capability of contact angle to evaluate surface heterogeneity. Electron microscopy has been used for several years to study polymer morphology and surface properties. Recently, significant progress in the analysis of block copolymer surface structure has been reported by Goodman et al.[9] Attenuated total reflectance Fourier transform infrared spectroscopy (ATR-FTIR) has been used by Knutson[10] and by Gardella[11] to study surface-related material phenomena. Calorimetry and other bulk characterization methods, such as dynamic mechanical analysis or nuclear magnetic resonance, can similarly be used to study surface phenomena.[12] By studying material property changes as a function of surface to bulk ratios, calorimetry, spectroscopy, and mechanical methods can be useful in studying surface structure. Although these methods are useful, they require particles of varying size. Inverse chromatography has been developed to study surface structure, particularly surface dispersive and acid–base character.[13] Inverse gas chromatography is sensitive to subtle surface changes such as those involving heterogeneity in a segmented copolymer. Application of inverse liquid chromatography extends the method into aqueous environments.[14] Fluorescence spectroscopy has been used to study surface structural phenomena. Sakashita[15] and Nishijima[16] have used intrinsic and extrinsic fluorescence probes in liquid environments to study copolymer and blend domain structure. Although electron spectroscopy for chemical analysis (ESCA), requires high-vacuum environments for analysis, methods are available to study hydrated polymer surfaces by freezing-in the polymer's hydrated structure.[4] Atomic force microscopy[17] and computer simulation of interacting molecules[18] are now becoming important tools in imaging and predicting polymer surface microheterogeneity.

We have been developing methods to evaluate polymer surface structure in an in situ aqueous environment. Polyurethanes are phase-separated block copolymers, which result in domains of the order of 50–250 Å in size. The glass transition temperature of one of the phases is usually below room temperature; such phases can, therefore, respond to changes in the environment. The structure of a typical polyurethane is presented in Figure 1. Polyurethanes have been popular candidate materials in several blood-contacting applications, and their good blood compatibility has been attributed to their multidomain structure interfacing with the multicomponent and multidomain structure of proteins and cells in blood.[19] Although they have presented correlations between bulk morphology and biocompatibility, definitive information on in situ surface structure is generally lacking. It is our goal to characterize polyurethane surface structures, to evaluate their dependence upon bulk properties and their local environment, and to determine the significant material properties controlling blood compatibility. In this paper we introduce our perspective of appropriate characterization of the microheterogeneity of dynamic surfaces. We present, herein, several methods that differentiate material structure in aqueous or dry environments. Additional methods now being developed will

(6) Andrade, J. D.; Smith, L. M.; Gregonis, D. F. In *Surface and Interfacial Aspects of Biomedical Polymers*; Andrade, J. D., Ed.; Plenum: New York, 1985; Chapter 7, p 249.
(7) (a) Johnson, R. E.; Dettre, R. H. *Surf. Colloid Sci.* **1969**, *2*, 85. (b) Dettre, R. H.; Johnson, R. E. *J. Phys. Chem.* **1965**, *69*, 1507.
(8) Schwartz, L. W.; Garoff, S. *Langmuir*, **1985**, *1*, 219.
(9) Goodman, S. L.; Li, C.; Pawley, J. B.; Cooper, S. L.; Albrecht, R. M. In *Surface Characterization of Biomaterials*; Ratner, B. D., Ed.; Elsevier: Amsterdam, 1988; p 281.
(10) Knutson, K. S.; Lyman, D. J. In *Biomaterials: Interfacial Phenomena and Applications*; Cooper, S. L., Peppas, M. A., Eds.; Advances in Chemistry 199; American Chemical Society: Washington DC, 1982; p 109.
(11) Gardella, J. A., Jr.; Vargo, T.-G.; Hook, T. J.; Grobe, G. L., III; Salvati, L., Jr.; Hautaniem, J. In *Surface Characterization of Biomaterials*; Ratner, B. D., Ed.; Elsevier: Amsterdam, 1988; p 145.
(12) Mackenzie, R. C.; Paterson, E.; Swaffield, R. *J. Therm. Anal.* **1981**, *22*, 269.
(13) (a) Suzuki, T.; Murakami, Y.; Immi, T.; Takegami, T. *Polym. J.* **1981**, *13*, 1027. (b) Bogue, D.; Gamet, D. L.; Schreiber, H. P. *J. Adhes.* **1986**, *20*, 15.
(14) Gao, S.; Qingfang, B. *J. Liq. Chromatogr.* **1989**, *12*, 2083.
(15) Sakashita, J.; Yamamoto, M.; Nishijima, Y. *Rep. Prog. Polym. Phys. Jpn.* **1985**, *28*, 457.
(16) Nishijima, Y.; Yamamoto, M.; Fujimoto, T.; Ito, S. *Rep. Prog. Polym. Phys. Jpn.* **1984**, *33*, 237.
(17) Albrecht, T. R. *J. Appl. Phys.* **1988**, *64*, 1178.
(18) (a) Mansfield, K. F.; Theodorou, D. N. *Polym. Prepr. (Am. Chem. Soc., Div. Polym. Chem.)* **1989**, *30*, 76. (b) Vaz, R. Presentation, Center for Biopolymers at Interfaces, University of Utah, April 1990.
(19) (a) Okano, T.; Aoyagi, T.; Kataoka, K.; Abe, K.; Sukurai, Y.; Shimada, M.; Shinohara, I. *J. Biomed. Mater. Res.* **1986**, *20*, 919. (b) Takahara, A.; Tashita, J.; Kajiyama, T.; Takayemaji, T.; McKnight, W. J. *Polymer* **1985**, *26*, 987.

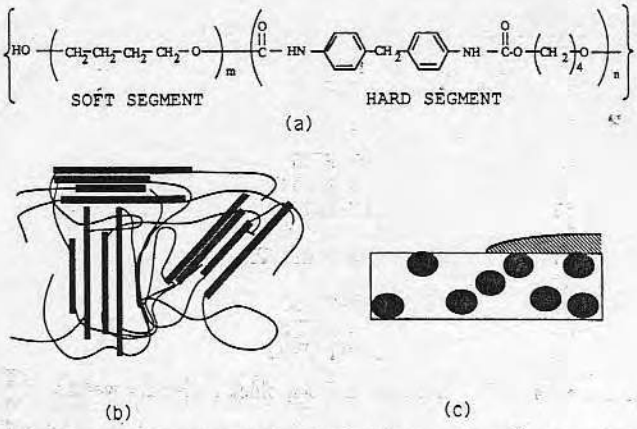

Figure 1. Polyurethane structure. (a) Primary chemical structure of poly(ether urethane). The polyether soft segment is enclosed in the left bracket and the polyurethane hard segment in the right bracket. (b) Phase separation of the blocks can result in some degree of ordering as domains of soft polyether (fine lines) and rigid polyurethane (heavy lines). (c) The macroscopic surface structure can be modeled as multiphases whose surface composition and morphology are chemically and environmentally dependent. Dark hard-segment domains and their shaded interphases are represented in a sea of continuous-phase soft segment. The effect of water on surface structure is represented under the cross-hatched region representing a water droplet on the upper right surface.

enhance our ability to characterize micromorphology in situ and are briefly discussed herein.

Early work on polyurethanes has lead to structural models of the polyurethane bulk.[20] Subsequent studies by Knutson and others suggest that composition and domain-phase purity at the surface are different from the bulk.[10] Polyurethane properties can be engineered by controlling the bulk structure through variations in monomer chemistry, block molecular weights, and processing parameters. Conflicting correlations of surface chemistry with interfacial response have been reported,[21] suggesting that more complete models of surface structure are required.

Matsuda[22] discussed the complexity of phase-separated block copolymers and their reorientation behavior as related to minimization of the interfacial free energy. He presented a thermodynamic criterion for surface enrichment in the two-phase polymer system. He demonstrated, using interfacial energies, that the phase with the lowest interfacial energy will spread over the second phase to minimize the free energy of the total system. As the environment at the surface changes, due, for example, to hydration or protein adsorption, the interfacial energy changes, subsequently driving a response in the polymer surface morphology. If the total surface interfacial energy is minimized by the spreading of the second phase, a change in surface composition will result.

We want to develop models of the surface of polyurethanes of varying composition and evaluate the interfacial response of the polymer as a function of bulk and surface structure.

Materials and Methods

Contact angle experiments were performed on a Wilhelmy Plate contact angle apparatus. Polymer films were prepared by extrusion through a ribbon die or spin cast onto clean glass cover slips. Several advancing and receding angles were measured on at least four samples of each material. The contact angles were measured as a function of hydration time. The samples were hydrated under static conditions and the water was changed prior to each measurement to reduce the possible effects of leachable contaminants or bacterial growth. Clean water was used as the probe fluid and changed after each sample was analyzed. In some cases, the samples were also dried under vacuum at room temperature to evaluate the reversibility of the system.

Infrared analyses of polyurethanes were performed at the Center for Biomedical Fourier Transform Infrared Spectroscopy (FTIR), Battelle, Columbus, OH.[23] Polyurethane films were spin cast from filtered 0.1% dimethylacetamide (DMAC) solutions onto germanium internal reflectance elements. Solvent evaporation and film curing were performed under 25-in. water vacuum at 60 °C for 12 h. The coated Ge crystals were analyzed in the Battelle attenuated total reflectance (ATR) FTIR flow cell previously described.[24] Reference spectra were collected with 4-cm^{-1} resolution in a Digilab 3200-60 spectrometer with a mercury–cadmium–telluride (MCT) detector. Subsequent spectra were collected under these conditions as 450–2000 coadded scans, depending on the desired rate of spectral accumulation. The films were exposed to water at flow rates of 15 mL/min for 5 h, followed by vacuum for 5 h; this cycle was repeated once. The water bands in the spectrum were individually and manually subtracted from each spectrum to form a flat base line in the region between 1600 and 1700 cm^{-1}. The spectral characteristics of the principal bands were determined from algorithms supplied from the Canadian Research Council.[25]

Inverse liquid chromatography was performed using a peristaltic pump to drive soluble synthetic peptide probes, in phosphate buffer, through an 85-mm-long column, 10 mm in diameter. The columns were packed with polyurethane particles dispersed in methanol, which was exchanged for phosphate buffer following column packing. Preparation of the polyurethane particles has been described.[26] Retention volumes were determined by monitoring fluid passage with an electronic mass balance and a differential refractometer (Waters Associates,R401). Peptide probes included tryptophan (Trp), phenylalanine (Phe), phenylalanine–tryptophan (Phe–Trp), and tryptophan–tryptophan (Trp–Trp) and were purchased from Sigma.

All of the noncommercial experimental resins were supplied by Becton Dickinson Polymer Research; the commercial resins (Biomer, Mitrathane, and Pellethane) were all supplied by other sources. Commercial as well as experimental polyurethanes are based on methyl diphenyl diisocyanate (MDI) hard segment. The experimental polyurethanes, designated with PU prefixes, were formed by one-step polymerization methods, resulting in a distribution of hard-segment block molecular weights. Chemical formulations of the polyurethanes studied are presented in Table II. Pellethane, Mitrathane, and Biomer are commercial polyurethanes whose compositions are mostly proprietary. Belisle et al. have published a comprehensive characterization of Biomer tht indicates that surface-active ingredients are present in Biomer and will effect its surface properties.[27] Commercial polyurethane compositional data indicated in Table II are based on observations reported by Lelah and Cooper.[28] The other polyurethanes used in our studies can be subdivided into three logical series:

In the first series, the bulk composition of the soft-segment polyether, was varied by changing the ratio of poly(ethylene oxide) (PEO) and poly(tetramethylene oxide) (PTMO) soft-segment blocks used in formulating the polyurethane. This series is designated as PU–PEO(X), where the variable X represents the

(20) Cooper, S. L.; Tobolksy, A. V. *J. Appl. Polym. Sci.* **1966**, *10*, 1837.
(21) (a) Hanson, S. R.; Harker, L. A.; Ratner, B. D.; Hoffman, A. S. *J. Lab. Clin. Med.* **1980**, *95*, 289. (b) Sa Da Costa, V.; Brier-Russell, D.; Salzman, E. W.; Merrill, E. W. *J. Colloid Interface Sci.* **1981**, *80*, 445.
(22) Matsuda, T.; Akutsu, T. *Org. Coat. Appl. Polym. Sci. Proc.* **1983**, *48*, 647.
(23) The Center for Biomedical Infrared Spectroscopy no longer exists and was dismantled in 1989.
(24) Gendreau, R. M. In *Spectroscopy in the Biomedical Sciences*; Gendreau, R. M., Ed.; CRC Press: Boca Raton, FL, 1986; Chapter 1.
(25) Cameron, D. G.; Kauppinen, J. K.; Moffatt, D. J.; Matsch, H. H. *Appl. Spectrosc.* **1982**, *36*, 245.
(26) Lambert, J. M. *Polym. Prepr. (Am. Chem. Soc., Div. Polym. Chem.)* **1989**, *30*, 583.
(27) Belisle, J.; Maier, S. K.; Tucker, J. A. *J. Biomed. Mater. Res.* **1985**, *24*, 15.
(28) Lelah, M. D.; Cooper, S. L. *Polyurethanes in Medicine*; CRC Press: Boca Raton, FL, 1986.

Table II. Polyurethane Compositions Studied[a]

polymer/form	extender	% hard segment	soft segment
biomer/commercial dispersion	diamine		PTMO
Mitrathane/commercial dispersion	diamine		PTMO
Pellethane/extrudable pellets	diol		PTMO
PU–PEO(100)/experimental film	diol	55	1450 PEO
PU–PEO(67)/experimental film	diol	55	67% 1450 PEO, 33% 1000 PTMO
PU–PEO(33)/experimental film	diol	55	33% 1450 PEO, 67% 1000 PTMO
PU–PTMO-1000/experimental film	diol	55	1000 PTMO
PU–FPTMO/experimental film	diol	35	1000 P(diF)TMO
PU/experimental film	diol	100	none
PU–PTMO-650 S/experimental beads	diol	65	650 PTMO
PU–PTMO-1000 S/experimental beads	diol	65	1000 PTMO
PU–PTMO-2900 S/experimental beads	diol	65	2900 PTMO

[a] Copolymer structure is related to the chemistry of the prepolymers, the percentage of each phase, and the block molecular weight.

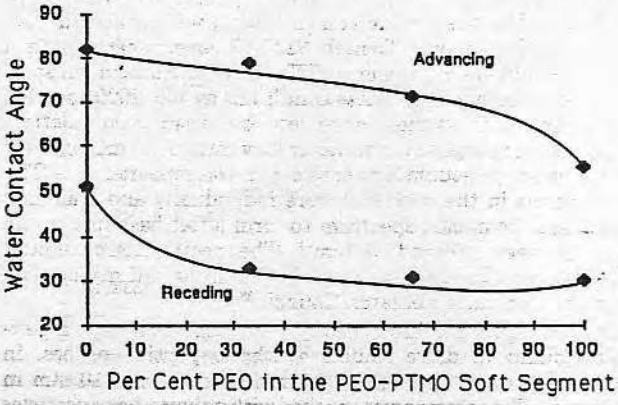

Figure 2. Wilhelmy Plate advancing and receding angles for samples PU–PTMO-1000, PU–PEO(33), PU–PEO(67), and PU–PEO(100).

percent of PEO in the soft-segment block of the copolymer. The polymer PU–PTMO-1000 is also a logical component of this series with no PEO in the soft segment. The -1000 suffix designates the molecular weight of the soft-segment PTMO block.

A second series of experimental urethanes were formed as particles in a suspension. These polymers are listed as PU–PTMO-*Y* S, where the variable *Y* is indicative of the PTMO block molecular weight, and the S indicates that the polymer was prepared by a suspension polymerization technique.[26] The molecular weight of the polyether in this series varies from 650 to 2900 amu.

The remaining polyurethanes listed in the table include a pure hard-segment urethane control containing no polyether (PU), and an interesting hydrophobic polyurethane composed of a fluorinated poly(tetramethylene oxide) with approximately two fluorine atoms on each tetramethylene oxide unit (PU–FPTMO). The sample PU–PTMO-1000 serves as a polyurethane control.

Results and Discussion

The contact angles of the hydrophobic and hydrophilic polyurethanes, made from a combination of PEO and PTMO, are plotted (Figure 2) as a function of bulk composition of the hydrophilic component of the soft-segment block. Advancing and receding angles are presented for each material. The contact angles do not appear to be linear with composition; the advancing angle appears to remain fairly constant up to very high concentrations of the hydrophilic phase, while the receding angle remains relatively constant up to very high concentrations of the hydrophobic phase. The data correspond well to the model developed by Johnson and Dettre[7] for heterogeneous surfaces. The more hydrophobic surface components act as pinning points for the advancing water causing high advancing angles representative of the hydrophobic phase. The hydrophilic phase acts as channels in which the water can recede, causing low receding angles, representative of the hydrophilic phase, even at high concentrations of hydrophobic phase. Interpretation of contact angle hysteresis is difficult because hysteresis originates from several different material phenomena, as previously discussed. The hysteresis observed for this series might be interpreted as restructuring of the soft-segment domains; however, contact angle changes observed in the hydration experiments, which are more indicative of reorientation, result in reorientation-induced contact angle value changes no greater than 15° over several hours. The hysteresis in these experiments, observed in a matter of minutes, is much larger, ranging from 35° to 52°. In this instance, therefore, hysteresis is attributed to morphology, where relaxation times are not a critical parameter and much larger contact angle values are not inconsistent with data accumulated in the hydration experiments. Much of the polyurethane literature indicates that a single phase predominates at the surface;[29] however, the data for these complex block copolymers, formed from three components, suggest that domains do indeed exist at the surface and are of sufficient size and concentration to be detected by contact angle measurements.

Table III. Equilibrium Contact Angle Variations between Dried and Hydrated Films and between Dried and Hydrated PU–FPTMO

(a) Dried and Hydrated Films

polymer	contact angle, deg: dry	contact angle, deg: wet	change, deg (±2°)
PU	86	82	4
PU–PTMO-1000	82	75	7
PU–PEO(100)	55	40	15
PU–PEO(33)	79	70	9
PU–FPTMO	129	119	10

(b) Hydration Cycling of PU–FPTMO

hydration state	contact angle, deg: adv (±1°)	contact angle, deg: rec (±1°)
cast, cured dry	129	38
equilibrium wetted	119	37
vacuum dried	124	39
equilibrium rewetted	119	39
vacuum redried	123	39

Contact angle analysis of additional polyurethane copolymers suggests that hydration of the copolymer causes surface structural rearrangement of the polar and nonpolar phases. Table IIIa shows advancing contact angle values for polyurethane formulations in "wetted" and "dried" states. The samples selected were chosen because of their similarity in structure and processing history. Because only the changes in the advancing angle, rather

(29) Ratner, B. D.; Yoon, S. C.; Kaul, A.; Rahman, R. In *Polyurethanes in Biomedical Engineering II*. Planck, H., Ed.; Elsevier: Amsterdam, 1987; p 213.

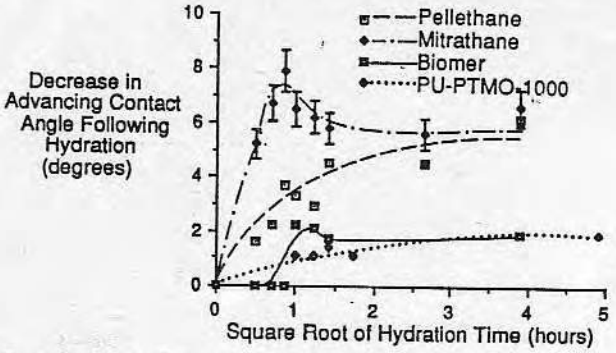

Figure 3. Time-dependent decrease in advancing contact angle of commercial polyurethanes. The error bars shown for Mitrathane are representative of the standard deviation in contact angle for all polymers presented.

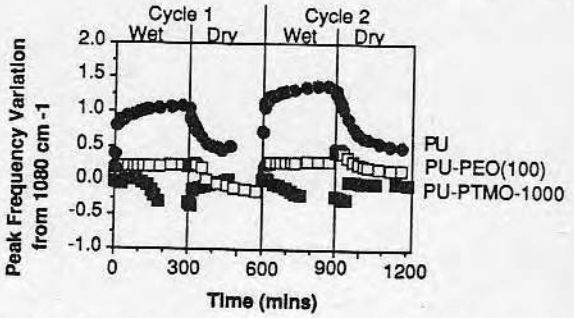

Figure 4. Change in the center of gravity calculated infrared absorption frequency at 1080 cm^{-1}, the ether stretch associated with the carbamate moiety. Closed circles represent hard-segment homopolymer PU. Open squares represent PU–PEO-(100). Closed squares represent PU–PTMO-1000.

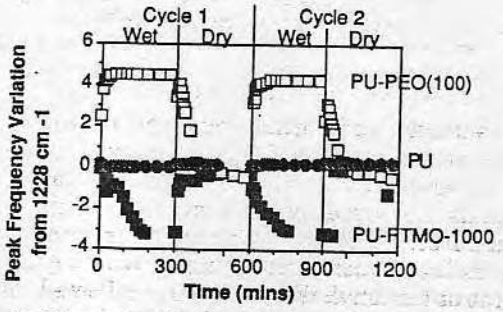

Figure 5. Change in the center of gravity calculated infrared absorption frequency at 1228 cm^{-1}, the C–N stretch associated with the hard segment. Closed circles represent hard-segment homopolymer, PU. Open squares represent PU–PEO(100). Closed squares represent PU–PTMO-1000.

than hysteresis, have been reported, the complications in interpretating hysteresis are removed. The data suggest that changes in surface chemistry are occurring upon hydration. Not surprisingly, the PU homopolymer, which is homogeneous on a molecular scale and could only respond structurally with side-chain rotations, shows little reduction in advancing contact angle. The phase-separated block copolymers show a larger decrease in the advancing angle. These polyurethanes are multiphase and can restructure at a larger scale to minimize interfacial energy. Table IIIb indicates the reversibility of the contact angle through several hydration–dehydration cycles, indicating that the phenomenon is not due to leachables or contaminants. There does appear to be a significant decrease in the dried advancing angle after the first hydration step. This suggests that the ability of the polymer film to restructure is dependent on processing conditions. The structure developed by dehydration will be different from the structure produced from solvent evaporation when the film was initially formed.

Figure 3 presents the contact angles of commercial diamine and experimental diol-extended polyurethanes as a function of hydration time. Hydration time is plotted as the square root of time. If linearity between contact angle and the square root of hydration time does exist, diffusion alone may account for variations in the contact angle. Although the scatter in the data makes curve fitting difficult, the curve shapes indicate that the change in the advancing angle must be attributed to more than only diffusion of water into the bulk. The decrease in the advancing contact angle as a function of hydration suggests an enhancement of the surface concentration of the hydrophilic hard segment, reducing the interfacial free energy of the film. The relative maxima in the Biomer and Mitrathane data are not yet explained, but may be related to a nonequilibrium "overshoot" in restructuring the surface. These samples are the diamine-extended polyurethanes, whose most distinguishing characteristic from the diol-extended polyurethanes (Pellethane and PU–PTMO-1000) is their more complete phase separation. We believe, therefore, that the small overshoot in the hydration time-dependent contact angle (Figure 3) is surface morphology related. These contact angle results are consistent with models of surface heterogeneity and with the multiphase nature of polyurethane surfaces. They also indicate that this multiphase structure is related to the environment and processing conditions of the material.

Infrared spectra of hydrated and dehydrated films were collected in the ATR mode. Figures 4 and 5 present the infrared spectral frequency shift of the 1080- (O=C—O—C stretch) and 1228-cm^{-1} (C—N stretch) hard-segment bands as a function of film hydration and dehydration for a model hard-segment homopolymer (PU), a hydrophobic polyether polyurethane (PU–PTMO-1000), and a hydrophilic polyether polyurethane (PU–PEO(100)). Because we anticipated that the spectral frequency changes would be subtle, polymers that were quite different in composition and structure were studied. Although the frequency shifts are small, the results are consistent and fairly reproducible from the first to the second cycle. Both bands presented are complex bands, and the specific interactions responsible for their frequency shifts are difficult to establish.[30] It should be noted, however, that the frequency shifts in both the C—N and O=C—O—C stretches of the hydrophilic and hydrophobic polyurethanes occur in opposite direactions upon wetting, indicating different responses to hydration.

The infrared response to hydration of the pure hard segment (PU) indicates little change in the C–N stretch, suggesting stable hydrogen bonding between the secondary amine and the carbonyl functionality of the homopolymer. However, the large variations in the carbamate ether stretch suggest hydrogen bonding of water with the free carboxy ethers.

The decrease in the spectral shifts of both the 1080- and 1228-cm^{-1} bands for the PU–PTMO-1000 copolymer suggests, respectively, a decrease in the hydrogen-bonding strength of the amine or carbonyl functionality and an increase in the hydrogen-bonding strength of the free carboxy. This suggests that the introduction of water to the hard-segment phase in PU–PTMO-1000 results in a partial breakdown and broadening of the hard-segment–soft-segment interphase. This broadening of the interphase may be attributed to structural accommodation of the polymer to allow soft segment to uncover the hard domains

(30) Ishihara, H.; Kimura, I.; Saito, K.; Ono, H. *J. Macromol. Sci., Phys., B* **1974**, *10*, 52.

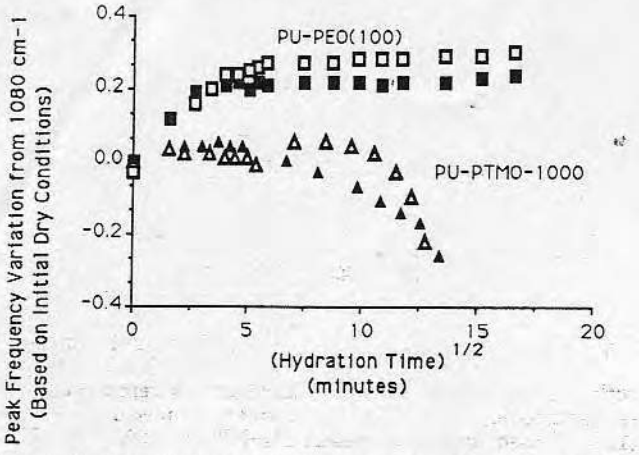

Figure 6. Change in the center of gravity frequency of the 1080-cm^{-1} band, the ether stretch associated with the carbamate moiety, plotted as a function of the square root of hydration time. The closed symbols represent the first hydration cycle and the open symbols represent the second cycle.

near the surface, exposing more of the polar hard-segment phase to minimize interfacial free energy.

The increases in the PU–PEO(100) spectral shifts of both bands are suggestive of a poorly organized hard-segment phase. The increase in the frequency of the C–N stretch indicates increased hydrogen bonding of either the amine or carbonyl. From the data collected thus far, we are unable to determine if this is indicative of improved inter- or intrachain hydrogen bonding, or if the shift to higher frequency is a result of water interaction with the amine and carbonyl functionality in the hard-segment block. These combined results indicate, however, that polymer restructuring is material dependent and suggest that surface restructuring of phases does occur in the case of the hydrophobic polyurethane, PU–PTMO-1000, and may also be occurring in the hydrophilic PEO polyurethanes.

Figure 6 presents the spectral shift of the 1080-cm^{-1} carbamate stretch for two hydration cycles as a function of the square root of time. The hard segment of the more hydrophilic polyurethane responds very rapidly and spectral changes occur linearly with the square root of hydration time until steady-state conditions become apparent. However, the more hydrophobic polyurethane spectrum is relatively unchanged for the initial 30 min and slowly begins to show spectral variations consistent with a diffusion-related phenomenon. We have interpreted this delay time as an indication of the reorientation of the surface-dominant hydrophobic phase to permit interaction of the water with the hydrophilic hard-segment domains. Once the hydrophilic hard-segment domains are exposed to the surface, the interaction of water with the hard phase results in a diffusion-controlled response. This further supports the interpretation of the specific band shifts in PU–PTMO-1000 as an indication of phase reorientation.

We have observed from the water contact angle and water hydration studies that the heterogeneity of the hard and soft phases of the polyurethane appears to vary as a function of their bulk composition. Initially, the more hydrophilic soft-segment materials contain higher surface concentrations of hard segment than the hydrophobic PTMO soft-segment materials. An increase in the concentration of the surface hard-segment domain is observed, however, upon hydration of the more hydrophobic polyurethanes.

Work is currently underway to evaluate the surface concentration of the hard-segment phase by studying the

Table IV. Retention of Peptide Probes Normalized to Water Retention in Polyurethane Inverse Liquid Chromatography Columns[a]

	peptide probe retention ratio			
polymer	Trp	Phe	Phe–Trp	Trp–Trp
PU–PTMO-650 S	1.0	1.0	1.1	1.5
PU–PTMO-1000 S	1.0	1.0	1.0	1.1
PU–PTMO-2900 S	1.0	1.0	1.1	1.3

[a] Increased peptide retention ratio correlates with the surface concentration of hard segment aromatic groups.

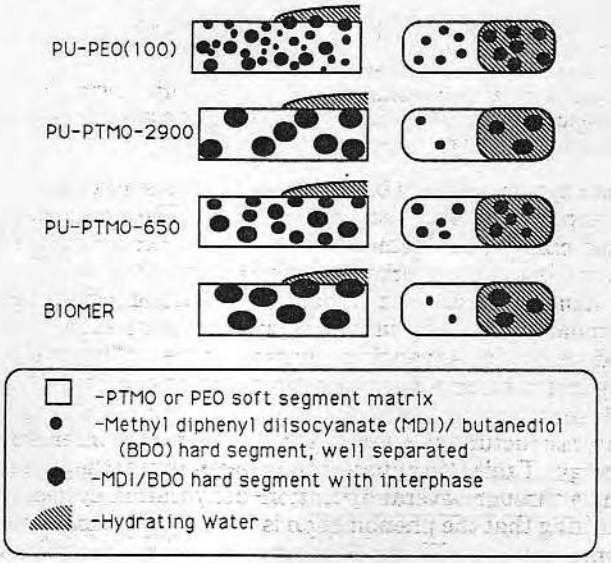

Figure 7. Polyurethane surface structural models, depth profile view on the left and surface view on the right. Scale would be approximately 500 × 1200 Å. Key: (a) PU–PEO(100). (b) PU–PTMO-2900. (c) PU–PTMO-650. (d) Biomer.

retention of aromatic peptide probes on chromatographic columns of polyurethane beads equilibrated in phosphate-buffered saline.[31] Inverse chromatographic analysis was performed on high surface area polyurethane particles, which is the uncharacterized stationary phase. It is probed with well-characterized peptides, which act as the mobile phase. The polyurethanes available in particle form were used in this study because of their high surface area to volume ratio. Peptide combinations of phenylalanine and tryptophan, amino acids containing conjugated unsaturation in their side chains, are introduced into the column as an aqueous solution. The retention of the probes relative to water indicate enhanced interaction of the peptide solute with the polyurethane stationary phase. The retention of probes designed to study charge transfer of aromatic species has been previously studied.[32] Studies confirming the specific interaction of the conjugated unsaturation in the amino acids with the aromatic groups of the hard segment are now underway. Table IV presents preliminary data and indicates that PU–PTMO-1000 S has the lowest interaction with the peptide probes. Differential scanning calorimetry has indicated that the high-temperature thermal transitions of PU–PTMO-1000 S are more similar to the pure hard-segment PU than any other polyurethane in the series.[33] This indicates that phase separation is optimized for the intermediate soft-segment block size. The low peptide retention times suggest that the concentration of the hard-segment aromatic groups is lower

(31) Sibrell, K.; Caldwell, K. D.; Andrade, J. D. Presented at the 63rd Colloid and Surface Science Symposium, Seattle, WA, 1989.
(32) Porath, J.; Caldwell, K. D. *J. Chromatogr.* 1977, *133*, 180.
(33) Sibrell, K.; Tingey, K. G.; Lambert, J. M.; Caldwell, K. D.; Andrade, J. D.; Solomon, D. D., in preparation.

than PU–PTMO-650 S, and PU–PTMO-2900 S in the surface layer. From this we conclude that the surface hard-segment concentration is minimized with hard-segment-phase purity. Additional inverse liquid chromatography studies are now underway to further investigate this phenomenon.

Based on these experiments and analyses, we have begun to develop models of both dry and wet polyurethane surfaces. We have characterized the vacuum surface composition of these surfaces by X-ray photoelectron spectroscopy. The bulk morphology has been investigated via differential scanning calorimetry. Surface energetics in air are being probed by use of inverse gas chromatography. Bulk composition has been quantitated by elemental analysis and transmission infrared techniques. These bulk properties and additional surface characterizations, important in developing the models, have been reported elsewhere.[33] Representative surface models of selected polyurethanes studied thus far are presented in Figure 7. In the figure the surface or top view is shown (right) as well as a cross section of the surface (left). A water droplet is shown in the figure to emphasize the significance of environmentally induced phase reorientation. The hydrophilic PEO polyurethanes are phase mixed and do not appear to differentiate much between water and air environments. The hydrophobic PTMO polyurethanes displayed in the figure do, however, reorient at the surface to minimize the interfacial free energy. The purity, size, and reorientation potential of the domains presented in the model vary with chemical composition.

We want to test the hypothesis that surface heterogeneity is important in determining the blood compatibility of phase-separated copolymers. The models of the multiphase nature of these complex surfaces have been important in interpreting what we have begun to learn about protein adsorption and platelet adhesion on these polyurethanes.[34] The domains of similar polyurethanes previously studied have been shown to be from 80 to 100 Å in diameter.[35] This is the same order of magnitude as typical protein domains composed of 100–150 amino acid residues, which result in domains of roughly 25 Å in diameter.[36] The polyurethane domains or the interphase regions separating the copolymer phases may accommodate the domain nature of adsorbed proteins. This accommodation of the protein at the surface may have little effect on the protein's native secondary or tertiary structure. In the adsorbed native or near-native state, the protein may be sufficiently unchanged so that the foreign body or coagulation responses initiated by proteins are not triggered. We have recently observed correlations between hard-segment-phase purity and protein adsorption.[34] These findings are in agreement with similar observations made by others.[37] This indicates the significance of surface morphology in interaction with biological media. Further investigations into in situ interfacial microheterogeneity of polymers will help us better understand these interfacial mechanisms and may lead to the ability to engineer complex polymers to achieve their desired surface properties.

(34) Tingey, K. G.; Sibrell, K.; Lambert, J. M.; Caldwell, K. D.; Andrade, J. D.; Solomon, D. D. *Transactions*, 17th Meeting of the Society for Biomaterials, 1991; p 83.

(35) (a) Ophir, Z.; Wilkes, G. L. *J. Polym. Sci., Polym. Phys. Ed.* **1980**, *18*, 1409. (b) Blackwell, J.; Lee, C. D. *J. Polym. Sci., Polym. Phys. Ed.* **1983**, *21*, 2169.

(36) Schulz, G. E.; Schirmer, R. H. *Principles of Protein Structure*; Springer Verlag: New York, 1979; p 87.

(37) (a) Takahara, A.; Tashita, J.-I.; Kajiyama, T.; Takayanagi, M.; MacKnight, W. J. *Polymer* **1985**, *26*, 978. (b) Grasel, T. G.; Cooper, S. L. *Biomaterials* **1986**, *7*, 315.

Future Work

ESCA analysis of frozen hydrated polyurethanes is being conducted to enhance the accuracy of our models. By freezing the hydrated sample to liquid nitrogen temperatures the structure of the hydrated surface will be "locked in". The surface water can be sublimed below the glass transition temperature of the polymer and the surface composition evaluated. We hope to observe the restructuring of the surface to the vacuum-equilibrated state by further increasing temperature above the glass transition temperature of the mobile phase.

Additional studies probing surface heterogeneity and domain size are now being developed in our laboratories utilizing fluorescence spectroscopy. Similar techniques have been previously utilized to study the bulk domain formation in random copolymers and blends.[15,16] The conjugated unsaturation in the hard-segment monomer leads to characteristic intrinsic fluorescence of the hard-segment phase. The fluorescence spectrum of the surface hard segment can be shifted relative to the bulk spectrum to give a measure of surface hard-segment concentration through selective adsorption of fluorescent probe molecules, which interact with the surface hard segment. These fluorescence studies should be useful in determining the surface hard-segment concentration and domain size. These experiments are only in preliminary stages, but we are hopeful that they will contribute to our understanding of the surface character of these complex segmented copolymers.

We are also attempting to apply computer simulation of these phase-separated systems to study the structural reorientation of the heterogeneous surface in the presence of a simulated field mimicking the dielectric character of water. A simulated domain matrix model of the copolymer can be developed by using the chemical structure of the molecule, its density, and the thermal properties that determine the mobility of the phases. We would like to investigate the uncovering of the hydrophilic phase upon introduction of simulated water, as suggested by the contact angle and infrared data discussed in this paper. The interaction between a model protein and homopolymers that model polyurethane phases has been studied with this technique. Vaz observed different degress of repulsion between the free protein and each of the two homopolymer phases,[18b] indicating that interactions of proteins may occur preferentially with one phase relative to the other. An understanding of dynamic surface structure may enable us to simulate dynamic protein–polymer surface interactions. This complex interaction between polymers and proteins may result in simultaneous polymer and protein structural reorientations, which may be partially responsible for their complex adsorption phenomena.

Summary

We have shown the applicability of contact angle, infrared spectroscopy, and inverse liquid chromatography for detecting the surface structure of polyurethanes. These techniques have all differentiated specific surface or material properties between the hydrated and dehydrated state of the material. We have shown that, although the concentration at the surface of the soft-segment phase is enhanced above its bulk concentration, these polyurethanes have multiphase surfaces with domains of sufficient size and concentration to be detected by contact angle methods. We have also shown that the surfaces of the polymers are dynamic in nature and respond to the environment by minimizing the surface free energy through

domain reorientation at the surface. The morphology of the multiphase structure, particularly hard-segment-phase purity, affects the ability of the polymer to reorient in response to environmental changes. We have developed surface composition and structural models of phase-separated polyurethanes to help us correlate protein and platelet interactions with these copolymer surfaces. Additional avenues have been proposed to further develop these models and to evaluate hypotheses relating surface structure and blood compatibility.

Acknowledgment. We acknowledge K. Sibrell and Dr. K. D. Caldwell for providing the unpublished inverse chromatography data. We acknowledge Dr. K. K. Chittur and the NIH Center for Biomedical Infrared Spectroscopy for their participation in the infrared analysis and for their financial support. We also acknowledge Drs. J. M. Lambert and D. D. Solomon and Becton Dickinson Polymer Research for supplying polymers and for providing financial support.

Registry No. Mitrathane, 97343-15-2.

Surface modification and evaluation of some commonly used catheter materials. I. Surface properties*

Philip M. Triolo† and Joseph D. Andrade‡
Department of Bioengineering, University of Utah, Salt Lake City, Utah 84112

Double catheter systems consisting of a stiff outer catheter and a flexible, buoyant, flow-directed, inner catheter which is often balloon-tipped have been employed with increasing frequency recently in both therapeutic and diagnostic procedures. Their use, however, has been restricted because of the excessive friction generated between the two catheters. In an attempt to decrease friction between polymers commonly used as catheter materials, oxidation of polyethylene, fluorinated ethylene–propylene copolymer, poly(vinyl chloride), silicone rubber, and polystyrene surfaces was induced by exposing the polymers to radio frequency glow discharge (RFGD) in a helium environment. All polymers were surface characterized utilizing x-ray photoelectron spectroscopy (XPS), scanning electron microscopy (SEM), and contact angle measurements before and after oxidation. This article describes the materials and methods used to fabricate and characterize the polymer surfaces and the results of the characterization. The results indicate that increases in oxygen concentration at the surface of the polymers and decreases in air–water contact angles occur with increased RFGD exposure time. Plateau values were usually obtained after 5–30 s exposure time, yet no apparent changes in surface topography were noted by scanning electron microscopy. The hydrophilic surfaces produced were stable for up to three months storage time in air.

INTRODUCTION

The use of catheters has gained widespread acceptance by the medical profession. Catheters are used frequently in such routine procedures as the delivery of intravenous fluids to and the removal of urine from compromised patients, and with increasing frequency in such complicated procedures as the compression of plaques in coronary arteries and the obstruction of blood flow to specific areas of the body. Catheters provide the pathway by which heretofore inaccessible body areas can be reached for both diagnostic and therapeutic procedures, thereby reducing the need for surgery. A modest review of some of the varied uses of catheters appears elsewhere.[1]

The more complicated catheter procedures often require the use of two-catheter systems. Their use has been restricted because of excessive friction

* Submitted by P. T. in partial fulfillment of the requirements for the M.S. degree in Bioengineering, University of Utah, Salt Lake City, UT 84112.
† Current address, Sorenson Research, 4455 Atherton Dr., Salt Lake City, UT 84107.
‡ To whom reprints and correspondence should be addressed.

Journal of Biomedical Materials Research, Vol. 17, 129–147 (1983)

CCC 0021-9304/83/010129-19$02.90

and power supply characteristics.[30] The electrode configuration and power supply characteristics are fixed for the equipment used in this study, a commercial Plasmod unit.* The temperature is primarily determined by other parameters (pressure, power). Therefore, the most easily altered variables are gas composition, pressure, and power. Discharge power affects the number of active species generated. The rate of weight loss of polymer films exposed to plasmas exhibits a marked dependence on power.[37] The intent of this study was to oxidize the polymer surface and yet keep weight loss or other potentially surface roughening effects to a minimum. Therefore, a low (15 W) power setting was chosen.

The flow rate of the system and, hence, the system pressure can be adjusted to the working pressure compatible with atomic lifetimes and mean free paths of the activated species.[30] Studies indicate that over a very limited low-pressure range [(1.2×10^{-12})–(4.6×10^{12}) μm Hg] plasma reactions proceed faster at lower pressures.[32] The lower the pressure, however, the greater the chance of sputtering SiO_2 off the glass walls of the chamber and onto the sample. A pressure of 200 μm Hg was found to result in a reaction rate that produced various degrees of oxidation of the test surfaces involved when the exposure time was varied from 5–300 s, yet no sputtering of SiO_2 onto the surfaces was revealed by x-ray photoelectron spectroscopy (XPS). Two hundred μm Hg pressure was used throughout this study.

Polymers

Catheters are most commonly fabricated from silicone rubber (SR), polyethylene (PE), poly(vinyl chloride) (PVC), and Teflon (fluorinated ethylene–propylene copolymer) (FEP). In addition polystyrene (PS) was included as a control.

Commercially available polymers usually contain plasticizers, fillers, and other additives in order to enhance their properties. In order to simplify the study, such additives were avoided wherever possible.

Until recently, most surface treatments of polymers were undertaken in hopes of improving their adhesion to other materials. In general, RFGD plasma treatment resulted in increased surface energy of the polymers, as indicated by increased wettability and decreased air–water contact angles. Also, oxidation of the polymers occurred even when the polymers were treated in inert atmospheres, most probably as a result of interaction with water vapor present as an impurity in the discharge chamber.[38]

A more detailed discussion of the surface treatment methods and their resultant effects on the surface properties of SR, PE, FEP, PS, and PVC has been presented elsewhere.[1] Surface treatments of PVC have been hampered by the presence of plasticizer and other additives at its surface. The presence of plasticizer is known to render the PVC surface hydrophobic.[39] Even when plasticizer had been extracted, it quickly migrated back to the surface.[39] It

* Tegal Corp., Richmond, CA.

should, therefore, be difficult to produce any lasting surface modifications of this polymer, especially those affecting wettability because the properties of the plasticizer largely determine the properties of the surface. Unplasticized PVC films were used in this study.

MATERIALS

Poly(vinyl chloride) (PVC) films were spin cast from a 1% solution of PVC (secondary standard, Lot 01 M_n = 83,500, M_w = 37,400)* in tetrahydrofuran (THF, reagent grade).† The solution was filtered through a prefilter and a 1 μm PTFE Millipore filter under 15 psi argon (>99.995% pure).§

One percent silicone rubber (SR) solutions were prepared from SR received as a gift from R. Ward‡ and designated SR-RTV-80-68M-0IL, 100% solids, filtered. It was a silica-free, one-component RTV poly(dimethyl siloxane) with M_n = 23,000. The SR was dissolved in chloroform (reagent grade)† and filtered through a 1 μm PTFE filter as above in preparation for spin casting.

Polystyrene (PS) (secondary standard, M_n = 84,600, M_w = 321,000, Lot 03§ was dissolved in toluene (reagent grade† to form a 1% solution, and filtered in the same manner as SR in preparation for spin casting.

The polyethylene (PE) used was Alkathene 33§§ a low-density polyethylene (LDPE) film with no additives, received as a gift from D. Briggs of ICI. Polyethylene was used as received.

Fluorinated ethylene–propylene copolymer** was originally purchased as a film (Type A, heat-sealable) and provided as a gift by D. J. Lyman, University of Utah. FEP was extracted overnight in acetone, methanol, and water, then vacuum dried in a desiccator prior to use. No differences in the XPS spectra of cleaned or as-received FEP were noted.

Films of PVC, PS, and SR were spin cast on cleaned, silanized coverslips*** for contact angle, XPS, and SEM studies. All water used for hydration and contact angle work was doubly distilled.

METHODS

All microscope slides and coverslips were rinsed in tap water, cleansed in a solution of Micro†† using cotton balls as swabs, then rinsed in singly distilled water, placed in a hot chromic acid bath (80–90°C) for 5 min, rinsed three times in singly distilled filtered water, rinsed twice in filtered ethanol (reagent grade)† and vapor degreased for 5 min in Freon (trichlorotrifluoroethane)†††

* Aldrich Chemical Company, Milwaukee, WI.
† Fisher Scientific, Fair Lawn, NJ.
§ Scientific Products, Inc., Webster, NY.
‡ AVCO Medical Products, Everett, MA.
§§ ICI Ltd., Hertfordshire, U.K.
** Teflon, FEP, DuPont, Wilmington, DE.
*** No. 2, 25 mm square, Corning Glass Works, Corning, NY.
†† International Products Corporation, Trenton, NJ.
††† Freon TF, DuPont, Wilmington, DE.

to remove all traces of ethanol. The SR, PE, and extracted FEP films were cleaned in Micro, rinsed three times in singly distilled filtered water, twice in methanol, and allowed to air dry before use.

In order to improve the adhesion of the polymer films to the glass substrates, the chromic acid-cleaned glass was vapor silanized. A solution of 200 mL *p*-xylene‡, 10 mL *n*-propyltriethyoxysilane§ and 3 mL 2,6 lutidine (practical grade)§§ was placed in a 500 mL round bottom flask equipped with stirring bar and attached to a reflux chamber and condensing column. The glassware was continually exposed to the silane vapor for at least 8 h before removal. Contact angles were measured on at least one piece of glassware from each silanized batch as a quality control check.

One percent filtered polymer solutions of PVC in THF, PS in toluene, and SR in chloroform were deposited on clean, silanized microscope slides or coverslips using chromic acid-cleaned pipets. The slips or slides were spun at 4000 rpm for 15 s on a spinning apparatus** designed for producing thin, reproducible films for the semiconductor industry. All cleaning and spinning was done on a filtered, laminar flow bench. Substrates of PS and PVC were immediately cured at 60°C for at least 3 h under a steady flow of nitrogen to drive off excess solvent. The SR-coated substrates were placed above petri dishes filled with distilled water for 24 h to allow for the water-initiated crosslinking of the room temperature vulcanizing (RTV) polymer. They were then placed in a drying oven for 3 h at 100°C under a steady flow of nitrogen (pure grade).***

Polymer surfaces were treated for 5, 30, 120, and 300 s in an RFGD plasma at 15 W and 200 μm Hg. The chamber was cleaned by striking a discharge in oxygen at the beginning of each treatment after the unit had been inactive.[1] Coverslip size samples 25 mm sq. were placed in ceramic holders on a glass rack in the vertical center of the cylindrical discharge chamber. Microscope slides were placed in the center of the chamber as if they were coverslips. Squares of PE, FEP, and SR films, 2.5 × 2.5 cm in size, were treated in the same manner as coverslips. All samples were handled with tweezers and rubber gloves. Further preparation details are available.[1]

The contact angle apparatus is described elsewhere[40,41] and was designed to permit underwater measurements. Bubbles of air or octane were formed and distributed on the underwater polymer surfaces using a microsyringe.[40] All polymer samples were hydrated in distilled water prior to the contact angle measurements. The dimensions of the bubble were measured using micrometers on the goniometer apparatus and the angles calculated.[1,40] The measured angles correspond to the receding water angle and the advancing octane angle in a water environment. Contact angles were measured for each of five bubbles on each sample surface. Six samples of each polymer were used

‡ Eastman Chemical Co., Rochester, NY.
§ Petrarch Systems, Inc., Levittown, PA.
§§ Mallinckrodt Chemical Works, St. Louis, MO.
** Headway Research, Inc., Garland, TX.
*** Matheson, East Rutherford, NJ.

to obtain one contact angle datum point. These six consisted of three samples from two separate and identical RFGD treatments. Thus, each contact angle datum point is the average of 30 bubbles.

Twenty-four samples of each polymer were treated for each specified plasma exposure time. They were separated into four groups of six each. Each group consisted of three samples from two independent treatments of the same duration. They were stored separately in acid-cleaned glassware for 1 day in distilled water, and for 1 day, 1 week, 1 month, and 3 months in air. All samples were hydrated at least 24 h prior to contact angle determination. The 1 day sample was actually stored only in water for the 1 day duration. The rest were stored in air for the indicated time and then hydrated for at least 24 h prior to contact angle measurements. The effect of RFGD treatment time on contact angle was determined by treating 24 samples of each polymer for 5, 30, 120, and 300 s. RFGD-treated polymers were compared with hydrated controls of the same polymer.

The effect of storage time was investigated by determining the contact angle of the polymer surfaces exposed to different RFGD treatment times after the previously noted air storage times of 1 week, 1 month, and 3 months. These were also compared with hydrated controls of the same polymer. Results are reported as the mean ±1 standard deviation.

X-ray photoelectron spectroscopy (XPS) is a surface sensitive technique that yields the elemental composition of the first 50–70 Å of a surface and information about the immediate bonding environment of the atoms. The theory and technique are described by others.[42] XPS spectra were obtained with a Hewlett-Packard 5950B spectrometer utilizing monochromatic Alk_α 1,2 radiation at 1487 eV. Polymer samples were prehydrated for 36 h, vacuum desiccated, mounted on gold platens in air, inserted into the spectrometer, and analyzed at ambient temperatures in a 10^{-9} torr vacuum. Power at the x-ray source was 800 W. An electron flood gun operating at 0.3 mA and 5.0 eV supplied a flux of low-energy electrons to the polymer surfaces to minimize heterogeneous charging artifacts in the resulting spectra. Wide scans (0–1000 eV) were performed for surface elemental analyses as well as detailed 20 eV scans of the major elements indicated in the wide scan. C-1*s* scans were taken first and last to determine whether exposure to the x-rays and vacuum had any effect on the surfaces. All spectra were charge referenced to a C-1*s* line for alkyl-like carbon at 284 eV.

Scanning electron micrographs were taken using a Cambridge Mark II stereoscan scanning electron microscope. Samples of control and 300-s RFGD-treated PVC, PS, FEP, SR, and PE were hydrated in water and vacuum desiccated prior to viewing. An edge of each sample was coated with silver paint in order to ensure conductive contact between the samples and specimen holders. All samples were gold and carbon shadowed. The analyzing vacuum was approximately 10^{-4} torr.

Samples were also viewed under a Nikon Apophot research microscope to determine their surface roughness prior to SEM investigations.

RESULTS AND DISCUSSION

X-ray photoelectron spectroscopy

Scofield's theoretical cross sections[43] were used to semiquantitate the XPS data for PVC, PS, SR, and PE. Owing to the variation in the product of the mean free paths and throughput functions of the spectrometer used in this experiment, an additional correction factor was employed when comparing spectra whose main peak was outside the 0–600 eV binding energy range.[44] This factor was used when evaluating FEP spectra. Scofield-corrected C-1*s* and O-1*s* peak areas were multiplied by 1.224 and 1.136, respectively (see Fig. 24 of ref. 45) in order to obtain a more quantitative representation of the relative concentration of fluorine, carbon, and oxygen on the surface of FEP.

Polyethylene

X-ray photoelectron spectroscopy data revealed that the control PE surface was composed entirely of aliphatic carbon.[1] The C-1*s* peak was sharp with a full width at half-maximum intensity (FWHM) of 0.82 eV. No oxygen or other species were detected on the surface. Hydration of the polyethylene surface produced a small O-1*s* peak[1] and a noticeable high binding energy shoulder on the C-1*s* peak. The oxygen could be due to actual oxidation of the PE surface or surface rearrangement leading to the exposure of buried oxygen functionalities.[46] In general, RFGD treatment for increasing periods of time led to an increased FWHM for the C-1s spectrum accompanied by an increased shoulder on the high binding energy side of the C-1*s* peak and an increased relative O-1*s* intensity.[1]

The high binding energy C-1*s* shoulder was resolved into three peaks most probably representing carbon singly bound to oxygen, doubly bound to oxygen, and carbon bound to two oxygen functionalities—carboxylic acids and esters.[45,47]

An increase in oxygen concentration at the surface was noted previously for polyethylene treated in argon and nitrogen plasmas,[48] corona discharges,[49] and chromic acid.[50] Briggs, Brewis, and Konieczo[50] concluded that most of the oxygen was present as part of carbonyl functionalities or hydroxyl groups. Blythe et al.[49] found that in addition to these, carboxyl oxygen was present. The results of this study supported the above-mentioned results and further found that increased oxidation of the surface occurred with increased duration of exposure to a helium plasma (Fig. 1). The ratio of the different oxygen functionalities appeared to remain relatively constant as the degree of oxidation proceeded.

Polystyrene

As seen in Figure 2, the relative amount of oxygen at the surface of the PS increased with increased RFGD exposure time. The oxidation appeared to

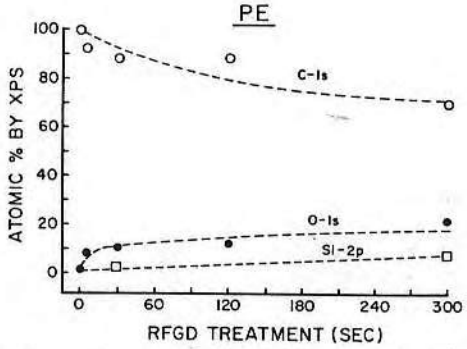

Figure 1. Relative surface elemental composition of polyethylene as a function of radio frequency glow discharge treatment time. Increased oxidation of the surface takes place with increased RFGD treatment, as indicated by an increased relative O-1*s* intensity and decreased C-1*s* intensity. The silicon appears as an impurity, probably from the walls of the RFGD chamber.

occur quite quickly since a plateau of the percent oxygen at the surface was reached in the first 5 s of treatment. Nitrogen appears as an impurity at longer exposure times.

Untreated polystyrene has a high binding energy peak approximately 6.9 eV from the parent aliphatic peak. This is a "shake-up" peak, as described by Clark and Dilks.[32] It was approximately 7% of the intensity of the parent peak and is indicative of the aromatic ring structure of the PS. The value of 7% for the shake-up peak was found for PS by others[1,51] using the instrument employed in this study, and is close to the value of 8.1% obtained by Clark and Feast.[52] This peak decreased with increasing RFGD treatment times.[1] This loss in the aromatic shake-up structure was accompanied by an increased oxygen concentration on the surface as revealed by a high binding energy

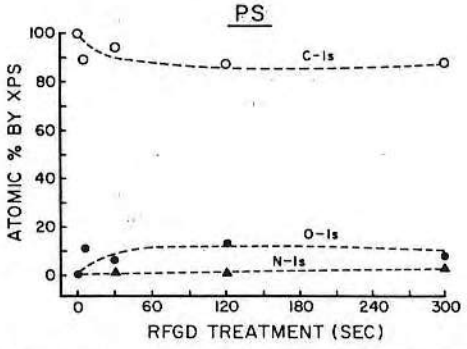

Figure 2. Relative surface elemental composition of polystyrene as a function of radio frequency glow discharge treatment time. Oxidation appears to take place quite rapidly and reaches a plateau within the first 2 min of treatment time. Nitrogen appears as an impurity.

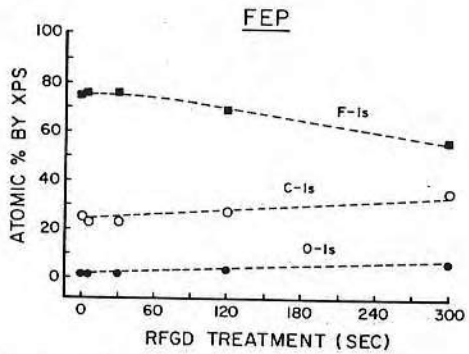

Figure 3. Relative surface elemental composition of fluorinated ethylene-propylene copolymer as a function of radio frequency glow discharge treatment time. The relative percent of carbon and oxygen at the surface increase with increased RFGD treatment time and the relative amount of fluorine decreases. Equilibrium does not appear to have been reached after 300 s of RFGD treatment.

shoulder on the C-1*s* peak as well as by an increased O-1*s* peak. The loss of the shake-up peak indicated a loss of phenyl side groups and/or a loss in aromaticity of the phenyl side groups. The addition of electron withdrawing groups to the aromatic ring is known to decrease the intensity of the shake-up peak.[53] A more detailed discussion of XPS data for PS is available.[40]

Approximately 13% of the PS carbon atoms in the surface volume analyzed were oxidized after RFGD treatment time greater than 5 s. This was less than the value of 22% found by Iwamoto, King, and Andrade[51] who discharged 50 W power in a helium environment at 400 μm Hg pressure, for 5 min. They, along with Yasuda,[38] noted a decrease in the shake-up peak after plasma exposure, indicating a decrease in aromaticity and/or increased unsaturation of the polystyrene backbone and/or oxidation of the phenyl side group.

Fluorinated ethylene-propylene copolymer (Fig. 3)

A small amount of aliphatic carbon was detected on the FEP surfaces. The C-1*s* peak for FEP treated by RFGD for 300 s revealed a substantial C–H peak along with a broad band of peaks located between the C–H and C–F_2 peaks. The broad band of peaks most probably consisted of carbon–oxygen and C–FH functionalities.[1]

An increase in the O-1*s* peak area occurred with increased RFGD treatment. As the O-1*s* peak increased, the shoulder intermediate between the C–H and C–F_2 peaks increased, indicating that it was, indeed, most probably indicative of carbon–oxygen functionalities.[1] Some C–FH groups were also probably present. The F-1*s* peak remained sharp with a FWHM of approximately 1.20 eV throughout the RFGD treatment. Its relative intensity to the other peaks, however, varied. The F/C ratio was approximately 2:1 for the control and cleaned samples, which was expected for the polymer.

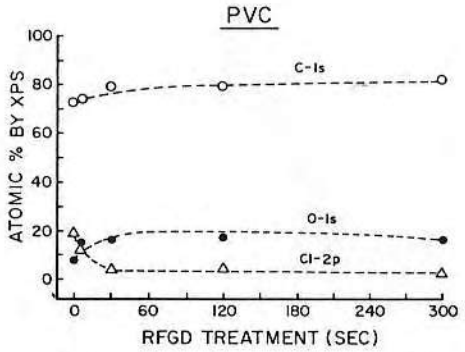

Figure 4. Relative surface elemental composition of poly(vinyl chloride) as a function of radio frequency glow discharge treatment time. Surface oxidation occurs rapidly reaching a plateau in the first 30 s of RFGD treatment.

Poly(vinyl chloride)

Oxidation of the PVC surface proceeded rather quickly and reached a plateau within the first 5 s of plasma treatment (Fig. 4). About 5% oxygen was present in the surface volume analyzed. The oxidation occurred largely at the expense of the chlorine atoms. A roughly 6.7% increase in oxygen over the hydrated control for the 5-s plasma treatment was matched with a 7.5% decrease in the amount of chlorine detected at the PVC surface (Fig. 4).

Poly(dimethyl siloxane)

XPS of control and prehydrated SR, poly(dimethyl siloxane), revealed the expected silicon/oxygen/carbon ratio of roughly 1:1:2. As RFGD treatment

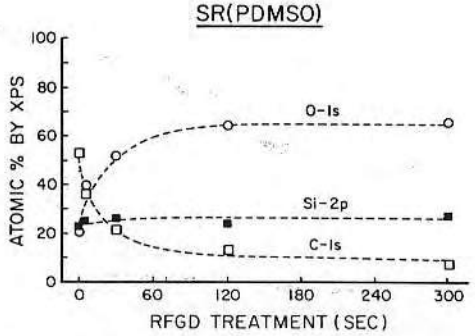

Figure 5. Relative surface elemental composition of silicone rubber as a function of radio frequency glow discharge treatment time. Oxidation reaches a plateau in roughly 120 s, producing a predominantly SiO_2 or SiO_2-like surface. Relative increases in oxygen at the surface are paralleled, almost identically, with relative decreases in carbon.

proceeded, an increase in oxygen present at the surface was noted, along with a concomitant decrease in carbon (Fig. 5). The relative percent of silicon remained unchanged at roughly 25% throughout RFGD treatment. The C-1s peak was shifted to higher binding energies as the treatment proceeded and its intensity decreased and FWHM increased.[1] The shift of the XPS C-1s peak revealed that the carbon became more bound to oxygen rather than to silicon alone as a function of treatment time. The O-1s peak also shifted to higher binding energies and its FWHM generally increased with increasing RFGD treatment.[1]

Feneberg and Krekeler[54] suggested that SiO_2 is the predominant species on the surface of PDMSO and other organopolysiloxane elastomers after ion bombardment. The results reported here also suggested the existence of SiO_2 on the surface. Enough energy was present in the plasma to rupture Si—C bonds as well as Si—O bonds. The freed organic portions of the elastomer could be volatilized and drawn from the plasma chamber by the vacuum. In the oxygen environment used by Feneberg and Krekeler,[54] oxygen was the only species capable of binding with the silicon, so SiO_2 was produced. In the helium environment used in this study, it was not possible for Si to bond with this inert gas. However, recombination with oxygen provided by water vapor present as an impurity in the chamber was possible, as was recombination with oxygen that was used to backfill the chamber in order to quench any unreacted surface radicals after the unit was turned off.

The Si peak remained at the same relative intensity throughout the plasma treatment, although it shifted to higher binding energies as the treatment proceeded. The peak was not indicative of one but rather of at least two species.

The RFGD treatment appeared to replace surface carbon with oxygen (Fig. 5). At 5 s a 16% increase in oxygen coincided with a 16% decrease in carbon; at 30 s a 28% increase coincided with a 31% decrease in carbon; and at 120 s a 41% increase was coincident with a 40% decrease in carbon. It was apparent that the methyl groups were being replaced by oxygen. Eventually, the backbone of the polymer was cleaved to yield SiO_2 molecules on the surface.

It is evident at 300 s exposure time that almost all of the silicon and carbon had to be bound to oxygens. The 27% silicon could thus account for 54% oxygen and the 7% carbon could account for 14% oxygen, bringing the total amount of oxygen to 68%, not much over the obtained value of 66% (Fig. 5). The surface consisted primarily, then, of SiO_2-like functionalities, with some oxidized carbon also present (carboxyl groups, aldehydes, etc.).

Gesser and Warriner[55] suggested that the pendant CH_3 groups of poly(methyl methacrylate) could be oxidized when placed in a water vapor discharge system. Similarly, the CH_3 pendant groups of the PDMSO appeared to be oxidized by the RFGD treatment in the helium used in this study. Some carbon–oxygen species may have been volatilized and escaped from the polymer surface. XPS did reveal, however, that RFGD treatment produced oxidation of the silicon of the SR backbone as well as of the carbon of the methyl side groups.

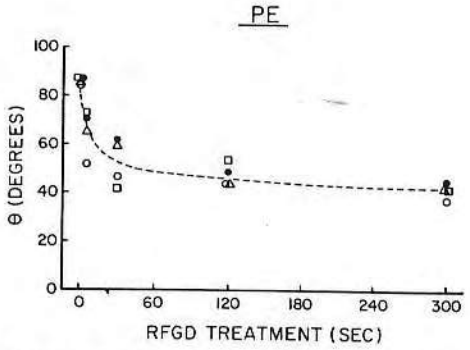

Figure 6. Air–water contact angle of polyethylene as a function of radio frequency glow discharge treatment time. Most of the decrease in contact angle occurred within the first 30 s of RFGD treatment. The contact angles remained relatively constant after three months storage in air. (□) 1 day; (●) 1 week; (Δ) 1 month; (○) 3 months.

Contact angle

The air–water contact angle for PE (Fig. 6) decreased with increased RFGD exposure time. The maximum decrease (from 87 to 42°) occurred within the first 30 s of treatment, yet increased oxidation was noted for up to 300 s by XPS. This most probably occurred because the contact angle is determined by the extreme outer surface molecules only. On the other hand, XPS monitors the first 70 Å of the surface.[44] Oxidation of the outermost surface layers was completed first and corresponded to a plateau of contact angle values. Subsequent oxidation led to further changes in XPS spectra but no change in contact angle.[56] The contact angles of the surfaces remained relatively unchanged over a 3-month storage time in air. Note that these contact angle

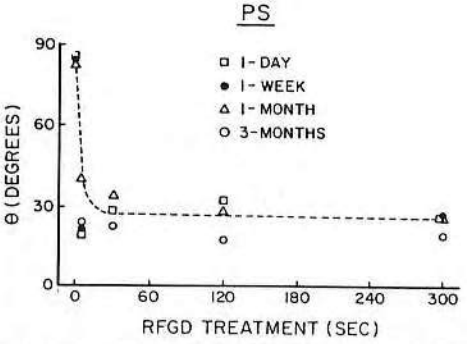

Figure 7. Air–water contact angle of polystyrene as a function of radio frequency glow discharge treatment time. Contact angle values appear to plateau at five seconds and remain relatively unchanged after three months storage in air.

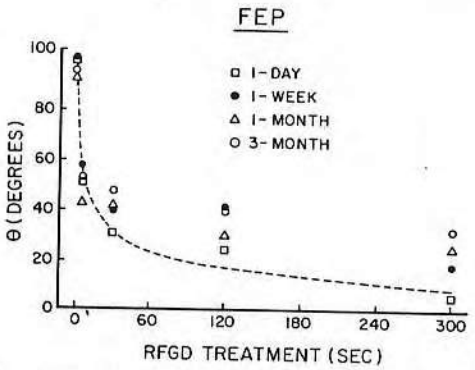

Figure 8. Air–water contact angle of florinated ethylene–propylene copolymer as a function of radio frequency glow discharge treatment time. It is difficult to tell whether or not the contact angle has reached its equilibrium value after 300 s of RFGD exposure. The contact angle gradually increased with storage time.

measurements were made after the appropriate air storage time by immersing the sample in H_2O for at least 24 h before measuring the angle of the fully hydrated surface underwater.

The results for polystyrene (Fig. 7) were qualitatively similar to those obtained for PE. Air–water contact angles decreased with increasing RFGD treatment, indicating an increase in surface free energy. The contact angle remained relatively constant over a 3-month storage time in air. The contact angle values reached plateaus after 5 s of RFGD treatment (from 86 to 19°), corresponding to a plateau reached in oxygenation of the PS surface.

Increased RFGD treatment led to a decreasing contact angle on FEP until the surface became totally wetting at 300 s exposure time (Fig. 8). The con-

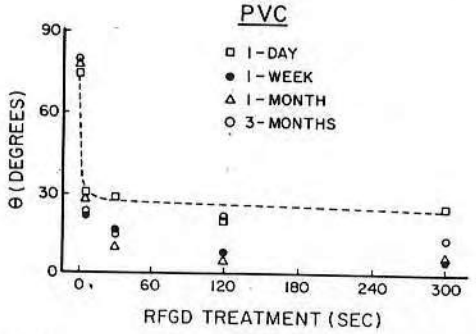

Figure 9. Air–water contact angle of poly(vinyl chloride) as a function of radio frequency glow discharge treatment time. The contact angle of the 1 day sample appears to plateau during the first 5 s of RFGD treatment. The contact angles tend to decrease after being stored in air.

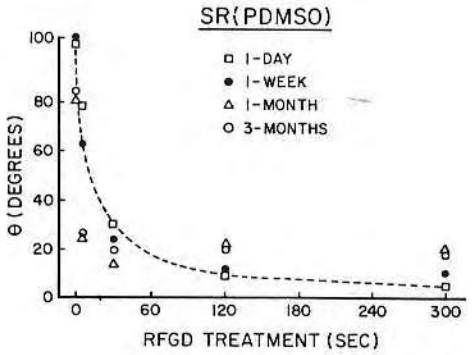

Figure 10. Air–water contact angle of silicone rubber as a function of radio-frequency glow discharge treatment time. The contact angle appears to plateau after roughly 120 s of RFGD treatment time, corresponding to a plateau in oxygen concentration as revealed by XPS data.

tinual decrease in contact angle with increased RFGD exposure time was paralleled by an increased surface oxygen concentration as revealed by XPS. A gradual increase of the contact angle with storage time for the initially totally wetting surface was noted. Otherwise, the results paralleled those of PS and PE.

Air–water (Fig. 9) contact angles decreased with increasing exposure of PVC to RFGD. The results were similar to those previously mentioned, except that the contact angle appeared to decrease slightly with increased storage time. The contact angle plateau at roughly 5 s corresponded to the oxygen plateau at 5 s revealed by XPS.

Air–water (Fig. 10) contact angles decreased with increased RFGD treatment of SR. The contact angles remained relatively constant over the 3-month storage time in air. The plateau in contact angle at approximately 120 s corresponded to the oxygen plateau as revealed by XPS.

In general, the experimentally obtained contact angle values for control surfaces fell within the range of the values reported in the literature (PE,[33] PS,[51,58] FEP,[44,57–59] PVC,[39,60] and SR[61]).

The PVC contact angle value obtained for the spin cast PVC (75.3°) was very close to that reported by Kim, Petersen, and Lee[39] for methanol-extracted PVC (78.2°), indicating that Kim's extraction process most probably removed all surface phthalates present. Plasticizers, bis(2-ethylhexyl)phthalate in particular, have been shown to cause surfaces to act more hydrophobically.[39] It is therefore essential to permanently remove plasticizers from the surface region of commercial polymers in order to produce a hydrophilic surface, regardless of the method of treatment used to induce hydrophilicity. It should be remembered that the polymers used in this study contained no plasticizer.

RFGD treatment of polymer samples for 300 s generally produced surfaces with lower contact angle values than treatments reported in the literature.

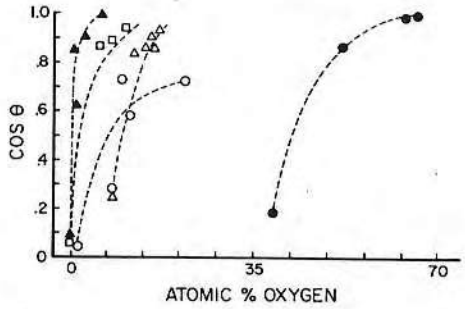

Figure 11. Cosine of air–water contact angle as a function of relative surface oxygen concentration for silicone rubber (●), fluorinated etylene–propylene copolymer (▲), poly(vinyl chloride) (△), polystyrene (□), and polyethylene (○). A relatively small change in the percent of oxygen found at the surface of the polymers results in a significant increase in the wettability.

This was especially noticeable for FEP, where other seemingly harsher treatments resulted in less significant contact angle changes. There are several possible explanations for these discrepancies. The experimental values were all determined by the underwater captive bubble technique and measured a receding air–water contact angle. All literature values quoted were for an advancing rather than receding air–water contact angle.

The treatments varied; gas, power, pressure, and exposure time for experiments reported in the literature were not the same as those used in this experiment. Also, the pressure used in this study for experimental RFGD treatment (200 μm Hg) was lower than that of any of the other treatments, indicating a greater mean free path for all active species.

Figure 11 shows that a relatively small percent of surface oxygen led to a significant decrease in the underwater air contact angle and, thus, in the surface free energy of the polymer. The fastest decrease in contact angle with increased surface oxygen concentration was seen for FEP followed by PS and PVC. Polyethylene appeared to reach a lower plateau of surface free energy (higher angle) than the other polymers.

The SR curve is misleading because SR already contained roughly 25% oxygen in the polymer before RFGD treatment. This oxygen, however, was part of the polymer backbone and therefore did not directly contribute to the surface nature, which was largely controlled by the methyl side groups of the SR. Figure 11 illustrates that the SR side groups were oxidized leading to increased wetting. If the curve for SR is transposed 25% to the left of its present position to compensate for the oxygen present in its backbone, a plot slightly to the right of the PVC curve is obtained.

Octane–water contact angle data did not add any significant information to that obtained from the air–water contact angle values. Coleman,[62] in fact, suggested that the two are related and that the octane–water angle can be inferred from the air–water value. It is suggested that air–water contact angle values alone are sufficient to assess roughly the surface energy of oxidized and unoxidized polymers, especially for routine quality control checks.

Scanning electron microscopy

Scanning electron micrographs were taken of cleaned and silanized glassware and RFGD-treated (30 s) and untreated PE, PS, FEP, PVC, and SR. Samples that were hydrated overnight and subsequently dried along with those samples that were never hydrated were investigated. No differences were noted between hydrated and control samples.

There was a significant difference between surfaces that were spin cast and commercially available films. The commercially available PE had a rough, specular surface with a ruddy appearance. The commercial FEP had a somewhat smoother topography. Not as many undulations of the FEP surface were noted as were noted for the PE surface yet the small-scale perturbances of the surface were of the same nature as those seen on the PE. In addition, the FEP surface was marked by grooves and striations in places, probably as a result of manufacturing processes. In contrast, spin-cast surfaces were much smoother. The granularity that was apparent was much finer and less pronounced than that of the commercial FEP and PE samples. Some particulate matter was, however, noted on the spin-cast surfaces, along with some areas that appeared to be composed of polymer aggregates. The SR surface was wrinkled in places and appeared to pull away from the glass substrate.

No difference in surface topography was noted as a result of RFGD treatment for 300 s for any of the polymers investigated. Lower pressures, greater exposure time, and increased power settings would lead to etching in the surface. These were deliberately avoided in this study.

CONCLUSIONS

Exposure of PE, PS, FEP, PVC, and SR to an-RFGD-produced plasma in helium (200 μm Hg pressure, 15 W power) for times of up to 300 s produced an oxidized surface on each of the polymers. X-ray photoelectron spectroscopic analysis suggested that the oxygen initially attacked the polymers' side groups instead of their backbones. The oxidation of the surface generally reached a plateau within 30 s exposure to RFGD for the conditions used and was probably accompanied by crosslinking of the polymer surface. RFGD treatment induced oxidation of the polymer surfaces with a consequent decrease in both air–water and octane–water contact angles. Very slight increases in surface oxygen were found to cause severe decreases in air–water contact angles. SEM revealed no apparent changes in surface topography.

RFGD tratment produced a hydrophilic surface on all polymers investigated for a storage time of up to 3 months in air.

Air–water contact angles alone were sufficient to assess roughly the surface energy of oxidized and unoxidized polymers. Octane–water contact angles are not necessary for routine surface characterization.

References

1. P. M. Triolo, "Surface Characterization and Modification of Some Commonly Used Catheter Materials," Masters Thesis, Department of Bioengineering, University of Utah, Salt Lake City, UT, 1980, pp. 1–152.
2. F. J. Miller, Personal Communication, Department of Radiology, University of Utah, Salt Lake City, UT, 1979.
3. J. D. Mortensen, "Clinical Sequelae from Arterial Needle Puncture, Cannulation, and Incision," *Circulation*, **35**, 1118–1123 (1967).
4. C. A. Crenshaw, L. R. Kelly, R. J. Turner, and D. Enos, "Bacteriologic Nature and Prevention of Contamination to Intravenous Catheter," *Am. J. Surg.*, **123**, 264–266 (1972).
5. W. R. Peters, W. H. Bush, R. D. McIntyre, and L. D. Hill, "The Development of Fibrin Sheath on Indwelling Venous Catheters," *Surg. Gynecol. Obstet.*, **137**, 43–47 (1973).
6. H. G. Spanos and J. F. Hecker, "Thrombus Formation on Indwelling Venous Cannulae in Sheep: Effects of Time, Size, and Materials," *Anesth. Intens. Care*, **4**, 217–224 (1976).
7. J. F. Hecker, G. C. Fish, and D. C. Farrell, "Measurement of Thrombus Formation on Intravascular Catheters," *Anesth. Intens. Care*, **4**, 225–231 (1976).
8. R. L. Mani and R. L. Eisenberg, "Complications of Catheter Cerebral Arteriography: Analysis of 5,000 Procedures. III. Assessment of Arteries Injected, Contrast Medium Used, Duration of Procedure, and Age of Patient," *Am. J. Roentgenol.*, **131**, 871–874 (1979).
9. R. L. Mani and R. L. Eisenberg, "Complications of Catheter Cerebral Arteriography: Analysis of 5,000 Procedures. II. Relation of Complication Rates to Clinical and Arteriographic Diagnoses," *Am. J. Roentgenol.*, **131**, 867–869 (1978).
10. G. H. Nachnani, L. S. Lessin, T. Motomiya, and W. Jensen, "Scanning Electron Microscopy of Thrombogenesis on Vascular Catheter Systems," *N. Engl. J. Med.*, **286**, 139–140 (1972).
11. J. H. Anderson, C. Gianturco, S. Wallace, and G. D. Dodd, "A Scanning Electron Microscope Study of Angiographic Catheters and Guide Wires," *Radiology*, **111**, 567–571 (1974).
12. M. G. Bourassa, M. Cartin, E. B. Sandborn, and E. Pederson, "Scanning Electron Microscopy of Surface Irregularities and Thrombogenesis of Polyurethane and Polyethylene Coronary Catheters," *Circulation*, **53**, 992–996 (1976).
13. G. D. Wilner, W. J. Casarella, R. Baier, and C. Fenoglio, "Thrombogenicity of Angiographic Catheters," *Circ. Res.*, **43**, 424–428 (1978).
14. R. G. Mason, N. F. Rodman, and D. E. Scarborough in *Artificial Heart Program Conference Proceedings*, R. J. Hegyeli, Ed., Government Printing Office, Washington, DC, 1969, p. 193.
15. K. Amplatz, "A Simple Non-Thrombogenic Coating," *Invest. Radiol.*, **6**, 280–289 (1971).
16. E. W. Salzman, W. G. Austen, G. J. Lipps, E. W. Merrill, E. R. Gilliland, and J. Joison, "A New Antithrombogenic Surface: Development and *In Vitro* and *In Vivo* Characteristics," *Surgery*, **61**, 1–10 (1967).
17. M. D. Freed, J. F. Keane, and R. Rosenthal, "The Use of Heparinization to Prevent Arterial Thrombosis After Percutaneous Cardiac Catheterization in Children," *Circulation*, **50**, 565–569 (1974).
18. C. C. Clawson and S. J. Boros, "Surface Morphology of Poly(vinyl Chloride) and Silicone Elastomer Umbilical Artery Catheters by Scanning Electron Microscopy," *Pediatrics*, **62**, 702–705 (1978).
19. G. Formanek, R. S. French, and K. Ampltaz, "Arterial Thrombus Formation During Clinical Percutaneous Catheterization," *Circulation*, **41**, 833–841 (1970).
20. B. Jacobsson and D. Schlossman, "Thromboembolism of Leg Following Percutaneous Catheterization of Femoral Artery for Arteriography: Predisposing Factors," *Acta Radiol Diag.*, **8**, 109–118 (1969).
21. J. B. Downs, R. L. Chapman, Jr., and S. F. Hawkins, "Prolonged Radial-Artery Catheterization," *Arch. Surg.*, **108**, 671–673 (1974).
22. P. N. Sawyer, W. Ramsey, B. Stanczewski, R. Turner, W. Liebig, G. W.

Kammlott, and B. Braun, "A Comparative Study of Several Polymers for Use as Intravenous Catheters," *Med. Instrum.*, **11**, 221–230 (1977).
23. C. V. Libsach and K. R. Kollmeyer, "Role of Catheter Surface Morphology on Intravascular Thrombosis of Plastic Catheters," *J. Biomed. Mater. Res.*, **13**, 459–466 (1979).
24. S. Durst, J. Leslie, R. Moore, and K. Amplatz, "A Comparison of the Thrombogenicity of Commercially Available Catheters," *Radiology*, **13**, 599–600 (1974).
25. D. J. Lyman, J. L. Brash, and K. G. Klein in *Artificial Heat Program Conference Proceedings*, R. J. Hejyele, Ed., Government Printing Office, Washington, DC, 1969, p. 113.
26. R. Cramer, R. S. French, and K. Amplatz, "A Preliminary Human Study with a Simple Nonthrombogenic Coating," *Radiology*, **100**, 421, 422 (1971).
27. P. Eldh and B. Jacobsson, "Heparinized Vascular Catheters: A Clinical Trial," *Radiology*, **111**, 289–292 (1972).
28. J. Hradil, J. Stamberg, A. L. Kaganov, and P. Synek, "Investigation of the Surface Structure of Polymers by Chromatographic Methods. I. Hydrophilized Polyethylene Capillaries for Medical Applications," *J. Polym. Sci. Symp.*, **47**, 123–129 (1974).
29. M. Hudis in *Techniques and Applications of Plasma Chemistry*, J. R. Hollahan and A. T. Bell, Eds., Wiley, New York, 1974, chap. 3.
30. A. Braley and J. D. Fales, "Prospects for Industrial Applications of Electrical Discharges," *Chem. Tech.*, 232–237 (1971).
31. F. K. McTaggert, *Plasma Chemistry in Electrical Discharges*, Elsevier, New York, 1967, chap. 3.
32. D. T. Clark and A. Dilks, "ESCA Studies of Polymers. VII. Shake-up Phenomena in Some Alkane-Styrene Copolymers," *J. Polym Sci. Polym. Chem. Ed.*, **14**, 533–542 (1976).
33. C. A. L. Westerdahl, J. R. Hall, E. C. Schramm, and D. W. Levi, "Gas Plasma Effects on Polymer Surfaces," *J. Colloid Interface Sci.*, **47**, 610–620 (1974).
34. J. R. Hollahan, "Research with Electrodelessly Discharged Gases," *J. Chem. Ed.*, **43**, A487–A512 (punctuated) (1966).
35. J. C. Mijovic and J. A. Koutsky, "Etching of Polymeric Surfaces: A Review," *Polym. Plast. Technol. Eng.*, **9**, 139–179 (1977).
36. J. C. von der Heide and H. L. Wilson, "Guide to Corona Film Treatment," *Mod. Plast.*, **38**, 199–206 (1961).
37. E. L. Lawton, "Adhesion Improvement of Tire Cord Induced by Gas Plasma," *J. Appl. Polym. Sci.*, **18**, 1557–1574 (1974).
38. H. Yasuda and H. C. Marsh, "ESCA Study of Polymer Surfaces Treated by Plasma," *J. Polym. Sci. Polym. Chem. Ed.*, **15**, 991–1019 (1977).
39. S. W. Kim, R. V. Petersen, and E. S. Lee, "Effect of Phthalate Plasticizer on Blood Compatibility of Polyvinyl Chloride," *J. Pharm. Sci.*, **65**, 670–673 (1976).
40. R. N. King, "Surface Characterization of Synthetic Polymers for Biomedical Applications," Ph.D. Thesis, University of Utah, 1980, pp. 1–174.
41. J. D. Andrade, R. N. King, D. E. Gregonis, and D. L. Coleman, "Surface Characterization of Poly(Hyroxyethyl methacrylate) and Related Polymers. I. Contact Angle Methods in Water," *J. Poly. Sci. Polym. Symp.*, **66**, 373–336 (1979).
42. D. T. Clark, "ESCA Applied to Polymers," *Adv. Polym Sci.*, **24**, 126–188 (1977).
43. J. H. Scofield, "Hartree-Slater Subshell Photoionization Cross-Sections at 1254 and 1487 eV," *J. Electron Spectrosc. Relat. Phenom.*, **8**, 129–137 (1976).
44. S. M. Hall, J. D. Andrade, S. M. Ma, and R. N. King, "Photoelectron Mean Free Paths in Barium Stearate Layers," *J. Electron Spectrosc. Relat. Phenom.*, **17**, 181–189 (1979).
45. B. J. Lindberg, "Can We Expect Any Meaningful Correlations Between NMR-and ESCA-Shifts?" *J. Electron Spectrosc. Relat. Phenom.*, **5**, 149–166 (1974).
46. A. Baszkin, M. Nishino, and L. Ter-Minassian-Saraga, "Solid–Liquid Adhesion of Oxidized Polyethylene Films: Effect of Temperature," *J. Colloid Interface Sci.*, **54**, 317–328 (1976).
47. D. T. Clark and H. R. Thomas, "Applications of ESCA to Polymer Chemistry. X. Core and Valence Energy Levels of a Series of Polyacrylates," *J. Polym. Sci. Polym. Chem. Ed.*, **14**, 1671–1700 (1976).
48. S. Braley, "The Chemistry and Properties of the Medical-Grade Silicones," *J. Macromol. Sci. Chem.*, **4**, 529–544 (1970).
49. A. R. Blythe, D. Briggs, C. R. Kendall, D. G. Rance, and V. J. I. Zichy, "Surface Modification of Polyethylene by Electrical Discharge Treatment and the Mechanism of Autoadhesion," *Polymer*, **19**, 1273–1278 (1978).
50. D. Briggs, D. M. Brewis, and M. B. Konieczo, "X-Ray Photoelectron Spectroscopy Studies of Polymer Surfaces. Part 3. Flame Treatment of Polyethylene," *J. Mater. Sci.*, **11**, 1270–1277 (1976).
51. G. K. Iwamoto, R. N. King, and J. D. Andrade in *Photon, Electron and Ion Probes of Polymer Structure and Properties*, D. Dwight, T. J. Fabish, and H. R. Thomas, Eds., ACS Symp. Ser. No. 162, American Chemical Society, Washington, DC, 1981, pp. 405–418.
52. D. T. Clark and W. J. Feast, "Application of ESCA to Studies of Structure and Bonding in Polymeric Systems," *J. Macromol. Sci. Rev. Macromol. Chem.*, **C12**, 191–286 (1975).
53. D. T. Clark, A. Dilks, J. Peeling, and H. R. Thomas, "Applications of ESCA to Studies of Structure and Bonding in Polymers," *Faraday Discuss.* **60**, 183–195 (1975).
54. P. Feneberg and U. Krekeler, "Process for the Production of Hydrophilic Surfaces on Silicone Elastomer Articles," U.S. Pat. 3,959,105 (1976).
55. H. D. Gesser and R. E. Warriner, "Contact Lenses," U.S. Pat. 3,925,178 (1975).
56. B. W. Malpass and K. Bright, "Glow Discharge Pretreatment of Polyethylene," in *Aspects of Adhesion*, 5, D. Jalney, Ed., CRC Press, Cleveland, OH, 1969, p. 214.
57. J. F. M. Pennings and B. Bosman, "Relaxation of the Surface Energy of Solid Polymers," *Colloid Polym. Sci.*, **257**, 720–724 (1979).
58. J. J. Bikerman, *The Science of Adhesive Joints*, 2nd ed. Academic, New York, 1968.
59. J. Galembeck, "Surface Modification of Teflon: Contact Angle Measurements," *J. Poly. Sci. Polym. Lett. Ed.*, **15**, 107–109 (1977).
60. N. J. DeLollis and O. Montoya, "Bondability of RTV Silicone Rubber," *J. Adhesion*, **3**, 57–67 (1971).
61. M. Hudis and L. E. Prescott, "A Study of the Contact Angle on RTV Silicone Treated in a Hydrogen Glow Discharge," *J. Appl. Polym. Sci.*, **19**, 451–459 (1975).
62. D. L. Coleman, "In Vitro Blood-Materials Interactions: A Multitest Approach," Ph.D. Dissertation, Department of Pharmaceutics, University of UT, 1980, pp. 1–167.

Received August 1981
Accepted July 29, 1982

Surface modification and characterization of some commonly used catheter materials. II. Friction characterization*

Philip M. Triolo† and Joseph D. Andrade‡
Department of Bioengineering, University of Utah, Salt Lake City, Utah 84112

The effects of the modification of polystyrene (PS), polyethylene (PE), poly(vinyl chloride) (PVC), silicone rubber (SR), and fluorinated ethylene propylene (FEP) copolymer by radio frequency glow discharge in a helium environment were presented in part I. The hydrated polymer surfaces were characterized by XPS, SEM, visual microscopy, and by contact angle measurements. In general, exposure of the polymers to RFGD produced an oxidized hydrophilic surface, yet the roughness of the surface was unaltered by the relatively mild plasma conditions used. In this article, the frictional behavior of oxidized and unoxidized SR, PE, and FEP in distilled water, isotonic saline, and blood plasma environments is examined experimentally. The results are discussed in relation to the properties generally believed to affect frictional phenomena and to the surface properties as determined in part I. Results indicate that RFGD-treated SR generates less friction than untreated SR when dragged across all untreated and treated polymer surfaces, whether the medium is distilled water or an isotonic saline solution. Friction is consistently lower in a blood plasma medium between all surfaces investigated, most probably because of the presence of adsorbed proteins at the polymer interfaces.

INTRODUCTION

Many of the more-complicated catheterization procedures employed today utilize two-catheter systems. A large-diameter, semirigid catheter is guided through the vasculature to serve as a pathway for a flexible, free-floating, balloon-tipped inner catheter. The space between these two catheters is usually filled with isotonic saline. A great deal of friction is often encountered when these catheter systems are used, diminishing their effectiveness or sometimes even preventing their successful use, thus necessitating the use of more risky, complicated, and costly procedures.

This study was initiated in order to elucidate some of the parameters affecting the friction between idealized polymer surfaces in saline and blood plasma environments. Its results are discussed in relation to properties gen-

* Submitted by P. T. in partial fulfillment of the requirements for the M.S. degree in Bioengineering, University of Utah, Salt Lake City, UT 84112.

† Current address: Sorenson Research, 4455 Atherton Dr., Salt Lake City, UT 84107.
‡ To whom requests for reprints and correspondence should be addressed.

Journal of Biomedical Materials Research, Vol. 17, 149–165 (1983)

CCC 0021-9304/83/DDPPPP-NN$ZZ.ZZ

erally believed to affect frictional phenomena and surface properties as determined in part I.[1] Flat sheets of polymer were studied rather than the tubular configuration of catheters because polymers in this geometry were more easily modified and characterized. PE, FEP, and SR films were oxidized by exposing them to a RFGD in helium to produce hydrophilic surfaces. It was hypothesized that the hydrophilic surfaces would adhere a thin boundary of water that could serve as a lubricant between contacting polymer surfaces. A general discussion of friction and particularly friction between polymers follows in order to acquaint the reader with the polymer properties and parameters that have been shown to affect frictional behavior.

Friction

Detailed treatments of polymer friction properties are available in the literature.[2-20] It is generally recognized that the frictional force between two surfaces in relative motion is composed of two principle parts[3,4]:

$$F_{Tot} = F_{Adhesion} + F_{Displacement} \quad (1)$$

The displacement component is sometimes subdivided into four distinct parts[3]: (1) elastic component, (2) plastic component, (3) shearing (cutting of bulk material), and (4) shearing of surface films. The relative importance of the contribution of each of the above to the total frictional force depends on the type of motion involved (sliding or rolling), the surface topography, and the physical and mechanical properties of the materials themselves. The fourth term, "shearing of surface films," is usually relatively unimportant with polymers because of their general lack of chemical reactivity with the environment. The adhesion component arises from adhesive forces over the real area of contact between the two surfaces. Bowden and Tabor[5] state that for most unlubricated polymers, the adhesion term dominates. In extreme cases, notably for elastomers, the friction can result entirely from elastic displacement and the energy losses arising from elastic hysteresis.

If a hard slider (representing a single asperity) traverses the surface of an elastomer, energy is fed into the surface in front of the slider and some energy is restored to the slider by the elastic recovery of the elastomer behind the slider, urging it forward. The net loss of energy to the elastomer accounts for the force of work required to maintain sliding. If a transient groove is formed in the elastomer, the net energy loss is related to the input energy and the loss properties of the material at the particular temperature, contact pressure, and rate of deformation involved.[6-8] In nonelastomers a certain amount of permanent set may occur and the polymer may be treated as a plastic solid with a well-defined yield pressure. In most situations the loss properties of the polymer are most relevant in frictional phenomena.[4]

If the hard slider has sharp corners or edges, it may cut or tear the surface of the counterface material. The ploughing force is increased and the surface is seriously damaged. With rubbers, Schallamach[9] showed that a sharp asperity stretches the material around it until local tensile failure occurs. Presumably the same situation exists for elastomers. A lip is left protruding for removal by subsequent asperity interaction. With polymers, a sharp asperity may act as a miniature cutting tool and remove material.[4] Wear produced in this way may be described as abrasion.

As a result of the irregular nature of even the smoothest surfaces available, two materials will touch only in isolated regions.[3,14] The real area of contact is thus always less than, or equal to, the apparent area of contact. Two surfaces will initially have at most only three points touching. Even for minute total loads, the pressure at these points is sufficient to cause deformation leading to more points of contact. The stresses on individual contact points are relatively high in comparison with those occurring within the bulk of the material, and locally high pressures and temperatures exist.

For elastomers at light loads,[3] the individual asperity contacts remain discrete, multiple contact conditions exist, and the coefficient of friction is independent of load. At heavier loads, the increasing size of the deforming asperities leads to interference between separate, adjacent regions of deformation. The real area of contact increases less rapidly than at lighter loads, the adhesion term rises less rapidly because adhesive forces require direct contact, and, hence, the coefficient of friction falls more rapidly with increasing load. Finally, at even higher loads, all the asperities of the elastomer may be deformed flat into the general plane of the surface. The real area of contact is then equal to the apparent area of contact.[3]

Cohen and Tabor[19] showed that when nylon slides on a hydrophilic surface such as glass, water can be an effective lubricant. On hydrophobic counterfaces such as polytetrafluoroethylene or polyethylene, water is completely ineffective. Similar results were obtained with rubber. There was no reduction in friction when using water as a lubricant for rubber sliding on polyethylene, but there was an appreciable reduction for rubber on glass or steel. The ability of water to wet the hydrophilic surfaces probably played a role in enhancing its effectiveness as a lubricant in the above instances.

The friction between elastomers, when separated by a lubricating film, is a complex process that is dependent on load, surface roughness, and other factors, and it is often difficult to predict. At light loads the energy required to shear the lubricating film becomes increasingly significant. As the load is reduced, the real area of contact decreases and the effective thickness of the lubricating film increases.[14] Hydrodynamic lubrication predominates.

Surface roughness has various effect on the frictional properties of the lubricated surfaces. On the one hand, increasing the surface roughness will decrease the real area of contact and lead to a lessening of the adhesive component of friction. On the other hand, increasing the surface roughness leads to increased deformation losses in the opposing elastomers. For clean, dry rubber surfaces, the adhesive component dominates; thus, increasing surface roughness usually leads to a decreased coefficient of friction.

The effects of plasma treatment on the frictional properties of polymers have

not yet been elucidated. Most plasma treatment is employed to increase the adhesion of the polymer to an adhesive in forming a three-component joint.

Plasma treatment can cause:

(1) oxidation of the polymer surface,[1,21] leading to increased polar interactions between materials;

(2) the formation of a hydrophilic surface[1,22] which should make water an effective lubricant;

(3) an alteration of the surface topography,[23] most probably roughening, which can affect the surface area of the contact region; and

(4) crosslinking of the polymer surface,[1,24] which can lead to a change in the viscoelastic properties of the surface layer, thereby altering frictional properties.

In short, many competing effects are produced, and the resultant frictional behavior will be a consequence of the relative importance and interactions of the surface alterations—oxidations, hydrophilization, topography changes, and crosslinking.

A more general discussion of RFGD treatment of polymers and its effects on surface properties is presented elsewhere.[1]

MATERIALS

The thin surface coatings produced by spin casting and used predominantly for part I of this study were found to be totally removed from their glass substrates in some places when the surfaces were dragged across each other during friction tests. Therefore, only intact polymer films were used for friction studies. The friction between commercially available polyethylene (PE),* fluorinated ethylene propylene copolymer (FEP)† and silastic rubber (SR) sheeting, 10 mils thick,‡ was determined using the test apparatus described below.

Water

All water used was singly distilled.

RFGD treatment of the polymers is described in part I.[1] Films used for friction work (1 × 2¾ in., 1.8 × 4.5 cm) were too flexible to stay upright in the ceramic holders. They were therefore treated on a rack placed in the middle of the RFGD chamber.

Friction measurements

A modification of ASTM-27:D 1894-63 was used to determine the coefficient of friction between the various treated and untreated polymer surfaces while

* Alkathene 33, ICI, Ltd., U.K.

† Teflon type A, DuPont; originally produced as a film and provided by D. J. Lyman, University of Utah, Salt Lake City, UT.

‡ Dow Corning Medical Products, Midland, MI, lot No. 059163.

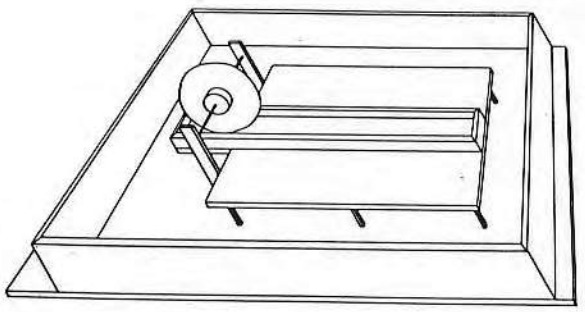

Figure 1. Friction testing apparatus. Stationary samples were taped to glass slides and firmly attached to the bottom of the trough which was filled with the appropriate test solution. The movable slide with attached polymer was connected to a piece of suture material which wrapped around the low-friction pulley and was attached to a load cell of an Instron tensile tester.

underwater, in an isotonic saline solution and in blood plasma. The apparatus (Fig. 1) consisted of a constant temperature bath, a trough into which the samples and the friction environment (air, water, blood plasma, etc.) were placed, a tensile testing machine (Instron Model TM5) to move one surface past another with a 500 g load cell used as a force transducer, a low-friction pulley used to transmit the vertical force supplied by the Instron to the horizontal motion of the polymers across one another, a sled on which samples were mounted for testing, and a piece of silk fishing line (Gudecase, 18-lb test) used to connect the sled to the load cell of the Instron. All samples were equilibrated for 24 h in filtered, distilled water prior to testing.

The samples placed on the movable slider were 1.8 cm wide × 4.2 cm long. The flat part of the slider in contact with the base surface was 2.1 cm wide × 1.5 cm long. The apparent surface contact area of the films was therefore 2.7 cm^2. The sample strips were fastened at the 1.8 cm edges to the top of the sled. Rubber gloves were worn at all times and care was taken to avoid contact with the sliding surfaces.

The stationary polymers were 1 in. wide × 2¾ in. long. They were fastened to the ends of acid-cleaned microscope slides with scotch tape. The slide was then fastened to the bottom of the sample trough, again with scotch tape, so that it abutted a slide permanently fastened to the bottom of the trough. This slide guaranteed that the sample could not move forward during the friction measurements.

A 20 g load was placed on the slider for all determinations. Friction between 300-s RFGD-treated polymers and control polymers was determined in en-

TABLE I

Friction Data for Control and Radio Frequency Glow Discharge-Treated Silicone Rubber, Polyethylene, and Fluorinated Ethylene–Propylene Copolymer in Distilled Water

	Base																							
	SR control				SR treated*				PE control				PE treated				FEP control				FEP treated			
Slider	Min†	Max‡	Type§	Average force or number of peaks**	Min	Max	Type	Average force or number of peaks	Min	Max	Type	Average force or number of peaks	Min	Max	Type	Average force or number of peaks	Min	Max	Type	Average force or number of peaks	Min	Max	Type	Average force or number of peaks
SR control	94	130	a	16	48	105	b	3	200	205	a	9	10	94	c	3	220	220	a	5	10	55	d	$\overline{25}$
	120	120		14	105	105	b	4	220	220		10	47	92		7	210	210		5	14	36	d	$\overline{24}$
	120	200		11	23	40	d	$\overline{23}$	230	230		12	26	105		5	194	210		9	15	60	d	$\overline{37}$
	220	220		9	65	90	b	3	220	220		10	42	59		5	100	180		6	8	58	d	$\overline{30}$
	160	300		6	85	110	b	3	220	220		10					170	170		6	12	57	d	$\overline{26}$
	160	205		10	110	110	b	2	240	250		6					210	210		10	8	90	e	$\overline{24}$
SR treated*	30	65	c	5	8	30	e	$\overline{20}$	100	110	a	7	19	19	d	$\overline{13}$	8	14	d	$\overline{10}$	6	31	e	$\overline{17}$
	30	105	c	5	12	35	e	$\overline{24}$	19	38	c	3	8	42	e	$\overline{24}$	10	18	d	$\overline{14}$	7	60	e	$\overline{24}$
	50	50	c	5	10	37	e	$\overline{21}$	12	15	d	$\overline{16}$	25	37	d	$\overline{27}$	24	105	b	6	6	15	d	$\overline{10}$
	20	30	d	$\overline{24}$	17	25	d	$\overline{20}$	10	100	b	5	18	44	d	$\overline{26}$	6	29	d	$\overline{21}$	9	30	e	$\overline{22}$
	20	110	c	3	7	12	d	$\overline{10}$	5	19	d	$\overline{15}$	11	16	d	$\overline{13}$	85	110	a	8	9	40	e	$\overline{22}$
	20	105	c	4									8	12	d	$\overline{9}$	50	110	a	8	11	58	e	$\overline{30}$
PE control	205	290	a	14	6	9	d	$\overline{7}$	4	12	d	$\overline{8}$	10	11	d	$\overline{8}$	13	33	e	$\overline{22}$	10	11	d	$\overline{8}$
	80	350		8	8	12		$\overline{10}$	10	10		$\overline{7}$	7	10		$\overline{7}$	12	17	d	$\overline{11}$	8	11		$\overline{10}$
	275	300		8					11	11		$\overline{7}$	7	8		$\overline{8}$	13	19	d	$\overline{14}$	7	10		$\overline{8}$
									8	8		$\overline{7}$	6	13		$\overline{11}$								
									7	14		$\overline{8}$	13	27		$\overline{18}$								
									7	9		$\overline{7}$	12	22		$\overline{19}$								
PE treated	100	105	a	4	10	11	d	$\overline{9}$	20	20	d	$\overline{16}$	11	14	d	$\overline{10}$	9	9	d	$\overline{8}$	5	15	d	$\overline{8}$
	103	115		8	63	63		$\overline{21}$	10	17		$\overline{14}$	12	13		$\overline{8}$	6	9		$\overline{8}$	9	12	d	$\overline{8}$
	130	150		4	12	25		$\overline{19}$	11	19		$\overline{13}$	7	11		$\overline{9}$	5	11		$\overline{8}$	11	11		$\overline{8}$
									8	8		$\overline{7}$	12	12		$\overline{8}$								
									9	9		$\overline{8}$	9	10		$\overline{8}$								
									9	10		$\overline{7}$	11	11		$\overline{8}$								
FEP control	Approached 500 g				12	12	d	$\overline{10}$	12	12	d	$\overline{7}$	9	9	d	$\overline{7}$	9	32	d	$\overline{10}$	8	11	d	$\overline{5}$
					10	15		$\overline{11}$	10	10		$\overline{7}$	8	8		$\overline{7}$	9	10		$\overline{6}$	5	8		$\overline{6}$
					9	17		$\overline{11}$	8	8		$\overline{7}$	10	11		$\overline{7}$	11	14		$\overline{7}$	6	8		$\overline{7}$
FEP treated	62	98	a	16	11	17	d	$\overline{14}$	10	10	d	$\overline{8}$	9	10	d	$\overline{8}$	7	8	d	$\overline{6}$	12	12	d	$\overline{7}$
	33	33	c	5	12	22		$\overline{15}$	7	8		$\overline{8}$	11	11		$\overline{9}$	8	8		$\overline{7}$	8	11		$\overline{9}$
					10	11		$\overline{7}$	8	8		$\overline{8}$	10	10		$\overline{8}$	10	10		$\overline{6}$	9	11		$\overline{8}$

*RFGD treatment is for 300 sec in all cases. All force measurements are in grams.

†The force of the first peak height.

‡The maximum force encountered.

§Qualitative assessment of the friction encountered. See text for details.

**Required to keep slider moving over the base. The numbers representative of averages have a bar above them. Numbers without bars indicate number of force peaks detected.

TABLE II

Friction Data for Control and Radio Frequency Glow Discharge-Treated Silicone Rubber, Polyethylene, and Fluorinated Ethylene–Propylene Copolymer Tested in an Isotonic Saline Solution and Blood Plasma*, †

	Base																	
	Saline									Blood plasma								
	SR control				SR treated				PE treated			SR control				SR treated				PE treated		
Slider	Min	Max	Type	Average force or number of peaks	Min	Max	Type	Average force or number of peaks	Min	Max	Type	Average force or number of peaks	Min	Max	Type	Average force or number of peaks	Min	Max	Type	Average force or number of peaks	Min	Max	Type	Average force or number of peaks
SR treated					9	13	d	$\overline{11}$									48	95	b	2				
					6	24	e	1									10	66	b	2				
					5	29	e	1									10	26	e	1				
																	10	91	e	1				
																	87	87	b	3				
																	75	75	b	3				
PE control	30	30	d	$\overline{11}$									16	21	d	$\overline{14}$								
	18	18	d	$\overline{12}$									13	50	c	3								
	124	220	a	7									17	17	d	$\overline{11}$								
	180	180	a	8									90	90	a	7								
													21	25	a	$\overline{17}$								
PE treated	44	110	c	5					9	12	d	$\overline{9}$	17	105	b	2					11	50	b	2
	55	55	d	$\overline{26}$					9	13	d	$\overline{11}$	13	16	d	$\overline{13}$					15	57	b	4
	38	38	d	$\overline{24}$					10	15	d	$\overline{8}$	12	14	d	$\overline{13}$					10	60	b	3
													27	90	b	2					22	62	b	1
													21	70	b	5					6	16	d	$\overline{18}$
FEP control	116	200	a	11									28	50	c	$\overline{37}$								
	220	300	a	7									24	35	d	$\overline{37}$								
	160	160	a	9									21	21	d	$\overline{16}$								
													30	30	d	$\overline{27}$								
													20	20	d	$\overline{14}$								
													31	31	d	$\overline{15}$								
FEP treated					12	21	d	$\overline{14}$									13	20	d	$\overline{14}$				
					9	15	d	$\overline{12}$									12	24	d	$\overline{16}$				
					9	16	d	$\overline{9}$									12	29	d	$\overline{23}$				
																	21	36	d	$\overline{24}$				
																	17	29	e	1				

*Friction generated in the blood plasma environment was generally lower than in either distilled water or saline environment.

†See Table 1 for explanatory notes.

vironments of singly distilled filtered water, an isotonic saline solution,* and expired blood plasma†. The speed used to slide the sled over the base was constant at 0.25 cm/s for all determinations.

The sled was attached to the silk fishing line by means of a hook designed for this purpose. The sled with attached polymer was then placed on top of the base polymer, and most air trapped between the two surfaces was eliminated by gently pressing on the sled. The sled was then removed from the base, yet kept in the friction environment, and placed gently atop the base before being pulled across it. This procedure helped to ensure that the real area of contact was due to the 20 g load and not the added pressure used for squeezing out air bubbles.

The force required to pull the slider over the base was measured by the load cell and recorded by a strip chart recorder. Graphs can be interpreted as force versus time or force versus sliding distance along the base. The slider speed was 0.25 cm/s and the recorder speed was 0.25 cm/s. The actual distance along the base during which a particular force was encountered can be determined from the graph.

Results were interpreted both quantitatively and qualitatively (Tables I and II). The "MIN" column on these tables is the force required to produce the first peak in the force versus sliding distance graphs. The "MAX" column gives the maximum force encountered during the experiment. Depending upon the type of results obtained, either the number of peaks or the average force required to move the slider was recorded in the tables.

DISCUSSION

The graphs produced for the friction between surfaces of PVC, PE, and SR in aqueous environments varied a great deal. Some were very smooth; others had frequent, high-amplitude spikes; still others had low-frequency, low-amplitude spikes. At least five different types of behavior were noted. They are described below and depicted in Figures 2 and 3.

Type A: Many high-amplitude, low-frequency spikes were seen in the force versus slider distance graph. The peaks were sharp with steep slopes.

Type B: High-amplitude, low-frequency spikes were separated by sections of lower force. Rise time was greater for these peaks than in type A. Peaks were sharp and fell rapidly, but rose slowly.

Type C: Low-amplitude, high-frequency spikes predominated.

* McGaw Laboratories, Division of American Hospital Supply Corp., Irvine, CA.
† University of Utah Hospital Blood Bank, Salt Lake City, UT.

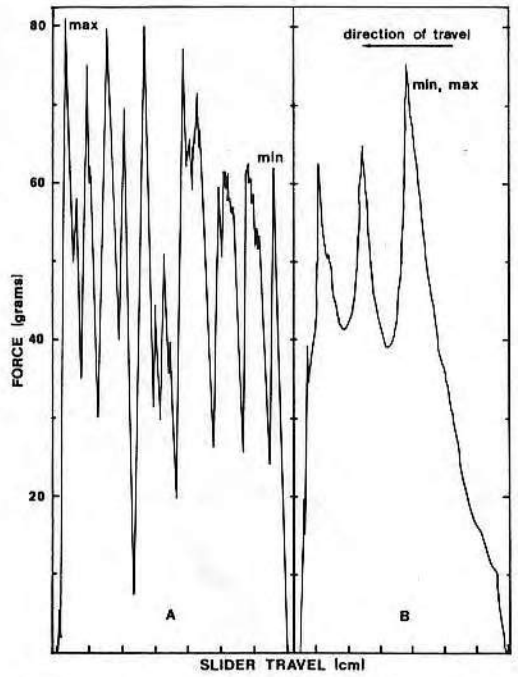

Figure 2. Representative graphs produced by friction types A and B. Type A appeared to be indicative of "stick-slip" friction. Type B appeared to be intermediate between types A and C (Fig. 3). Energy was released from the polymer more slowly than it was dissipated (accounting for the rise in the peak) until a critical level was reached and the energy was suddenly released. "Min" is the amount of force recorded as the first peak value. "Max" is the maximum force value obtained. See text for a more complete explanation.

Type D: A relatively smooth curve was obtained, usually with a slight spike at the beginning of the force versus distance curve, followed by a relatively flat graph at a nearly constant force.

Type E: Another smooth curve was produced, but this time the force required to keep the slider moving gradually increased with time.

The possible mechanisms responsible for the behavior that produced these curves are discussed below.

The number of spikes was recorded for the graphs (types A and B) that produced them. The area under the smooth curves was measured and converted into an average force for graph types C, D, and E. The area and number of peaks are recorded in Tables I and II.

Type A behavior appeared to be indicative of stick-slip friction of elastomers. The following mechanism is proposed to account for the observed behavior. When the two surfaces touched, a bond was formed between the slider and base because of mechanical interlocking and/or adhesive forces. In the case

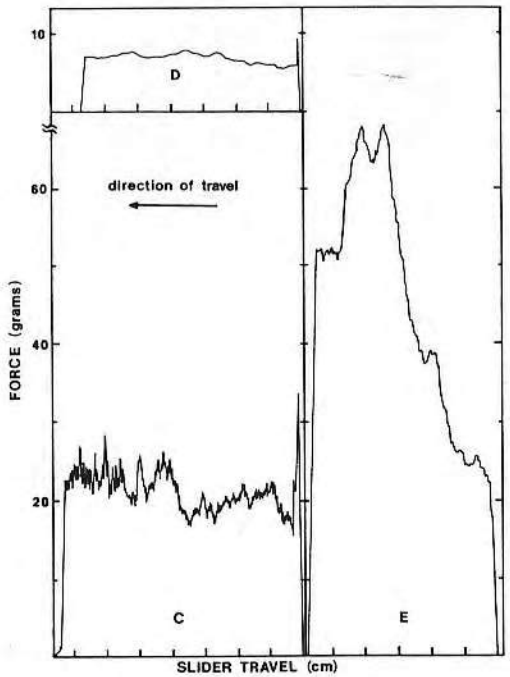

Figure 3. Representative graphs produced by friction types C, D, and E. Type C is similar to type A behavior except the surfaces were more rigid and/or the interfacial forces were not as great and/or the surface region of one of the two polymers was weak. Type D behavior is that which we would expect from frictional phenomena. An initially high resistance to friction indicative of static friction is followed by a region of nearly constant resistance indicative of dynamic friction. Type E behavior appears to be intermediate between types A and D. See text for details.

of the rigid solids, the bond had to be disrupted or mechanical failure of either of the solids had to occur before the slider could move. For the elastomers, however, a certain amount of elasticity was present in the surface layers. The surface could be stretched, storing energy in the elastomer. Eventually a point was reached where the crosslinked polymer chains could not be stretched any further without mechanical rupture of the material. If the cohesive force of the polymer exceeded the adhesive forces at the interface, interfacial failure occurred. If the adhesive force was greater than the cohesive force of the polymer, failure of the elastomer surface occurred. Normally, wholly interfacial or wholly cohesive failure does not occur and a combination of both is seen.[25] It is not known whether interfacial or cohesive failure dominated in this friction study.

The buildup of force in the force versus distance curves in type A behavior was created by the storage of energy in the elastomer before interfacial bond or cohesive failure occurred. The sharp drop at the other side of the peak occurred when the energy was released and the slider actually jumped forward on the base. This was observed for most samples exhibiting type A behavior. This jumping was probably caused by elastic recovery of the elastomer.

The surface mechanical properties probably determined how far the elastomer stretched before yielding. Increased crosslinking of the polymer chains would lead to a more rigid elastomer which would not store energy as well as a more loosely crosslinked network. More rigid polymers and elastomers would not, then, be expected to store as much energy as less rigid elastomers, yet they would not behave as totally rigid solids because some mobility of the chains at the polymer surface is possible.

Type C behavior, with high-frequency, low-amplitude spikes, was probably caused by the same mechanism as type A behavior, except the surfaces were more rigid and/or the interfacial forces were not as great, and/or the surface region of one of the two polymers was weaker. Increased rigidity would decrease the amount of energy that could be stored in the polymer and could cause adhesive or cohesive failure to occur more quickly. Lower interfacial forces or a mechanically weak surface layer would fail before a significant force was required to slide the polymers past each other. Stick-slip behavior could still occur; however, the amplitude of the force spikes would be decreased and they would occur with higher frequency. This is an apt description of type C behavior.

Type D behavior is usually associated with frictional phenomena. The initial force required to cause the surfaces to slide past each other was greater than the force required to keep them in relative motion. That is, static friction exceeded dynamic friction. Not much energy was stored in either surface, and interfacial bond or cohesive failure occurred readily and consistently at the same level.

Type E behavior was most likely caused by a combination of type D and type A behaviors. There was a net storage of energy in either of the polymer surfaces as a result of the force exerted there, resulting in an increased force required to keep the surfaces in relative motion. The degree to which the energy was stored, however, was less than that in type A behavior, and an abrupt failure of the interfacial forces or surface layers did not occur during the period of sliding examined in this experiment. Rather than an abrupt drop in the force, perhaps a plateau value would eventually have been reached where the net energy input was balanced by the elastic recovery of the system.

Type B behavior appeared similar to type A behavior, since it, too, produced spikes, and to type E behavior, since its rise time was also slower. Energy was released by the polymers, but not as quickly as it built up, accounting for the rise in the curves. When the energy reached a critical value, possibly because it was expended during the disruption of interfacial or cohesive bonds, it was released suddenly and a sharp fall occurred in these curves.

In general, those pairs of surfaces that exhibited type D or E behavior had a lower coefficient of friction that those that exhibited type A or B behavior; type C behavior fell midway between the two. Type A behavior is the least desirable because the spikes produced could be great enough to result in mechanical failure of the bulk as well as the surface of a material. Type D behavior is most desirable because no spike situation occurs and the force required to keep the slider moving is constantly low. The data are now analyzed with respect to the above discussion.

The results for friction studies in filtered, distilled water are displayed in Table I. The data are most easily interpreted by looking at four blocks simultaneously: for example, SR slider, treated and untreated, on SR base, treated and untreated. This reveals that the two treated surfaces exhibited types E and D behaviors with an average force of approximately 20 g required to keep the slider moving. In contrast, the two untreated surfaces exhibited type A behavior with forces in excess of 200 g experienced at some of the peaks. It is obvious that the RFGD treatment resulted in some change of surface properties that reduced the friction between the two surfaces. The SR (slider) versus FEP (base) results reveal that the two treated surfaces had the lowest coefficient of friction. Similar results were obtained for SR on PE.

The greatest differences are noted between SR untreated and treated surfaces when SR was the base. The treated surface always exhibited a lower coefficient of friction.

All but one of the PE versus FEP, FEP versus PE, PE versus PE, and FEP versus PE curves exhibited low-friction type D behavior. Some differences can be noted between the friction produced by these surfaces, but they are not nearly as striking as those for the SR.

The reasons for the preferred frictional properties of the RFGD-treated SR could be any or all of the following:

(1) Its hydrophilic surface could adsorb a water layer which acts as a lubricant by increasing the distance between the sliding surfaces so that short range adhesive forces are ineffective. A hydrodynamic friction regimen may be encountered.[14]

(2) The predominantly SiO_2 surface as revealed by XPS could favor low adhesion. Either it was a very weak layer and was disrupted easily or it was a strong, rigid surface that did not store energy. A rigid surface in combination with a low interfacial adhesive force (see above) would produce a low-friction surface.

(3) A surface roughness effect not revealed by SEM could lead to decreased mechanical interlocking of the opposing surfaces. Roughness could also result in a change in the wetting behavior of the polymer surfaces.

Six slider/base polymer pairs were selected for friction studies in a saline environment. These are listed in Table II. The results parallel those found in filtered, distilled water with the following exception: the treated PE slider on the control SR base exhibited type D behavior and a lower coefficient of friction. No explanation was apparent for this finding.

Studies in blood plasma

The maximum force values determined for friction in blood plasma were generally lower than those found in filtered, distilled water or saline. This difference was probably caused by adsorption of proteins from the blood plasma onto the polymer surfaces. The proteinaceous layer was not nearly as coherent as the underlying polymer, and interfacial failure could readily have occurred here. In itself, this layer might also have served as a gel-like layer, separating the true surface of the sliding polymers and resulting in decreased adhesion between the surfaces.

Very little type A behavior was noted. Even for an FEP control slider on an SR control base, the combination yielding the highest force values in distilled water and saline environments, type D behavior predominated and the frictional force was low.

For treated PE on treated PE, the behavior changed from predominantly type D behavior in water and saline to predominantly type B behavior in plasma. In fact, type B behavior occurred much more frequently in plasma than in either saline or water for all polymer pairs studied, indicating that this behavior was most probably produced by the plasma environment rather than by the polymers themselves. Protein adsorption and subsequent shearing or disruption of the adsorbed film was indicated as the probable cause of the change in behavior.

In general, the results for plasma appeared less varied than those for water or saline. The behavior of the adsorbed protein at the interface most probably determined the interfacial phenomena and was less variable than the behavior of the treated and untreated polymers investigated.

CONCLUSIONS

Friction experiments revealed that RFGD-treated SR (300 s) generates less friction than control SR when dragged across all treated and untreated polymer surfaces, whether the medium was filtered, distilled water, or an isotonic saline solution. This was not the case in a blood plasma medium where the presence of adsorbed proteins probably dominated the interfacial phenomena associated with friction. Friction was consistently lower in the blood plasma environment.

It appears that RFGD treatment of two catheter systems, especially those employing SR catheters, could substantially improve their frictional properties from the standpoint of ease of manipulation. A steady infusion of isotonic saline should be maintained and blood should be kept from accumulating between the catheters as much as possible in order to avoid thrombus formation. Treating the outside surface of the SR catheter without treating the inside surface of the catheter in which SR travels should be sufficient to improve frictional characterists of two-catheter systems employing SR as an inner catheter material. The composition of the outer catheter, whether it is fabri-

cated of PE, FEP, PVC, or even PS, should not affect the improved frictional performance of the treated SR catheter. Preliminary platelet retention tests indicated that the treated catheter might also be less thrombogenic. Modification of the outside surface of the SR catheter by RFGD and subsequent *in vivo* trials are suggested. A method must be found or developed, however, whereby one can assure a uniform treatment of the entire catheter surface.

Alternatively, introducing a steady flow of blood plasma between the catheters or preequilibrating the catheters in plasma proteins might reduce the friction between them, providing coagulation could be minimized. These methods are suggested and require subsequent tests to reveal the permanence, effectiveness, and biocompatibility of the treated surfaces.

Friction studies are necessary as a function of the number of passes the oxidized surfaces make over each other to see if the surfaces remain patent and reduced friction is still maintained. It is also necessary to see what effect an increased load will have on the modified surfaces.

Elucidation of the mechanism(s) responsible for the reduced friction of RFGD-treated SR would add to the understanding of the frictional process. SR with different crosslink densities could be investigated to see if the mechanical properties of the surface of the polymer are more important in determining its frictional characteristics than its chemical nature.

References

1. P. M. Triolo and J. D. Andrade, "Surface Modification and Evaluation of Some Commonly Used Catheter Materials. I. Surface Properties," preceding article, *J. Biomed. Mater. Res.*, **16**, 129–147 (1982).
2. J. J. Bikerman, "Adhesion in Friction," *Wear*, **39**, 1–13 (1976).
3. J. K. Lancaster in *Polymer Science*, A. D. Jenkins, Ed., North-Holland, Amsterdam, 1972, chap. 14.
4. B. J. Briscoe and D. Tabor, in *Polymer Surfaces*, D. T. Clark and W. J. Feast, Eds., Wiley, New York, 1978, chap. 1.
5. F. P. Bowden and D. Tabor, in *The Friction and Lubrication of Solids*, Parts I and II, Clarendon, Oxford, England, 1964.
6. D. G. Flom and A. M. Buech, "Theory of Rolling Friction for Spheres," *J. Appl. Phys.*, **30**, 1725–1730 (1959).
7. W. D. May, E. L. Morris, and D. Atack, "Rolling Friction of a Hard Cylinder over a Viscoelastic Material," *J. Appl. Phys.*, **30**, 1713–1724 (1959).
8. J. A. Greenwood and D. Tabor, "The Friction of Hard Sliders on Lubricated Rubber: The Importance of Deformation Losses," *Proc. Phys. Soc.*, **71**, 989–1001 (1958).
9. A. Schallamach, "Abrasion of Rubber by a Needle," *J. Polym. Sci.*, **9**, 385–404 (1952).
10. B. V. Deryagin, "Problems of Adhesion," *Research, London*, **8**, 70–74 (1955).
11. S. M. Skinner, R. L. Savage, and J. E. Rutzler, "Electrical Phenomena in Adhesion. I. Electron Atmospheres in Dielectrics," *J. Appl. Phys.*, **24**, 438–450 (1953).
12. H. G. Von Harrach and B. N. Chapman, "Charge Effects in Thin Film Adhesion," *Thin Solid Films*, **13**, 157–161 (1972).
13. J. H. Israelachvili and D. Tabor in *Progress in Membrane Science*, J. F. Danielli, M. D. Rosenberg, and A. D. Cadenhead, Eds., Academic, New York, 1973, Chap. 1.
14. W. Adamson in *Physical Chemistry of Surfaces*, 3rd ed., W. Adamson, Ed., Wiley, New York, 1976, chap. 10.
15. F. P. Bowden and E. H. Freitag, "The Friction of Solids at Very High Speeds I. Metal on Metal II. Metal on Diamond," *Proc. R. Soc. London*, **A248**, 350–367 (1958).
16. W. B. Hardy and I. Bereumshaw, "Boundary Lubrication—Plane Surfaces and the Limitations of Amonton's Law," *Proc. R. Soc. London*, **A108**, 1–27 (1925).
17. W. B. Hardy, Collected Works, Cambridge University Press, Cambridge, England, 1936.
18. H. W. Lox and W. A. Zisman, "The Spreading of Liquids on Low-Energy Surfaces. III. Hydrocarbon Surfaces," *J. Colloid Interface Sci.*, **7**, 428–442 (1952).
19. S. C. Cohen and D. Tabor, "The Friction and Lubrication of Polymers," *Proc. Roy. Soc. London*, **A291**, 186–207 (1966).
20. A. Schallamach, "How Does Rubber Slide?" *Wear*, **17**, 301–312 (1971).
21. H. Yasuda and H. C. Marsh, "ESCA Study of Polymer Surfaces Treated by Plasma," *J. Polym. Sci. Polym Chem.*, **15**, 991–1019 (1977).
22. M. Hudis and L. E. Prescott, "A Study of the Contact Angle on RTV-Silicone Treated in a Hydrogen Glow Discharge," *J. Appl. Polym. Sci.*, **19**, 451–459 (1975).
23. M. Hudis, in *Techniques and Applications of Plasma Chemistry*, J. R. Hollahan and A. T. Bell, Eds., New York, 1974, chap. 3.
24. D. T. Clark and A. Dilks, "ESCA Applied to Polymers. XVIII. RF Glow Discharge Modification of Polymers in Helium, Neon, Argon, and Krypton, *J. Polym. Sci.*, **16**, 911–936 (1978).
25. J. J. Bikerman, *The Science of Adhesive Joints*, 2nd ed. Academic, New York, 1968.

Received August 1981
Accepted July 29, 19892

JOURNAL OF COLLOID AND INTERFACE SCIENCE 173, 16–27 (1995)

Adsorption of Globular Proteins at the Air/Water Interface as Measured via Dynamic Surface Tension: Concentration Dependence, Mass-Transfer Considerations, and Adsorption Kinetics

BRIAN C. TRIPP,*,[1] JULES JOHN MAGDA,† AND JOSEPH D. ANDRADE‡

*Purification and Formulation Process Development, Genetics Institute, Inc., One Burtt Road, Andover, Massachusetts 01810;
†Department of Chemical and Fuels Engineering, University of Utah, 3290 MEB, Salt Lake City, Utah 84112; and
‡Department of Bioengineering, University of Utah, 2480 MEB, Salt Lake City, Utah 84112

Received April 8, 1994; accepted December 13, 1994

The pendant drop technique was used to measure the dynamic surface tension (DST) of eight globular proteins at the air/water interface as a function of protein bulk concentration (C_b) at C_b values of 0.01, 0.1, and 1.0 mg/ml. Initial periods of negligible decrease in the DST ("induction times") were observed for many of the proteins at C_b = 0.01 mg/ml, but were less common at higher C_b values. DST kinetic parameters varied by up to several orders of magnitude for different proteins, even those with similar bulk diffusion coefficients. All eight proteins achieved initial values of the mesoequilibrium surface tension (MST) within 15 h at C_b = 1.0 mg/ml, although only four of the proteins attained steady-state surface tension within this time. The 15-h MST value at C_b = 1.0 mg/ml did not vary much among the eight proteins, with an average value of 47 ± 6 mN/m. The DST data were numerically modeled by a 4-parameter Hua–Rosen equation and analyzed with respect to protein surface hydrophobicity, conformational stability, bulk depletion effects, and the apparent vs theoretical diffusion-limited rate of adsorption.

Key Words: Air/water interface; protein adsorption; surface tension.

INTRODUCTION

Many proteins lose their biological activity ("denaturation") after exposure of their solutions to the air/water (A/W) interface (1–4). This is due to adsorption and unfolding processes resulting from the amphiphilic (polar/nonpolar) nature and marginal stability (5) of globular proteins. This phenomenon is theoretically interesting and practically important because it can result in undesirable aggregation and precipitation of commercially important proteins (6). Furthermore, the A/W interface is a hydrophobic/hydrophilic interface which serves as a good model for blood/biomaterial interfaces important to biotechnology (7, 8).

Numerous surface tension studies have previously been performed on globular protein solutions (7–50). This work discusses experimental dynamic surface tension (DST) behavior of eight well-characterized globular proteins as measured by the pendant drop surface tension method. DST measurements were performed as a function of bulk solution protein concentration (C_b). The proteins used were hen egg lysozyme (Lys), bovine ribonuclease A (RNase), equine myoglobin (Myo), tuna heart cytochrome *c* (Cyt *c*), bovine erythrocyte superoxide dismutase (SOD), bovine milk β-casein (β-Cas), recombinant human growth hormone (hGH), and bovine serum albumin (BSA). Some key physical and structural properties of these proteins are listed in Table 1 (51–63). These eight proteins differ greatly in their amino acid composition, secondary structure, conformational stability, and surface distribution of nonpolar amino acid residues.

THEORETICAL CONSIDERATIONS

Protein structural hardness. Globular proteins with a high degree of conformational stability and a low degree of flexibility are considered to be rigid or "hard" (9, 64, 65) and tend to resist large, irreversible changes in conformation upon adsorption at interfaces (66). Conversely, "soft" globular proteins are relatively flexible and can rearrange their tertiary structures to facilitate adsorption at interfaces. Hard proteins are generally identified by their relatively great resistance to thermal, chemical, and shear-induced denaturation. Hard *single-domain* proteins may tend to have greater numbers of intrachain disulfide bonds, which result in more rigid folded structures.

Protein foamability. Foamability, as defined by the amount of foam created upon rapid mechanical mixing of an aqueous, surfactant-free protein solution with air, is another physical property indicative of protein hardness. Solutions of hard proteins should exhibit relatively low foamability, because the thin interfacial films of foam bubbles are thought to be stabilized by extended amphiphilic polymer segments of unfolded proteins, rather than by compact na-

[1] To whom correspondence should be addressed.

0021-9797/95 $12.00

TABLE 1
Model Globular Protein Physical and Chemical Properties

Protein	IEP[a]	Secondary[b]	No. aa[c]	MW[d] (kDa)	No. S-S[e]	T_m[f] (°C)	HIC[g] (min)	Foam[h] (mm)
Lys[i]	10.7	4-α/5-β	129	14.4	4	70	18.0	0.1
RNase[j]	9.6	3-α/3-β	124	13.7	4	68	8.7	1.5
Myo[k]	7.4	8-α	153	18.8	0	77	8.0	1.0
Cyt-c[l]	10.0	5-α	103	11.4	0	60	8.2	2.0
SOD[m]	4.6	8-β	151	15.5	1	92	7.3	0.5
β-Cas[n]	5.0	Random	209	24.1	0	—	∞	16
hGH[o]	5.0	4-α	146	22.0	2	81	16.0	16
BSA[p]	4.9	α(3-D)	582	67.0	17	65	6.7	15

[a] IEP is the abbreviation for the isoelectric point, the pH value at which the protein has zero net charge.

[b] This is the number of α-helices and β-sheet strands (secondary structures), as determined from X ray crystal structures. The 3-D notation for BSA denotes that it has three probable structural domains.

[c] No. aa denotes the number of amino acid residues in the protein primary sequence.

[d] MW is the molecular weight, in kiloDaltons, of the unglycosylated form of each protein.

[e] No. S-S is the number of covalent cross-links present in each protein structure, disulfide bonds either between cysteine residues or between cysteine residues and prosthetic heme groups.

[f] T_m is the thermal denaturation (melting/unfolding) temperature of each protein, as determined from differential scanning calorimetry of a C_b = 1–5 mg/ml solution of protein in pH = 7.4, standard buffers, as measured via a Hart Scientific Model 4207 differential scanning calorimeter, with an upward scan rate of 1°C min.

[g] Experimental retention time of 50–100 μl of protein at C_b = 1.0 mg/ml, in PBS buffer, in a 10-mm diameter × 10-cm length Pharmacia phenyl sepharose hydrophobic interaction chromatographic column, at T = 24°C, a pressure of 1.5 MPa, and a fluid flow rate of 0.7 ml/min. The eluting proteins were detected by measuring the elutant adsorbance at a wavelength of 280 nm, as recorded on a timed pen plotter. The retention times were estimated by using the time of maximum UV absorbance of the eluting protein peak.

[h] Foam height of 5 ml of pH = 7.4, C_b = 1.0 mg/ml protein solution, shaken for 30 s and allowed to coalesce for 30 s inside a 20-ml glass scintillation vial.

[i] Jollés and Jollés (51), Perutz (51), and Sarma (53).

[j] Dayhoff (54).

[k] Chmelík *et al.* (55).

[l] Mathews (56) and Dickerson (57).

[m] Richardson (58) and Getzoff (59).

[n] Dickinson and Stainsby (60).

[o] De Vos *et al.* (61).

[p] Peters (62) and Hamilton *et al.* (63).

tive-structure globular proteins (67). Thus, foamability is a measure of how easily protein molecules are unfolded by shear stress and exposure to the A/W interface. The foamability of globular proteins also directly correlates with their affinity for the A/W interface (68–70).

Protein effective surface hydrophobicity. The number and distribution of nonpolar amino acid residues on the surface of a globular protein molecule also influences its adsorption behavior at the A/W interface. A folded, globular protein which has many and/or large nonpolar surface regions is considered to have a high effective surface hydrophobicity (ESH), with a high affinity for amphiphilic interfaces, including the A/W interface. Conversely, a folded globular protein molecule with few and/or small nonpolar surface regions has a low ESH and a low affinity for the A/W interface. The ESH of a protein can be experimentally evaluated by hydrophobic interaction chromatography (HIC), a nondenaturing chromatographic procedure (71). Proteins with longer retention times in a HIC column are indicative of higher ESH values.

Both conformational stability and surface hydrophobicity influence the extent and rate of interfacial protein adsorption (9). Soft proteins with high ESH values should have fast adsorption rates, as indicated by rapid rates of DST decrease. Hard proteins with low ESH values should have slow adsorption rates, as reflected by slower DST kinetics. This hypothesis was examined via DST measurements on the eight previously discussed model proteins.

Surface tension kinetic regimes. For surface-active proteins, the general adsorption process at the A/W interface may be considered to be a three-step process (10–13, 21):

Step 1. Diffusion of solute molecules from bulk solution to the subsurface region.

Step 2. Adsorption of molecules from subsurface to the A/W interface.

Step 3. Conformational rearrangement of adsorbed protein molecules.

As protein molecules adsorb at the A/W interface, the surface tension (γ) will dynamically decrease from the pure

solvent value, until some lower equilibrium value is attained. The equilibrium surface tension is attained by solutions of structurally complex polymer surfactants only when adsorbed surfactant molecules have achieved both equilibrium surface concentration and conformation. The nonequilibrium surface tension is a function of both the adsorbed surfactant surface concentration (Γ) and the surfactant conformation. DST data are sensitive to all three steps in the adsorption process. Thus, DST measurements can be used to indirectly monitor the process of surfactant adsorption at the A/W interface. However, the dynamic and equilibrium surface tension of aqueous surfactant solutions are not directly proportional to Γ, at all possible values of Γ.

The DST of aqueous surfactant solutions can be characterized by up to three general kinetic surface tension regimes (72), prior to attainment of equilibrium surface tension, as illustrated in Fig. 1. The first possible regime is the induction time, during which $\gamma(t)$ remains nearly equal to the pure solvent value, with little or no apparent decrease. At very low values of Γ, the interface possesses the physicochemical properties of water, with an equilibrium surface tension characteristic of pure water, e.g., (73, 74). The solution surface tension will decrease from the pure solvent value only after a significant amount of surfactant has adsorbed at the A/W interface. For globular proteins adsorbing at the A/W interface, approximately 50% of the monolayer surface concentration must be attained before the surface tension will decrease significantly from the pure buffer value (16, 21, 22, 32, 36, 41, 43). Under dynamic conditions, the decoupled surface tension-surface concentration functionality at low values of the surface concentration may result in the observation of an induction time in the initial DST from milliseconds to hours. Induction times are not always observed, especially for highly concentrated or rapidly adsorbing surfactant solutions. In this work, the induction time is defined as the time after formation of the fresh A/W interface during which the magnitude of the rate of DST decrease ($|d\gamma/dt|$) is less than 0.2 mN/m-min and including any time of initial *increase* in the DST.

The second kinetic surface tension regime is depicted in Fig. 1 by regime 2 and is characterized by a rapid rate of decrease in γ, with point values of $d\gamma/dt$ for proteins in the range of -0.2 to -10 mN/m-min. Observation of this DST kinetic regime indicates that Γ is between 50% and 100% of its equilibrium value, i.e., full monolayer/multilayer surface coverage (21). If the surfactant C_b is relatively high and/or adsorption at the A/W interface is rapid, this will be the first DST kinetic regime observed.

The third DST kinetic regime is the mesoequilibrium surface tension (MST) regime, indicated by regime 3 in Fig. 1. Attainment of the MST regime is indicated by a large decrease in the magnitude of the DST slope, at the end of regime 2, with $d\gamma/dt$ values ranging from -0.02 to -0.001 mN/m-min for mesoequilibrium and $0.0 > d\gamma/dt > -0.001$ mN/m-min for equilibrium/steady-state (regime 4 in Fig. 1). The slow rate of decrease in γ during the MST regime is probably due to molecular reorientation and conformational changes in the adsorbed protein molecules. Slow rates of decrease in the long-term MST have been observed for solutions of proteins (21), liposomes (75), and other structurally complex polymer surfactants (72, 76, 77). Attainment of steady-state surface tension during the MST regime indicates that the adsorbed surfactant molecules have achieved their equilibrium conformation and surface concentration at the A/W interface.

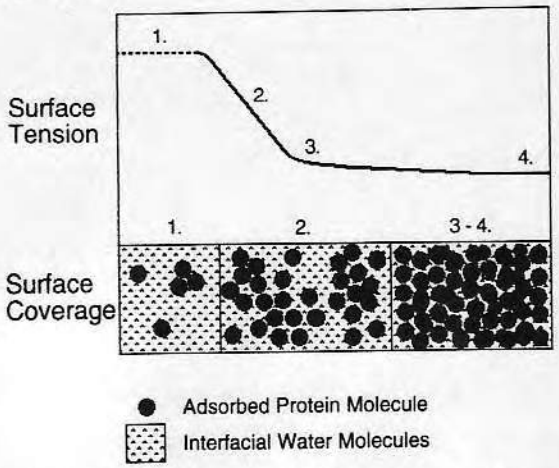

FIG. 1. Idealized diagram of dynamic surface tension–surface coverage relationship, illustrating the three possible dynamic surface tension kinetic regimes: 1, induction time, low to half monolayer surface coverage (optional, more commonly observed for lower C_b values and/or slowly adsorbing surfactants); 2, rapid surface tension decrease, half to full monolayer surface coverage; 3, mesoequilibrium surface tension, slow further decrease in surface tension, due to conformational changes (unfolding), packing rearrangements, ultimately resulting in 4, the equilibrium (steady-state) surface tension.

MATERIALS AND METHODS

Proteins and buffer solutions. The proteins used in this study were all single-domain proteins, with the exception of BSA, which has three domains. SOD exists only as a dimer in solution (78), β-Cas occurs in solution as large molecular weight multimers (79), and BSA self-associates in solution to a minor extent (Howard Li, personal communication). All of the other proteins used are present in solution only as monomers, over the range of concentrations used. This was verified during the retention time experiments with a hydrophobic interaction chromatography column, for C_b = 1.0 mg/ml solutions, which yielded single, symmetrical elution peaks, indicative of monomers (80).

3× crystallized and lyophilized hen egg lysozyme (prod. no. L-6876, lot no. 89F8276), tuna heart cytochrome *c* (prod. no. C-2011, lot no. 28F7120), bovine pancreas ribonuclease A type XII-A (prod. no. R-5500, lot no. 80H8020), bovine

milk β-casein (prod. no. C-6905, lot no. 67F9645), and horse skeletal muscle myoglobin (prod. no. M0630, lot no. 69F7165) were purchased from Sigma, St. Louis, Missouri. Crystalline BSA (prod. no. 12657, lot no. 001264) was purchased from Calbiochem, La Jolla, California. Purified bovine liver superoxide dismutase (lot no. 238-52) was purchased from DDI Pharmaceuticals, Inc., Mountain View, California. Recombinant human growth hormone (lot no. PS9033AX-GO42A), was provided by Genentech, Inc., South San Francisco, California. These were the purest commercial grades available of each protein, with small amounts of salts present as contaminants. Purity was demonstrated via sodium dodecyl sulfate–polyacrylamide gel electrophoresis, followed by staining with Coomassie blue, which resulted in single bands for each protein.

The hGH was reconstituted in a pH = 7.4, 0.005 *M* Na_2HPO_4, 0.25 *M* glycine buffer. All other proteins were dissolved in a pH = 7.4 phosphate buffered saline (PBS) solution, with the following composition: 0.0130 *M* KH_2PO_4, 0.0540 *M* Na_2HPO_4, 0.100 *M* NaCl. The components used in the buffers were analytical reagent-grade salts from Mallinckrodt, Inc., Paris, Kentucky. The water was obtained from a Millipore MilliQ reverse osmosis, ion exchange, and filtration apparatus, and had a conductivity of less than 18 Mohm-cm. Concentrated protein solutions (C_b = 1.0 mg/ml) were prepared by gently stirring in a gravimetrically measured amount of lyophilized protein into buffer solution, in a glass beaker, with a glass rod. More dilute solutions were prepared by addition of an aliquot of concentrated protein solution into buffer. Buffer and protein solutions were prepared and used on the same day.

Foamability measurement. Five milliliters of each protein–standard buffer solution at C_b = 1.0 mg/ml was prepared in clean glass 20-ml scintillation-counting vials. The high solution concentration was used in accordance with a recommendation by Kato and Yutani (35), who noted that the lowest protein concentration effective for observing interfacial properties (foaming and surface tension) was 0.5 mg/ml. Each solution was vigorously shaken by hand for 30 s and allowed to settle for 30 s, and then the foam height was measured with a ruler.

Effective surface hydrophobicity measurement. A Pharmacia phenylsepharose 10-mm-diameter × 10-cm-long chromatography column was used as the hydrophobic interaction substrate. The column was pressurized by a Pharmacia fast protein liquid chromatography (FPLC) system at a pressure of 1.5 MPa, a temperature of 24°C, and a fluid flow rate of 0.7 ml/min. The column was equilibrated with fresh PBS buffer (pH = 7.4) for 12 h prior to the experiment. The protein solutions were prepared in their standard buffers, at C_b = 1.0 mg/ml. Fifty to one hundred microliters of each solution was injected into the column, and the eluting solution absorbance was measured at a wavelength of 280 nm and recorded on a timed pen plotter. The retention time for each protein was determined from its maximum elution absorbance value.

Surface tension measurement. Initial DST experiments were performed using the Wilhelmy plate method for surface tension measurement. However, protein adsorption at the three-phase line during use of the Wilhelmy plate technique resulted in poor experimental accuracy and repeatability in DST measurements, as noted by others (9, 39, 43). To avoid these problems, a variant of the pendant drop technique was developed and used for measuring the DST of protein solutions. The pendant drop technique relies on shape analysis of mechanically static pendant drops, either through comparison of characteristic drop dimensions to published tables, or through a numerical analysis of the entire drop shape. The theory of the pendant drop method is derived from the Young–Laplace equation of capillarity and has been described in detail by various authors (81–86). The particular pendant drop method used in this work employed digital image analysis and a Simplex shape-fitting algorithm to determine the surface tension of pendant drops (87) and is termed the digital image pendant drop (DIPD) method. The DIPD method is very sensitive, accurate (±0.2 mN/m), independent of liquid meniscus contact angle, and repeatable within 2%, making it an ideal technique for DST measurement of protein and polymer solutions.

A diagram of the DIPD experimental apparatus is shown in Fig. 2. This apparatus consisted of an Apple Macintosh IIsi computer and a modified timer version of the image

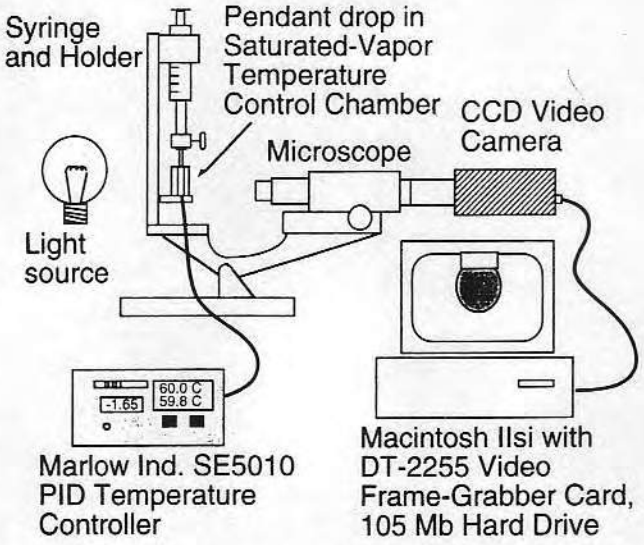

FIG. 2. Schematic diagram of the digital image pendant drop experimental apparatus, with a thermoelectrically heated/cooled environmental chamber for the pendant drop, microscope for image magnification, Sierra Scientific CCD video camera for obtaining grey-scale images of the pendant drop, a Macintosh IIsi computer with Data Translation DT-2255 frame-grabber card for digitization of video signal images, and a 105-Mb hard drive for storage of images.

analysis software *NIH Image* (National Institutes of Health, Bethesda, MD), termed *Image Timer*. This apparatus and software could automatically measure pendant drop data at intervals ranging from seconds to many hours, with a capacity of several hundred pendant drop images per experiment. A 10-gauge (4.17 mm diameter) stainless steel flat-tipped needle was used for suspending the pendant drop inside a controlled-temperature environmental chamber. Other details of the apparatus are given in (87). Stable aqueous pendant drops could be maintained in the environmental chamber for 24 h, with minimal change in volume, under saturated vapor conditions.

Prior to each DST experiment, the stainless steel needle, glass syringes, and connecting valve were ultrasonically cleaned and rinsed in pure ethanol and MilliQ water. Other glassware was cleaned in hot chromic–sulfuric acid and then repeatedly rinsed in MilliQ water. The DIPD device was assembled, heated or cooled to the desired temperature, and humidified, and the image of the needle tip was focused. Several drops of the protein solution were flushed through the system, and then a final stable pendant drop of the desired size was formed (drop volume ~0.04 ml), followed by activation of the data acquisition *Imagetimer* program. The time between drop formation and the beginning of the data acquisition was on the order of 5 s. The specified drop volume, in conjunction with the 10-gauge diameter needle, allowed the surface tension of aqueous solutions to decrease to approximately 30 mN/m, without detachment of the drop. After drop formation and timer activation, the environmental chamber was sealed for the duration of each DST experiment, which typically lasted for 17 h.

RESULTS

Foamability and hardness. Three of the eight model proteins had very high foamabilities (β-Cas, BSA, and hGH), three were slightly foamable (Cyt *c*, Myo, and RNase), and two (Lys and SOD) had very low foamability (Table 1). A comparative analysis of the model protein physical properties indicative of hardness (number of disulfide bonds, foamability, and thermal stability) yielded an approximate hardness ranking of the eight proteins, given in Eq. [1],

$$\text{SOD} > \text{Lys} > \text{RNase} > \text{Myo} > \text{Cyt } c > \text{hGH} > \text{BSA} > \beta\text{-Cas}; \quad [1]$$

SOD, Lys, and RNase had the hardest structures, while hGH, BSA, and β-Cas had the softest structures.

Effective surface hydrophobicity. The HIC retention times of the eight proteins used in this study are listed in Table 1. Of the eight proteins studied, β-Cas had the highest ESH, because it did not elute from the HIC column. Lys and hGH had the second and third highest ESH values, based on their relatively long retention times in the HIC column. The other five proteins had much lower ESH values, with BSA having the lowest ESH value. An approximate ESH ranking, from highest to lowest ESH, is given in Eq. [2]:

$$\beta\text{-Cas} > \text{Lys} > \text{hGH} > \text{RNase} > \text{Cyt } c > \text{Myo} > \text{SOD} > \text{BSA}. \quad [2]$$

Dynamic surface tension. The experimental DST data for each of the eight proteins, at $T = 24°C$, and initial C_b values of 1.0, 0.1, and 0.01 mg/ml (1.0 mg/ml = 0.1 wt.%) are plotted in Figs. 3–10. Many of the proteins exhibited induction times in their initial DST data at the lowest C_b value of 0.01 mg/ml. Only SOD exhibited an induction time at the highest C_b value of 1.0 mg/ml. Various experimental DST parameters for the eight protein solutions are summarized in Table 2, including initial 1-min DST decay rates for $C_b = 1.0$ mg/ml, induction times at 0.01 mg/ml, and 15 h MST values at all three C_b values. The protein DST data in Table 2 are vertically ranked from top to bottom on the basis of the initial rates of DST decrease at $C_b = 1.0$ mg/ml. The induction times were determined from enlarged plots of the initial DST data, subject to the mathematical criteria for induction times described above.

The DST data at $C_b = 1.0$ mg/ml were fit to an empirical Hua and Rosen (72) DST equation via nonlinear optimization with KaleidaGraph running on a Macintosh II computer. One form of the DST equation is given by

$$\gamma(t) = \gamma_m + \frac{\gamma_0 - \gamma_m}{1 + (t/t^*)^n}, \quad [3]$$

where $\gamma(t)$ is the surface tension at any time t, γ_0 is pure solvent surface tension, γ_m is the initial MST value, t is the time following fresh A/W interface formation, t^* is a time constant equal to 50% of the time to attain the initial MST, and n is a dimensionless exponent. Assuming that the value of γ_0 is held constant at the pure buffer surface tension value, there are three adjustable parameters: γ_m, t^*, and n. The value of the parameter t^* can be interpreted as the half-time required to attain the initial MST value. A kinetic parameter, the rate of surface tension decay at t^*, can be computed from the formula

$$\left.\frac{d\gamma}{dt}\right|_{t^*} = \frac{\gamma_0 - \gamma_m}{2t^*}. \quad [4]$$

The values of the fit Hua–Rosen parameters and the computed value of $(d\gamma/dt)_{t^*}$ are listed in the five right-most columns of Table 2.

DISCUSSION

Kinetic analysis. Ideally, a detailed analysis of the protein DST data should yield the surface concentration of adsorbed

TABLE 2
Protein Experimental and Model Dynamic Surface Tension Parameters

Protein	Ind. time C_b = 0.01 (min)[a]	$d\gamma_{ind}/dt$ C_b = 1.0 (mN/m-min)[b]	γ_{MST} C_b = 1.0 (mN/m)[c]	γ_{MST} C_b = 0.1 (mN/m)[d]	γ_{MST} C_b = 0.01 (mN/m)[e]	$d\gamma_{MST}/dt$ C_b = 1.0 (mN/m-min)[f]	$\gamma_{m\text{-}H\&R}$ C_b = 1.0 (mN/m)[g]	$t^*_{H\&R}$ C_b = 1.0 (min)[h]	$n_{H\&R}$ C_b = 1.0 (no unit)[i]	$d\gamma/dt^*_{H\&R}$ C_b = 1.0 (mN/m-min)[j]
β-Cas	1.0	48.7	44.3	47.1	49.4	−0.0014	40.5	0.0074	0.170	2142.0
hGH	0.0	21.2	37.8	43.8	47.7	−0.00050	35.2	0.548	0.360	33.6
Myo	13	13.1	41.6	43.6	44.4	−0.0026	41.2	1.68	0.648	9.17
BSA	0.0	7.0	52.7	53.8	55.2	−0.00074	43.6	6.83	0.150	2.08
SOD	200	3.4	48.0	51.4	55.5	−0.0031	48.7	12.3	1.036	0.947
Cyt *c*	6	5.7	49.9	49.4	49.7	−0.0027	45.1	18.0	0.371	0.747
Lys	40	3.4	46.5	51.5	57.5*	−0.0040	43.4	19.7	0.526	0.727
RNase	300	1.5	(55.4)	60.3	62.8*	−0.0043	51.1	93.1	0.539	0.112

Note. An asterisk indicates that the mesoequilibrium surface tension kinetic regime had not been attained within 15 h at C_b = 0.01 mg/ml, based on the large magnitude of $d\gamma/dt$ at t = 15 h, as shown in Figs. 9 and 10.

[a] Experimentally observed induction time in the initial DST at C_b = 0.01 mg/ml.

[b] Experimental 1 min decrease in initial DST from pure buffer value (72.0 mN/m) at C_b = 1.0 mg/ml.

[c] Experimental value of mesoequilibrium surface tension at t = 15 h for C_b = 1.0 mg/ml, with an error of ±0.2 mN/m. (Note: MST value for RNase was estimated by linear extrapolation of 12 DST data points at times ranging from 750 to 860 min)

[d] Experimental value of mesoequilibrium surface tension at t = 15 h for C_b = 0.1 mg/ml, with an error of ±0.2 mN/m.

[e] Experimental value of mesoequilibrium surface tension at t = 15 h for C_b = 0.01 mg/ml, with an error of ±0.2 mN/m.

[f] Numerically computed value of $d\gamma/dt$, the rate of mesoequilibrium surface tension decay, evaluated from linear fits of DST data at a time of 15 h for C_b = 1.0 mg/ml.

[g] Best-fit value of Hua–Rosen mesoequilibrium surface tension for C_b = 1.0 mg/ml DST data for each protein. (Note: γ_0 was fixed at a constant value of 72.0 mN/m for each of the proteins, based on the equilibrium surface tension value of pure PBS buffer at T = 24°C).

[h] Best-fit value of t^* parameter in Hua–Rosen equation for C_b = 1.0 mg/ml DST data for each protein.

[i] Best-fit value of dimensionless parameter n in Hua–Rosen equation for C_b = 1.0 mg/ml DST data for each protein.

[j] Computed value of $d\gamma/dt$, evaluated at $t = t^*$, for C_b = 1.0 mg/ml from Hua–Rosen equation parameters for C_b = 1.0 mg/ml DST data for each protein.

protein as a function of time and indicate whether the adsorption kinetics were limited by the rate of diffusional mass transfer to the A/W interface or limited by an adsorption energy barrier at the A/W interface. However, the small surface area and curved semi-spherical geometry of a typical pendant drop do not lend themselves to direct measurement of Γ via radiolabeling or ellipsometric methods. Conversion of DST data into surface concentration kinetics by application of polymer two-dimensional equations of state (88–91) requires many simplifying assumptions and may not be valid for nonequilibrium conditions.

The simple form of the Gibbs adsorption equation (92) is also considered to be inapplicable to modeling polymer/protein adsorption at the A/W interface (16, 17, 22, 24, 77) for several reasons. First, the chemical potential of adsorbed, dehydrated, unfolded globular proteins is poorly defined, relative to their solvated native states. Second, the Gibbs equation is valid only for reversible, equilibrium adsorptive processes, while proteins and other polymer surfactants frequently adsorb at the A/W interface in an irreversible manner (22, 24, 77, 93, 94), with greater extents of unfolding observed for slower adsorption rates (93, 95). Proteins adsorbed at the A/W interface may be desorbed by lateral compression of the interface (24, 96, 97), but this may result in precipitation, rather than resolvation of the adsorbed protein (98, 99).

For this work, a simplified approach was used to analyze the DST kinetics. Well-documented relationships between DST values and Γ were combined with limiting-case calculations for bulk depletion and diffusion-limited adsorption to estimate whether the adsorption kinetics of the eight proteins were diffusion-limited or adsorption rate-limited.

After approximately 4 s, any initial convective motion in the pendant drop should have dissipated (87). Surfactant adsorption kinetics at the pendant drop A/W interface may be limited by the rate of diffusional mass transfer from the interior region of the drop to the subsurface region (Step 1) if adsorption-induced bulk depletion is significant (100). Simple bulk depletion calculations performed using average pendant drop physical parameters (drop volume = 0.04 ml, drop surface area = 0.5 cm^2) and experimental equilibrium protein Γ values (Γ = 1–8 mg/m^2), (16, 22, 24, 42, 93, 101) indicate that bulk depletion due to interfacial adsorption is significant (10–100%) only for initial $C_b \leq 0.01$ mg/ml (87). The minimum theoretical time required for complete surface coverage (e.g., monolayer/multilayer) to be attained via diffusion-limited adsorption can be estimated from the equation proposed by Ward and Tordai (102)

$$\Gamma = 2C_b\left(\frac{Dt}{\pi}\right)^{1/2}, \qquad [5]$$

where D is the protein bulk diffusion coefficient, t is the time elapsed since the formation of the fresh A/W interface, and π is the numerical constant 3.1416 . . . .

Simple calculations with Eq. [5] can be used to estimate the theoretical diffusion-limited time required for a specified protein to attain near-equilibrium Γ values. This theoretical adsorption time can then be compared with the experimental time required to attain near-equilibrium surface coverage, as indicated by the time for attainment of the initial MST (as discussed above). The approximate time at which the initial MST is achieved can be estimated from the value of $2t^*$, where t^* is one of the fit parameters in Eq. [3].

This method of kinetic analysis was applied to the DST data of the three proteins β-Cas, BSA, and Lys. The bulk diffusion coefficients, adsorption kinetics, and equilibrium surface tension–surface concentration relationships of these proteins have been experimentally measured by other researchers (16, 21–23, 32, 42, 103). The theoretical diffusion-limited times required for the equilibrium Γ to be attained at $C_b > 0.1$ mg/ml, as calculated for β-Cas, Lys, and BSA, from Eq. [5], indicate that for $C_b > 0.1$ mg/ml, the equilibrium Γ of each protein should be achieved within 0.3 to 4 s (87). The values of $2t^*$ for each protein, at which time the initial MST and the equilibrium Γ were presumably attained, were 0.9 s for β-Cas, 14 min for BSA, and 40 min for Lys. Reasonably close agreement between the theoretical and experimental adsorption times was apparent only for β-Cas, a protein which is known to adsorb at the A/W interface in a diffusion-limited manner (16, 42). The much larger experimental adsorption times observed for Lys and BSA suggest that these two proteins both adsorb in an adsorption rate-limited manner (Step 2), in agreement with experimental radiolabeling studies (32, 42).

The other five proteins used in this study had values of $2t^*$ of at least two orders of magnitude greater than the β-Cas value (Table 2). Four of these five proteins had lower molecular weights (with the exception of dimeric SOD) and much more compact folded structures than the random-coil protein β-Cas, suggesting that their bulk diffusion coefficients and rates of diffusional mass transfer to the A/W interface would be faster than that of β-Cas. However, the much slower DST kinetics observed for these proteins under conditions of minimal bulk depletion suggest that their net rates of adsorption at the A/W interface are limited by some type of energy barrier to adsorption (Step 2).

The significant bulk depletion which can occur at C_b = 0.01 mg/ml may partly account for the long induction times and slow attainment of initial MST values observed for many of the proteins at this C_b. However, the long induction time (ca. 4 min) observed for SOD at C_b = 1.0 mg/ml is probably due to some type of energy barrier to adsorption, as bulk depletion should be insignificant at this C_b. The DST behavior of each of the eight proteins is discussed and analyzed in further detail in the following sections.

β-Cas. The DST behavior of β-Cas (Fig. 3) was similar to the DST behavior exhibited by aqueous solutions of simple detergents at C_b values below their critical micelle concentrations (CMCs). At the highest C_b of 1.0 mg/ml, β-Cas exhibited the fastest initial rate of surface tension decrease of all eight proteins, based on the large values of $d\gamma_{init}/dt$, $d\gamma/dt^*_{H\&R}$, and the small value of $t^*_{H\&R}$ (Table 2). Other researchers have also observed rapid equilibration of β-Cas surface tension at similar C_b values (36, 43). The adsorption of β-Cas at the A/W interface has also been demonstrated to be a reversible process (104). The great flexibility [1] and hydrophobic amino acid composition and surface character [2] of this random-coil protein may both contribute to its high, yet reversible affinity for the A/W interface.

hGH. The initial rate of hGH adsorption at the A/W interface was very rapid, with no induction time observed at any of the experimental C_b values (Fig. 4) and the second fastest initial DST decay rate at C_b = 1.0 mg/ml (Table 2). The equilibrium surface tension of the C_b = 1.0 mg/ml solution (γ = 38 mN/m) was the lowest observed for the eight proteins. hGH has a relatively high ESH [2] and a low degree of hardness [1]. Some surface regions of the folded hGH molecule may be relatively unstructured and flexible, unless the molecule is bound to its receptor protein (61). The rapid adsorption of hGH at the A/W interface may be mediated by partial unfolding and exposure of its strongly amphiphilic α-helices to the nonpolar air phase (30, 31, 36).

Myo. Myo exhibited a measurable induction time at C_b = 0.01 mg/ml (Fig. 5). However, Myo had the third fastest initial rate of DST decrease at C_b = 1.0 mg/ml (Table 2), despite its hydrophilic surface character [2]. At all bulk concentrations studied, the long-term Myo MST converged to approximately the same value of 42 ± 1.0 mN/m within 2–13 h, depending on the C_b value. The long-term MST in-

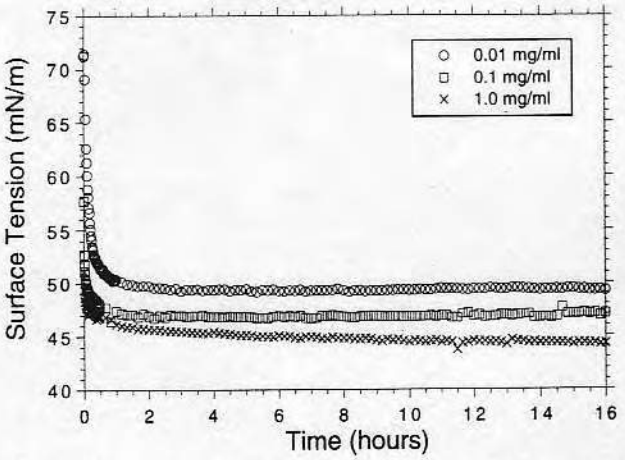

FIG. 3. Dynamic surface tension of bovine β-casein as a function of initial C_b, C_b = 0.01, 0.1, 1.0 mg/ml, T = 24°C, pH = 7.4, 0.125 M phosphate buffer.

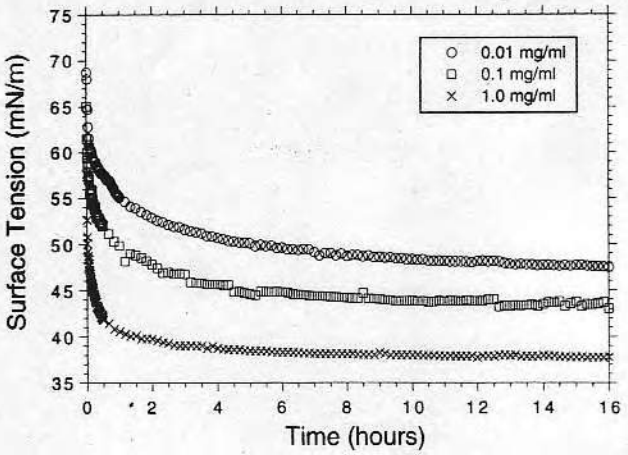

FIG. 4. Dynamic surface tension of human growth hormone as a function of initial C_b, C_b = 0.01, 0.1, 1.0 mg/ml, T = 24°C, pH = 7.4, 0.005 M Na_2HPO_4, 0.25 M glycine buffer.

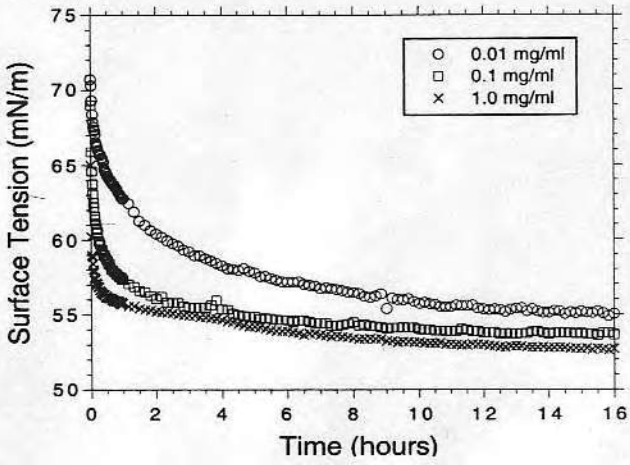

FIG. 6. Dynamic surface tension of bovine serum albumin as a function of initial C_b, C_b = 0.01, 0.1, 1.0 mg/ml, T = 24°C, pH = 7.4, 0.125 M phosphate buffer.

dependence of C_b is similar to the behavior of simple surfactants at C_b values above their CMCs. The high amphiphilic α-helical content of Myo, coupled with its intermediate stability [1] and its low net charge at pH 7.4 (IEP = 7.4, Table 1), may contribute to its apparently rapid adsorption rate.

BSA. BSA (Fig. 6) did not exhibit a measurable induction time at the lowest C_b of 0.01 mg/ml, while the initial DST kinetics at the highest C_b of 1.0 mg/ml were the fourth fastest (Table 2) of all eight proteins. Similar kinetic and long-term DST behavior was also observed for BSA by Watanabe *et al.* (37) and Absalom *et al.* (26). Despite its extremely hydrophilic surface [2], BSA adsorption at the A/W interface appears to be a rapid process. BSA is known to adsorb onto hydrophobic solids (105). It is likely that the relatively soft BSA molecule [1] partially unfolds upon adsorption at the A/W interface (23, 26, 34, 106), possibly via partial unfolding of the least-stable domain I (107). The long-term MST behavior of BSA had a low dependence on C_b, with 15-h MST values in the range of 53–55 mN/m. Similar long-term MST behavior has also been observed by Busscher *et al.* (108), who concluded that BSA had an apparent CMC at C_b = 0.005 mg/ml.

SOD. SOD exhibited very unusual initial DST behavior at both low and high C_b values. At C_b = 0.01 mg/ml, an increase from 68 to 72 mN/m was observed in the initial DST, followed by an extremely long induction time of 200 min (Fig. 7). The reason for this increase in the initial DST is unknown, but this observation was repeatable. At C_b = 1.0 mg/ml an induction time of 4 min was observed in the initial DST. No induction times were observed for any of

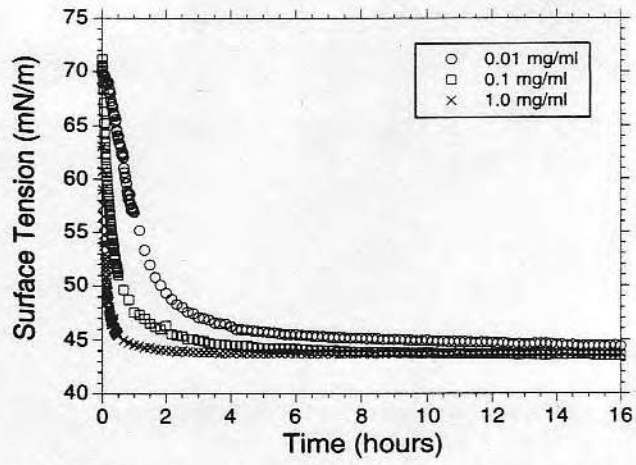

FIG. 5. Dynamic surface tension of equine myoglobin as a function of initial C_b, C_b = 0.01, 0.1, 1.0 mg/ml, T = 24°C, pH = 7.4, 0.125 M phosphate buffer.

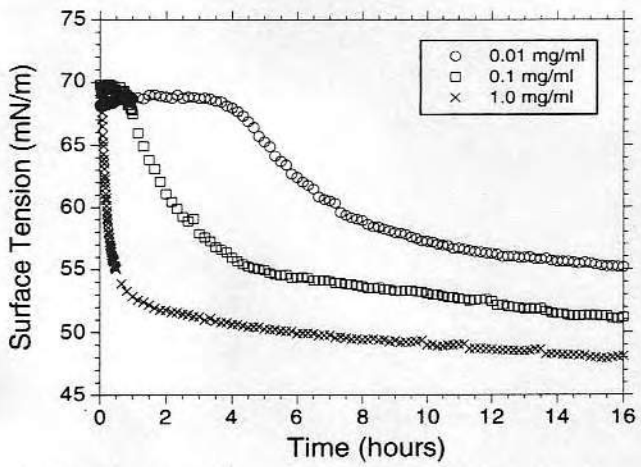

FIG. 7. Dynamic surface tension of bovine superoxide dismutase as a function of initial C_b, C_b = 0.01, 0.1, 1.0 mg/ml, T = 24°C, pH = 7.4, 0.125 M phosphate buffer.

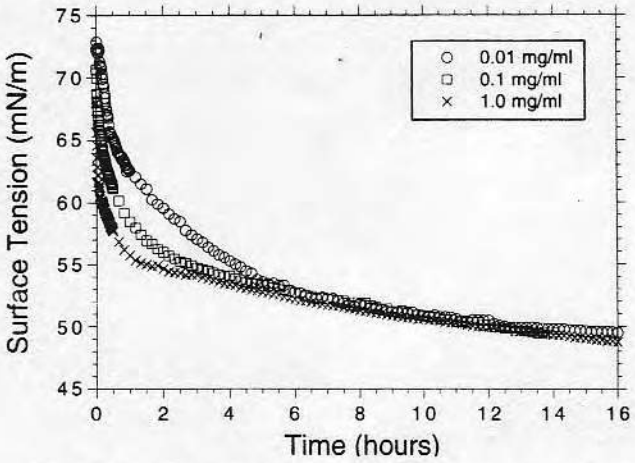

FIG. 8. Dynamic surface tension of tuna cytochrome *c* as a function of initial C_b, C_b = 0.01, 0.1, 1.0 mg/ml, T = 24°C, pH = 7.4, 0.125 *M* phosphate buffer.

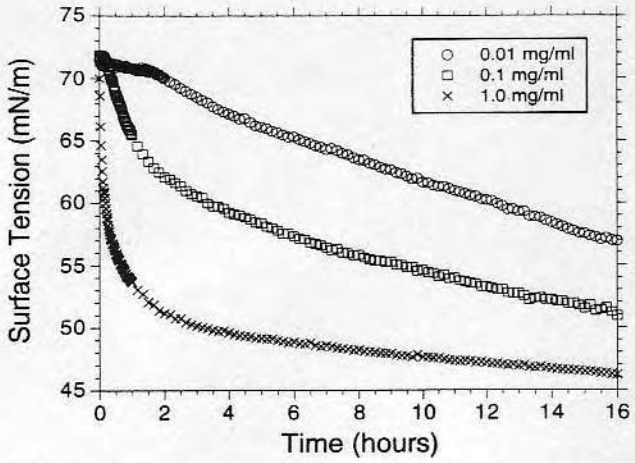

FIG. 9. Dynamic surface tension of hen lysozyme as a function of initial C_b, C_b = 0.01, 0.1, 1.0 mg/ml, T = 24°C, pH = 7.4, 0.125 *M* phosphate buffer.

the other model proteins at C_b = 1.0 mg/ml. Similar initial DST behavior has also been noted for SOD by Wei (9). The long induction times observed for SOD at each C_b suggest a very slow initial rate of SOD adsorption at the A/W interface. SOD is present as a dimer in solution (58, 59), resulting in a larger effective molecular weight and a smaller bulk diffusion coefficient than those of the six other single-domain proteins. However, BSA has a much larger molecular weight than the SOD dimer, yet faster DST kinetics and no induction times (Table 2) were observed for BSA. Thus, the slow apparent rate of SOD adsorption cannot strictly be attributed to mass-transfer limitations; the hydrophilic surface [2] and the great degree of hardness [1] of SOD may also contribute to its slow apparent rate of adsorption.

Cyt c. The short 6-min induction time at C_b = 0.01 mg/ml and the rapid DST decay rate at C_b = 1.0 mg/ml (Table 2) indicate that Cyt *c* adsorbed fairly rapidly, despite its intermediate ESH value [2]. Two important features were apparent in the long-term DST of Cyt *c* (Fig. 8). Like Myo, Cyt *c* exhibited a long-term convergence of its MST, independent of initial C_b value. Unlike Myo, the steady-state surface tension of Cyt *c* was not attained within the time of the experiment, even for the C_b = 1.0 mg/ml solution. The MST continued to slowly decrease in an almost linear manner, even after 16 h, suggestive of a slow unfolding process by adsorbed Cyt *c* molecules.

Lys. The initial DST kinetics of Lys were strongly dependent on C_b (Fig. 9), with induction times of 12 and 90 min observed for C_b values of 0.1 and 0.01 mg/ml, respectively, and a slightly slower DST decay rate at C_b = 1.0 mg/ml than Cyt *c*. Lys has a relatively hydrophobic surface [2], possibly due to a hydrophobic surface patch apparent in its X ray crystal structure (109), which probably dominates its interactions with hydrophobic surfaces (110). Lys has been shown to adsorb irreversibly at the A/W interface (22, 93); this irreversible process may be caused by unfolding upon adsorption (21). Lys is a very rigid protein [1], and the slow rate of decrease in the 15-h MST at C_b = 0.1 and 1.0 mg/ml may reflect a slow process of conformational change. The rate of MST decrease was inversely proportional to C_b, suggesting that the rate and ultimate extent of unfolding by adsorbed Lys molecules were higher when the bulk and surface concentration were lower, as observed in other interfacial adsorption studies (23, 93).

RNase. The initial and long-term DST kinetics of RNase were among the slowest of all the proteins and were very dependent on the C_b. A slow rate of MST decrease was also observed for RNase by Wei (9). At C_b = 0.1 mg/ml, the DST data set was very noisy (Fig. 10), possibly due to an

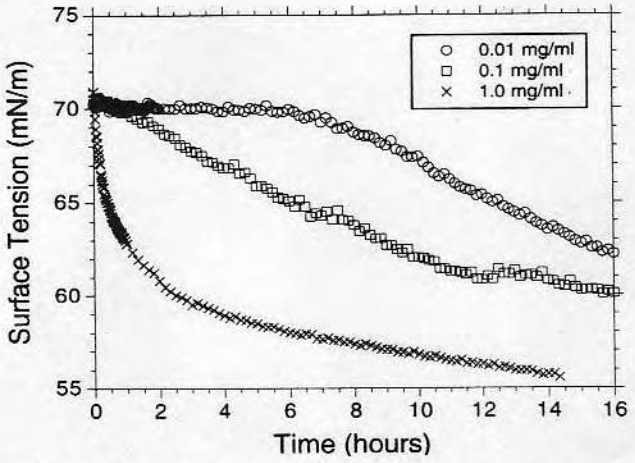

FIG. 10. Dynamic surface tension of bovine ribonuclease *a* as a function of initial C_b, C_b = 0.01, 0.1, 1.0 mg/ml, T = 24°C, pH = 7.4, 0.125 *M* phosphate buffer.

asymmetrical pendant drop shape. RNase can be characterized as a relatively hydrophilic protein [2], with an intermediate hardness [1]. The linear rate of MST decrease at C_b = 1.0 mg/ml suggests that the adsorbed RNase molecules were undergoing a slow conformational rearrangement process, as observed during RNase adsorption at solid–liquid interfaces (111).

Summary. All eight of the proteins adsorbed at the A/W interface, based on the large differences between the pure buffer surface tension and the experimental 15-h MST values at C_b = 1.0 mg/ml. A large degree of variation was observed in the initial DST kinetics of the eight proteins at all experimental C_b values (Table 2). At the highest C_b value of 1.0 mg/ml, the time required for attainment of the initial MST, as estimated from $2t^*$, varied by several orders of magnitude for the different proteins, ranging from 0.9 s for β-Cas to 190 min for RNase. After attainment of initial MST values (at C_b = 1.0 mg/ml), four of the protein solutions exhibited further decreases in their long-term MST, including the three most rigid proteins: Lys, SOD, and RNase [1]. The 15-h experimental MST values at C_b = 1.0 mg/ml did not vary greatly between different proteins, with an average value of $\gamma = 47.0 \pm 5.7$ mN/m. This average MST value is higher than that typically observed for solutions of simple ionic detergents and nonionic polymer surfactants at equivalent C_b values. For example, an aqueous C_b = 1.0 mg/ml solution of Tween 20 has an equilibrium surface tension of 30 mN/m (unpublished data).

At the lowest C_b of 0.01 mg/ml, induction times of the eight proteins varied by over two orders of magnitude (Table 2). Large differences in induction times at low C_b values have also been noted for SOD, Lys, RNase, sperm whale Myo, and Cyt *c* (9), and for β-lactoglobulin, α-lactalbumin, and BSA (49). The initial MST was achieved by six of the eight proteins within 15 h at this C_b, indicating that the adsorption step was over for these six proteins by the end of each experiment. Lys and RNase, two of the most rigid proteins [1], were the only two proteins which did not attain initial MST values at C_b = 0.01 mg/ml, based on the visibly steep slope of their DST data at t = 15 h (Figs. 9, 10).

The eight proteins can be grouped into three general categories by their DST behavior, hardness, and ESH values. The first category consists of the three soft [1], highly foamable proteins hGH, β-Cas, and BSA (Table 1). β-Cas and hGH have relatively high ESH values [2], and BSA is known to have a strong affinity for hydrophobic surfaces, as discussed above. These three proteins exhibited very ideal DST behavior with no or very brief induction times at low C_b values (0–1 min at C_b = 0.01 mg/ml), rapid attainment of initial MST values (Table 2), and eventual attainment of near steady-state surface tension values within 15 h at the high C_b of 1.0 mg/ml.

The second category consists of two proteins that have intermediate values of hardness [1], ESH [2], and foamability (Table 1), namely, Myo and Cyt *c*. These two proteins exhibited relatively complex, nonideal DST behavior, with medium-length induction times on the order of 10 min at C_b = 0.01 mg/ml and intermediate initial DST decay rates at C_b = 1.0 mg/ml (Table 2). The long-term MST values of Cyt *c* and Myo converged to single values within 16 h, suggesting independence of the long-term surface coverage on C_b over the experimental range of C_b.

SOD, Lys, and RNase constitute the third category of protein. These three proteins have the hardest structures [1], with low or intermediate foamabilities (Table 1), and highly variable ESH values [2]. These proteins exhibited the slowest DST kinetics at both low and high C_b (Table 2). SOD was the only protein to exhibit an induction time at C_b = 1.0 mg/ml. Lys and RNase were the only two proteins which did not attain initial MST values at C_b = 0.01 mg/ml, within the time of the experiments.

The differences in the initial DST kinetics of the eight proteins clearly indicate that the rate of protein adsorption at the A/W interface is very dependent on the protein type and composition. Proteins with rapid initial DST kinetics tended to attain lower long-term MST values. An attempt to statistically correlate ESH, foamability, and hardness parameters with measured DST kinetic parameters was largely unsuccessful (87). However, some trends were apparent; the softest proteins (β-Cas, BSA, hGH) had much faster rates of initial DST decrease than the hardest proteins (SOD, Lys, RNase). The effect of the ESH on DST kinetics was less clear. The fastest DST kinetics were exhibited by the most hydrophobic protein, β-Cas, and for two pairs of proteins with similar bulk diffusion coefficients (103), i.e., β-Cas vs BSA and Lys vs RNase, the more hydrophobic protein in each pair (β-Cas and Lys) exhibited faster DST kinetics. The ESH of a native protein is not always indicative of its affinity for amphiphilic interfaces. A soft, initially hydrophilic protein, e.g., BSA, may unfold during adsorption, resulting in exposure of normally buried hydrophobic residues to the A/W interface. High foamability was a better indicator of rapid DST kinetic behavior than low thermal stability; e.g., hGH had a high thermal unfolding temperature, but was very foamable and had the second-fastest DST kinetics at C_b = 1.0 mg/ml.

CONCLUSIONS

The observation of large decreases in the DST of aqueous protein solutions indicates that many different globular proteins adsorb at the A/W interface. The initial rate of DST decrease is much more dependent on the protein composition and physical properties than the long-term MST value, even at high C_b values. Both conformational stability (hardness) and surface hydrophobicity have a large influence on the adsorption rate of globular proteins at the A/W interface, although hardness is the more important variable. Soft, easily

foamable proteins with hydrophobic surfaces exhibited the fastest adsorption rates, while hard, poorly foamable proteins with hydrophilic surfaces exhibited the slowest adsorption rates. However, globular protein adsorption rates cannot always be predicted solely on the basis of their folded tertiary structure and surface characteristics; unfolding can occur during the adsorption process, resulting in a manifestation of higher than expected affinity for the A/W interface.

The initial C_b is also an important variable in protein adsorption kinetics at the A/W interface. Adsorption-induced bulk depletion is significant only at initial C_b values at or below 0.01 mg/ml in the DIPD method used in this work. At high initial C_b values, e.g., $C_b = 1.0$ mg/ml, mass-transfer rates to the subsurface region do not appear to be the limiting factor in protein adsorption rates at the A/W interface, with the exception of β-Cas. Based on the fitted values of the H&R parameter t^*, the adsorption kinetics of the other seven globular proteins at $C_b = 1.0$ mg/ml are not diffusion-limited, but are much slower, due to an energy or probabilistic barrier to adsorption. Thus, any general kinetic model that describes protein adsorption at high C_b must also account for the influence of protein structural properties, as well as mass-transfer rates, to the A/W interface.

ACKNOWLEDGMENTS

This work is based, in part, on the Ph.D. dissertation by Tripp (87). Financial support from the University of Utah Center for Biopolymers at Interfaces, the Patricia Robert Harris Fellowship Program, the NIH Biotechnology Training Grant Program, and Genentech, Inc., is gratefully acknowledged. Assistance and helpful conversations with A.-P. Wei, P. Dryden, A. Pungor, V. Hlady, K. Caldwell, J. Herron, T. Oolman, G. Nyquist, and Y. Gao, among others, and the gift of the ADSA-P software by A. W. Neumann are also appreciated.

REFERENCES

1. Augensteine, L. G., and Ray, B. R., *J. Phys. Chem.* **61,** 1385 (1957).
2. James, L. K., and Augenstein, L. G., *Adv. Enzymol. Relat. Subj. Biochem.* **28,** 1 (1966).
3. Donaldson, T. L., Boonstra, E. F., and Hammond, J. M., *J. Colloid Interface Sci.* **74,** 441 (1980).
4. Browne, M., Cecil, R., and Miller, J. C., *Eur. J. Biochem.* **33,** 233 (1973).
5. Dill, K. A., *Biochemistry* **29,** 7133 (1990).
6. Manning, M. C., Patel, K., and Borchardt, R. T., *Pharm. Res.* **6,** 903 (1989).
7. Bagnal, R. D., *J. Biomed. Mater. Res.* **11,** 947 (1977).
8. Andrade, J. D., Hlady, V., Wei, A.-P., Ho, C. H., Lea, A. S., Jeon, S. I., Lin, Y. S., and Stroup, E., *Clin. Mat.* **11,** 67 (1992).
9. Wei, A.-P., MA Thesis, Department of Bioengineering, University of Utah, 1991.
10. Cumper, C. W. N., and Alexander, A. E., *Rev. Pure Appl. Chem.* **1,** 121 (1951).
11. MacRitchie, F., and Alexander, A. E., *J. Colloid Sci.* **18,** 453 (1963).
12. MacRitchie, F., and Alexander, A. E., *J. Colloid Sci.* **18,** 458 (1963).
13. MacRitchie, F., and Alexander, A. E., *J. Colloid Sci.* **18,** 464 (1963).
14. Yamashita, T., and Bull, H. B., *J. Colloid Interface Sci.* **27,** 19 (1968).
15. Mitchell, J., Irons, L., and Palmer, G. J., *Biochim. Biophys. Acta* **200,** 138 (1970).
16. Benjamins, J., de Feijter, J. A., Evans, M. T. A., Graham, D. E., and Phillips, M. C., *Faraday Discuss. Chem. Soc.* **59,** 218 (1975).
17. Benjamins, J., de Feijter, J. A., Evans, M. T. A., Graham, D. E., and Phillips, M. C., *Faraday Discuss. Chem. Soc.* **59,** 254 (1975).
18. Blank, M., Lee, B. B., and Britten, J. S., *J. Colloid Interface Sci.* **50,** 215 (1975).
19. Elbaum, D., Harrington, J., Roth, E. F., and Negel, R. L., *Biochim. Biophys. Acta* **427,** 57 (1976).
20. Tornberg, E., *J. Colloid Interface Sci.* **64,** 391 (1978).
21. Graham, D. E., and Phillips, M. C., *J. Colloid Interface Sci.* **70,** 403 (1979).
22. Graham, D. E., and Phillips, M. C., *J. Colloid Interface Sci.* **70,** 415 (1979).
23. Graham, D. E., and Phillips, M. C., *J. Colloid Interface Sci.* **70,** 427 (1979).
24. Phillips, M. C., and Sparks, C. E., *Ann. NY Acad. Sci.* **348,** 122 (1980).
25. Ward, A. J. I., and Regan, L. H., *J. Colloid Interface Sci.* **78,** 389 (1980).
26. Absolom, D. R., van Oss, C. J., Zingg, W., and Neumann, A. W., *Biochim. Biophys. Acta* **670,** 74 (1981).
27. Tornberg, E., and Lundh, G., *J. Colloid Interface Sci.* **79,** 76 (1981).
28. Trapeznikov, A. A., Vins, V. G., and Shirokova, T. Yu., *Colloid J. USSR* **43,** 262 (1981).
29. Tornberg, E., Granfeldt, Y., and Håkansson, C., *J. Sci. Food Agric.* **33,** 904 (1982).
30. Krebs, K. E., and Phillips, M. C., *Biochim. Biophys. Acta* **754,** 227 (1983).
31. Krebs, K. E., and Phillips, M. C., *FEBS Lett.* **175,** 263 (1984).
32. De Feijter, J. A., and Benjamins, J., *in* "Food Emulsions and Foams" (E. Dickinson, Ed.), p. 72. Royal Society of Chemistry, London, 1986.
33. Song, K. B., and Damodaran, S., *J. Agric. Food Chem.* **35,** 236 (1987).
34. Damodaran, S., and Song, K. B., *Biochim. Biophys. Acta* **954,** 253 (1988).
35. Kato, A., and Yutani, K., *Protein Eng.* **2,** 153 (1988).
36. Krebs, K. E., Ibdah, J. A., and Phillips, M. C., *Biochim. Biophys. Acta* **959,** 229 (1988).
37. Watanabe, N., Shirakawa, T., Iwahashi, M., and Seimiya, T., *Colloid Polym. Sci.* **266,** 254 (1988).
38. MacRitchie, F., *Colloids Surf.* **41,** 25 (1989).
39. Coke, M., Wilde, P. J., Russell, E. J., and Clark, D. C., *J. Colloid Interface Sci.* **138,** 489 (1990).
40. Damodaran, S., and Song, K. B., *Colloids Surf.* **50,** 75 (1990).
41. Song, K. B., and Damodaran, S., *Langmuir* **7,** 2737 (1991).
42. Damodaran, S., and Song, K. B., *in* "Interactions in Food Proteins" (N. Parris and R. Burford, Eds.), Chap. 8, ACS Symposium Series Vol. 454. Amer. Chem. Soc., Washington, DC, 1991.
43. Ivanova, M. G., Verger, R., Bois, A. G., and Panaiotov, I., *Colloids Surf.* **54,** 279 (1991).
44. Levine, H. L., Ransohoff, T. C., Kawahata, R. T., and McGregor, W. C., *J. Parenter. Sci. Technol.* **45,** 160 (1991).
45. MacRitchie, F., *Anal. Chim. Acta* **249,** 241 (1991).
46. Maksymiw, R., and Nitsch, W., *J. Colloid Interface Sci.* **147,** 67 (1991).
47. Busscher, H. J., van der Vegt, W., Noordmans, J., Schakenraad, J. M., and van der Mei, H. C., *Colloids Surf.* **58,** 229 (1991).
48. Voigt, A., Thiel, O., Williams, D., Policova, Z., Zingg, W., and Neumann, A. W., *Colloids Surf.* **58,** 315 (1991).
49. Paulsson, M., and Dejmek, P., *J. Colloid Interface Sci.* **150,** 394 (1992).
50. Xu, S., and Damodaran, S., *Langmuir* **8,** 2021 (1992).
51. Jollés, P., and Jollés, J., *Mol. Cell. Biochem.* **63,** 165 (1984).
52. Perutz, M. F., *Proc. R. Soc. London.* **167,** 348 (1966).
53. Sarma, R., *in* "Conformation in Biology, the Festschrift Celebrating the Sixtieth Birthday of G. N. Ramachandran" (R. Srinivasan and R. H. Sarma, Eds.). Adenine Press, New York, 1983.

54. Dayhoff, M. O., Ed., "Atlas of Protein Sequence and Structure," Vol. 5. National Biomedical Research Foundation, Washington, DC, 1972.
55. Chmelík, J., Deml, M., Janca, J., *Anal. Chem.* **61,** 912 (1989).
56. Mathews, F. S., *Prog. Biophys. Mol. Biol.* **45,** 1 (1985).
57. Dickerson, R. E., *Sci. Amer.* **4,** 58 (1972).
58. Richardson, D. C., *in* "Superoxide and Superoxide Dismutase" (A. M. Michelson, J. M. McCord, and I. Fridovich, Eds.). Academic Press, New York, 1977.
59. Getzoff, E. D., *in* "Superoxide and Superoxide Dismutase in Chemistry, Biology, and Medicine" (G. Rotilio, Ed.), p. 135. Elsevier, New York, 1986.
60. Dickinson, E., and Stainsby, G., "Colloids in Food." Applied Science, London, 1982.
61. De Vos, A. M., Ultsch, M., and Kossiakoff, A. A., *Science* **255,** 306 (1992).
62. Peters, T., Jr., "Albumin, an Overview and Bibliography." Research Products Division, Miles Laboratories, Elkhart, IN, 1980.
63. Hamilton, J. A., Era, S., Bhamidipati, S. P., and Reed, R. G., *Proc. Natl. Acad. Sci. USA* **88,** 2051 (1991).
64. Arai, T., and Norde, W., *Colloids Surf.* **51,** 1 (1990).
65. Norde, W., and Anusiem, C. I., *Colloids Surf.* **66,** 73 (1992).
66. Norde, W., and Favier, J. P., *Colloids Surf.* **64,** 87 (1992).
67. Fligner, K. L., and Mangino, M. E., *in* "Interactions of Food Proteins" (N. Parris and R. Barford, Eds.), Chap. 1, ACS Symposium Series, Vol. 454. Amer. Chem. Soc., Washington, DC, 1991.
68. Cumper, C. W. N., *Trans. Faraday Soc.* **49,** 1360 (1953).
69. Mita, T., Nikai, K., Hiraoka, T., Matsuo, S., and Matsumoto, H., *J. Colloid Interface Sci.* **59,** 172 (1977).
70. Mita, T., Ishida, E., and Matsumoto, H., *J. Colloid Interface Sci.* **64,** 143 (1978).
71. Ingraham, R. H., *in* "High-Performance Liquid Chromatography of Peptides and Proteins: Separation, Analysis, and Conformation" (C. T. Mant and R. S. Hodges, Eds.). CRC Press, Baton Rouge, 1991.
72. Hua, X.-Y., and Rosen, M. J., *J. Colloid Interface Sci.* **124,** 652 (1988).
73. Hua, X.-Y., and Rosen, M. J., *J. Colloid Interface Sci.* **141,** 180 (1991).
74. Neu, T. R., Härtner, T., and Poralla, K., *Appl. Microbiol. Biotechnol.* **32,** 518 (1990).
75. Denizot, B. A., Tchoreloff, P. C., Proust, J. E., Puisieux, F., Lindenbaum, A., and Dehan, M., *J. Colloid Interface Sci.* **143,** 120 (1991).
76. Serrien, G., and Joos, P., *J. Colloid Interface Sci.* **139,** 149 (1990).
77. Lankveld, J. M. G., and Lyklema, J., *J. Colloid Interface Sci.* **41,** 454 (1972).
78. Steinman, H. M., *in* "Superoxide Dismutase, Volume I" (L. W. Oberley, Ed.), Chap. 2. CRC Press, Boca Raton, 1982.
79. Payens, T. A. J., Brinkhuis, J. A., and van Markwijk, B. W., *Biochim. Biophys. Acta* **175,** 434 (1969).
80. Grinberg, N., Blanco, R., Yarmush, D. M., and Karger, B. L., *Anal. Chem.* **61,** 514 (1989).
81. Rotenburg, Y., Boruvka, L., and Neumann, A. W., *J. Colloid Interface Sci.* **93,** 169 (1983).
82. Girault, H. H. J., Schiffrin, D. J., and Smith, B. D. V., *J. Colloid Interface Sci.* **101,** 277 (1984).
83. Anastasiadis, S. H., Chen, J.-K., Koberstein, J. T., Siegel, A. F., Sohn, J. E., and Emerson, J. A., *J. Colloid Interface Sci.* **119,** 55 (1987).
84. Boucher, E. A., Evans, M. J. B., and Jones, T. G. J., *Adv. Colloid Interface Sci.* **27,** 43 (1987).
85. Jennings, Jr., J. W., and Pallas, N. R., *Langmuir* **4,** 959 (1988).
86. Hansen, F. K., and Rødsrud, G., *J. Colloid Interface Sci.* **141,** 1 (1991).
87. Tripp, B. C., Ph.D. Dissertation, Department of Chemical Engineering, University of Utah, 1993.
88. Singer, S. J., *J. Chem. Phys.* **16,** 872 (1948).
89. Frisch, H. L., and Simha, R., *J. Chem. Phys.* **27,** 702 (1957).
90. Douillard, R., *Colloids Surf. B: Biointerfaces* **1,** 333 (1993).
91. Uraizee, F., and Narsimhan, G., *J. Colloid Interface Sci.* **146,** 169 (1991).
92. Aveyard, R., and Haydon, D. A., "An Introduction to the Principles of Surface Chemistry." Cambridge Univ. Press, New York, 1973.
93. Hunter, J. R., Carbonell, R. G., and Kilpatrick, P. K., *J. Colloid Interface Sci.* **137,** 462 (1990).
94. Bagnal, R. D., *J. Biomed. Mater. Res.* **11,** 947 (1977).
95. Furuno, T., and Sasabe, H., *J. Colloid Interface Sci.* **147,** 225 (1991).
96. Adams, D. J., Evans, M. T. A., Mitchell, J. R., Phillips, M. C., and Rees, P. M., *J. Polym. Sci.: Part C* **34,** 167 (1971).
97. MacRitchie, F., *J. Colloid Interface Sci.* **61,** 223 (1977).
98. MacRitchie, F., *J. Colloid Sci.* **18,** 555 (1963).
99. MacRitchie, F., and Owens, N. F., *J. Colloid Interface Sci.* **29,** 66 (1969).
100. Bianco, H., and Marmur, A., *J. Colloid Interface Sci.* **151,** 517 (1992).
101. Damodaran, S., *in* "Food Proteins" (J. E. Kinsella and W. G. Soucie, Eds.) Chapter 3. The American Oil Chemists' Society, Champaign, Illinois, 1991.
102. Ward, A. F. H., and Tordai, L., *J. Chem. Phys.* **14,** 453 (1946).
103. Tyn, M. T., and Gusek, T. W., *Biotechnol. Bioeng.* **35,** 327 (1990).
104. Hunter, J. R., Kilpatrick, P. K., and Carbonell, R. G., *J. Colloid Interface Sci.* **142,** 429 (1991).
105. Andrade, J. D., and Hlady, V., *Ann. NY Acad. Sci.* **516,** 158 (1987).
106. Burgess, D. J., Longo, L., and Yoon, J. K., *J. Parenter. Sci. Technol.* **45,** 239 (1991).
107. Andrade, J. D., Hlady, V., Wei, A.-P., and Gölander, C.-G., *Croat. Chem. Acta* **63,** 527 (1990).
108. Busscher, H. J., van der Vegt, W., Noordmans, J., Schakenraad, J. M., and van der Mei, H. C., *Colloids Surf.* **58,** 229 (1991).
109. Horsely, D., Herron, J., Hlady, V., and Andrade, J., *in* "Proteins at Interfaces: Physiochemical and Biochemical Studies" (J. L. Brash and T. A. Horbett, Eds.), p. 290, ACS Symposium Series, Vol. 343. Am. Chem. Soc., Washington, DC, 1987.
110. Fausnaugh, J. L., and Regnier, F. E., *J. Chromatogr.* **359,** 131 (1986).
111. Lee, C.-S., and Belfort, G., *Proc. Natl. Acad. Sci. USA* **86,** 8392 (1989).